



저작자표시-비영리-변경금지 2.0 대한민국

이용자는 아래의 조건을 따르는 경우에 한하여 자유롭게

- 이 저작물을 복제, 배포, 전송, 전시, 공연 및 방송할 수 있습니다.

다음과 같은 조건을 따라야 합니다:



저작자표시. 귀하는 원저작자를 표시하여야 합니다.



비영리. 귀하는 이 저작물을 영리 목적으로 이용할 수 없습니다.



변경금지. 귀하는 이 저작물을 개작, 변형 또는 가공할 수 없습니다.

- 귀하는, 이 저작물의 재이용이나 배포의 경우, 이 저작물에 적용된 이용허락조건을 명확하게 나타내어야 합니다.
- 저작권자로부터 별도의 허가를 받으면 이러한 조건들은 적용되지 않습니다.

저작권법에 따른 이용자의 권리는 위의 내용에 의하여 영향을 받지 않습니다.

이것은 [이용허락규약\(Legal Code\)](#)을 이해하기 쉽게 요약한 것입니다.

[Disclaimer](#)

Ph.D. Thesis

박사 학위논문

Molecular mechanisms underlying surface trafficking and
lipid regulation of acid-sensing ion channels (ASICs)

Hae-Jin Kweon (권혜진 權惠珍)

Department of Brain & Cognitive Sciences

DGIST

2017

Molecular mechanisms underlying surface trafficking and lipid regulation of acid-sensing ion channels (ASICs)

Advisor: Professor Byung-Chang Suh

Co-Advisor: Professor Il-Sung Jang

by

Hae-Jin Kweon

Department of Brain & Cognitive Sciences

DGIST

A thesis submitted to the faculty of DGIST in partial fulfillment of the requirements for the degree of Doctor of Philosophy in the Department of Brain & Cognitive Sciences. The study was conducted in accordance with Code of Research Ethics¹⁾.

8. 24. 2016

Approved by

Professor Byung-Chang Suh (Signature)
(Advisor)



Professor Il-Sung Jang
(Co-Advisor)

(Signature)


1) Declaration of Ethical Conduct in Research: I, as a graduate student of DGIST, hereby declare that I have not committed any acts that may damage the credibility of my research. These include, but are not limited to: falsification, thesis written by someone else, distortion of research findings or plagiarism. I affirm that my thesis contains honest conclusions based on my own careful research under the guidance of my thesis advisor.

Molecular mechanisms underlying surface trafficking and
lipid regulation of acid-sensing ion channels (ASICs)

Hae-Jin Kweon

Accepted in partial fulfillment of the requirements for the degree of
Doctor of Philosophy

8. 31. 2016

Head of Committee 김 은 경 (Signature) 

Prof. Eun-Kyoung Kim

Committee Member 김 규 형 (Signature) 

Prof. Kyuhyung Kim

Committee Member 이 승 배 (Signature) 

Prof. Sung Bae Lee

Committee Member 장 일 성 (Signature) 

Prof. Il-Sung Jang

Committee Member 서 병 창 (Signature) 

Prof. Byung-Chang Suh

Ph.D./BS
201145001

권혜진. Hae-Jin Kweon. Molecular mechanisms underlying surface trafficking and lipid regulation of acid-sensing ion channels (ASICs). Department of Brain & Cognitive Sciences. 2017. 68 p. Advisor Prof. Byung-Chang Suh, Co-Advisor Prof. Il-Sung Jang.

Abstract

Acid-sensing ion channels (ASICs) are proton-activated cation channels that play important roles as typical proton sensors in the nervous system. Protons are released in pain-generating pathophysiological conditions such as inflammation, ischemic stroke, infection, and cancer. During normal synaptic activities, protons also act as a neurotransmitter. Perception of physiological pH changes through ASICs are implicated in nociception, itch, mechanosensation, taste transduction, learning and memory, and fear. In spite of their importance in proton sensing, regulatory mechanisms of these channels still need to be further investigated. In this study, we studied the regulatory mechanisms of ASICs by dividing into two parts. In the first part, we examined whether these channels are regulated by membrane phospholipids, which are general cofactors of many receptors and ion channels. In the second part, we investigated differential surface trafficking mechanisms of ASIC subunits.

Firstly, we studied the sensitivity toward membrane phospholipids of ASICs by comparing with that of another proton-sensitive ion channel, transient receptor potential vanilloid 1 (TRPV1) channel. We observed that ASICs do not require membrane phosphatidylinositol 4-phosphate (PI(4)P) or phosphatidylinositol 4,5-bisphosphate (PI(4,5)P₂) for their function. However, TRPV1 currents were inhibited by simultaneous breakdown of PI(4)P and PI(4,5)P₂. By using a novel chimeric protein, CF-PTEN, that can specifically dephosphorylate at the D3 position of phosphatidylinositol 3,4,5-trisphosphate (PI(3,4,5)P₃),

we also observed that neither ASICs nor TRPV1 activities were altered by depletion of PI(3,4,5)P₃ in intact cells. Finally, we compared the effects of arachidonic acid (AA) on two proton-sensitive ion channels. We observed that AA potentiates the currents of both ASICs and TRPV1, but that they have different recovery aspects. Taken together, ASICs and TRPV1 have different sensitivities toward membrane phospholipids, such as PI(4)P, PI(4,5)P₂, and AA, although they have common roles as proton sensors.

In the second part, we investigated the regulatory mechanisms of ASICs by revealing surface trafficking mechanisms of ASICs. It is important that newly synthesized receptors or ion channels correctly target their final cellular destinations for their function. Diverse physiological disorders are linked with defects in ion channel surface trafficking. In this study, we focused on ASIC2 subunits in particular. Among the ASIC subunits, ASIC2a and ASIC2b are alternative splicing products from the same gene, *ACCNI*. It has been shown that ASIC2 isoforms have differential subcellular distribution: ASIC2a targets the cell surface by itself, while ASIC2b resides in the ER. However, the underlying mechanism for this differential subcellular localization remained to be further elucidated. By constructing ASIC2 chimeras, we found that the first transmembrane (TM1) domain and the proximal post-TM1 domain (17 amino acids) of ASIC2a are critical for membrane targeting of the proteins. We also observed that replacement of corresponding residues in ASIC2b by those of ASIC2a conferred proton-sensitivity as well as surface expression to ASIC2b. We finally confirmed that ASIC2b is delivered to the cell surface from the ER by forming heteromers with ASIC2a, and that the N-terminal region of ASIC2a is additionally required for the ASIC2a-dependent membrane targeting of ASIC2b. Together, our study supports an important role of ASIC2a in membrane targeting of ASIC2b.

In addition, we also found that ASIC2a has an important role in facilitating ASIC3 surface expression. ASIC2a also efficiently delivered ASIC3 which are predominantly

accumulated in the ER with partial distribution in the plasma membrane to the cell surface. We also observed that the ASIC2a-dependent surface trafficking of ASIC3 remarkably enhanced the sustained component of the currents. Our study demonstrates that ASIC2a can increase the membrane conductance sensitivity to protons by facilitating the surface expression of ASIC3 through heteromeric assembly.

Keywords: acid-sensing ion channel (ASIC), endoplasmic reticulum (ER), membrane lipid, protein assembly, surface trafficking

CONTENTS

| | |
|--|------------|
| Abstract | i |
| List of contents | iv |
| List of tables | v |
| List of figures | v |
| | |
| I . INTRODUCTION | 1 |
| 1. 1. Regulation of acid-sensing ion channels (ASICs) by membrane phospholipids | 2 |
| 1. 2. Surface trafficking mechanisms of acid-sensing ion channels (ASICs) | 4 |
| II . MATERIALS AND METHODS | 6 |
| | |
| III. RESULTS | 15 |
| 3. 1. Regulation of acid-sensing ion channels (ASICs) by membrane phospholipids | 15 |
| 3. 2. Surface trafficking mechanisms of acid-sensing ion channels (ASICs) | 28 |
| IV. DISCUSSION | 58 |
| 4. 1. Regulation of acid-sensing ion channels (ASICs) by membrane phospholipids | 58 |
| 4. 2. Surface trafficking mechanisms of acid-sensing ion channels (ASICs) | 62 |
| V . REFERENCES | vii |
| | |
| VI. SUMMARY IN KOREAN | xix |

List of tables

Table 1. Primers and templates used for chimera construction

List of figures

Fig. 1. An ASIC subunit and formation of a trimeric channel

Fig. 2. The activity of TRPV1 is dependent on phosphoinositides

Fig. 3. Homomeric ASIC currents are insensitive to PI(4)P and PI(4,5)P₂

Fig. 4. Heteromeric ASIC currents are insensitive to PI(4)P and PI(4,5)P₂

Fig. 5. Neither ASICs nor TRPV1 activities are affected by depletion of PI(3,4,5)P₃

Fig. 6. Potentiation of ASICs by AA

Fig. 7. Potentiation of TRPV1 by AA

Fig. 8. Different subcellular localization and proton-sensitivity between ASIC2a and ASIC2b in HEK293T cells

Fig. 9. Differential subcellular localization of ASIC2a and ASIC2b

Fig. 10. Replacement of the first 129 amino acids in ASIC2b by corresponding regions of ASIC2a conferred surface expression and proton-sensitivity

Fig. 11. The TM1 and the proximal post-TM1 domain of ASIC2a are critical regions for surface trafficking of ASIC2

Fig. 12. The N-terminus and the TM1 domain regulate the channel properties

Fig. 13. H72 and E78 are critical for proton-sensitivity, whereas D77 is involved in determining subcellular localization and proton-sensitivity

Fig. 14. ASIC2b traffics to the cell surface by heteromeric assembly with ASIC2a

Fig. 15. Control experiments for BiFC assay

Fig. 16. Surface expression of ASIC2b is increased in the presence of ASIC2a in SH-SY5Y cells

Fig. 17. The N-terminal region of ASIC2a is necessary for the ASIC2a-dependent membrane targeting of ASIC2b

Fig. 18. Different subcellular distribution of ASIC2a and ASIC3 in HEK293T cells

Fig. 19. N- or C-terminal deletion or both N- and C-terminal deletion from ASIC3 does not rescue ASIC3 from ER accumulation

Fig. 20. ASIC2a enhances the surface expression of ASIC3 by heteromeric assembly

Fig. 21. N- and C-terminal regions of ASIC3 are involved in heteromeric assembly with ASIC2a

Fig. 22. ASIC2a-dependent surface trafficking of ASIC3 increases sustained currents

Fig. 23. ASIC2a-dependent surface expression of ASIC3 in SH-SY5Y cells and proton-induced currents in native neurons

Fig. 24. N-terminal 15-30 amino acids of ASIC2a are critical for membrane targeting of ASIC2a and ASIC2a-dependent surface trafficking of ASIC3

I . INTRODUCTION

Acid-sensing ion channels (ASICs) are voltage-independent, proton-gated cation channels widely expressed in the nervous system (Price et al., 1996; Waldmann et al., 1997; Wemmie et al., 2013). They belong to the epithelial Na⁺ channel/degenerin (ENaC/DEG) superfamily of ion channels. Extracellular acidification commonly occurs in pathological conditions such as inflammation, tissue injury, ischemic stroke, and cancer (Smith et al., 1986; Deval et al., 2008; Deval et al., 2010). Protons have also been reported to act as a neurotransmitter in the brain, and it is well known that synaptic vesicles are acidic (Miesenböck et al., 1998; Du et al., 2014). Therefore, detection of physiological pH changes during pathological events and normal synaptic activities is indispensable for cellular activities (Kweon et al., 2015). ASICs play roles as typical proton sensors in the central and peripheral nervous system (Kweon and Suh, 2013). They are implicated in nociception, learning and memory, fear, taste transduction, and mechanosensation (Wemmie et al., 2002; Ugawa et al., 2003; Wemmie et al., 2003; Deval et al., 2008; Ikeuchi et al., 2008; Chen and Wong, 2013). There are six subunits (ASIC1a, ASIC1b, ASIC2a, ASIC2b, ASIC3, and ASIC4) encoded by four genes (*ACCN2*, *ACCN1*, *ACCN3*, and *ACCN4*). *ACCN2* and *ACCN1* each produce two alternative splicing variants: ASIC1a and ASIC1b from *ACCN2*, and ASIC2a and ASIC2b from *ACCN1*. The crystal structure of chicken ASIC1 has provided insight into the structure and the function of channels (Jasti et al., 2007; Gonzales et al., 2009). An ASIC subunit is composed of two transmembrane (TM) domains, a large extracellular loop, and short cytoplasmic N- and C-termini (Kweon and Suh, 2013) (Fig. 1). Structural studies have revealed that three subunits assemble to form a functional homo- or heterotrimeric channel (Fig. 1). However, among the subunits, ASIC2b and ASIC4 are not known to form functional homomeric channels. Unlike ASIC4,

ASIC2b has been shown to modulate the properties of other ASICs by forming heteromeric channels (Lingueglia et al., 1997; Schwartz et al., 2015).

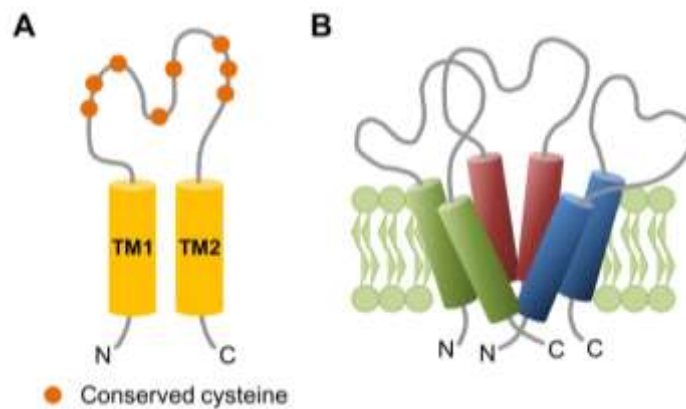


Fig. 1. An ASIC subunit and formation of a trimeric channel. (A) One ASIC subunit has two hydrophobic transmembrane domains, a large cysteine-rich extracellular loop, and short intracellular N- and C-termini. (B) Three subunits assemble to form a functional homo- or hetero- trimeric channel.

1. 1. Regulation of acid-sensing ion channels (ASICs) by membrane phospholipids

A signaling lipid, PI(4,5)P₂, which is a minor acidic phospholipid in the inner leaflet of the eukaryotic cellular membranes, has received attention as a functional cofactor for membrane receptors and ion channels (Suh and Hille, 2008; Falkenburger et al., 2010). Cleavage of PI(4,5)P₂ by receptor-activated PLC generates two second messengers: membrane-bound lipid diacylglycerol (DAG) and soluble inositol 1,4,5-trisphosphate (IP₃). Depletion of PI(4,5)P₂ during PLC signaling also inhibits the currents of several ion channels (Suh and Hille, 2008), including inwardly rectifying K⁺ (Kir) channel (Hilgemann et al., 1996), KCNQ channel (Suh and Hille, 2002; Suh et al., 2006), voltage-gated Ca²⁺ channel (VGCC) (Suh et al., 2010), ENaC (Yue et al., 2002; Pochynyuk et al., 2006; Pochynyuk et al., 2007), and several members of the transient receptor potential (TRP) channel family (Hardie, 2007).

In the first part of this study, we focused on determining the sensitivities of ASICs

toward phospholipids by comparing them to transient receptor potential vanilloid 1 (TRPV1) channels. Capsaicin- or thermal stimuli-activated TRPV1 channels are also proton sensors primarily expressed in sensory neurons (Jordt et al., 2000; Ryu et al., 2003; Aneiros et al., 2011). Although many interesting studies revealed that the plasma membrane (PM) phosphoinositide PI(4,5)P₂ is a regulator of TRPV1 channels, whether PI(4,5)P₂ has inhibitory or potentiating effects on their activities has been debated over the past decade (Chuang et al., 2001; Liu et al., 2005; Stein et al., 2006; Lukacs et al., 2007; Klein et al., 2008; Cao et al., 2013; Lukacs et al., 2013a, Lukacs et al., 2013b, Senning et al., 2014). In the case of ASICs, whether these channels have dependence on the phosphoinositides for their function has not been determined yet (Kweon and Suh, 2013). Dorofeeva *et al.* reported that homomeric ASIC1a channels can be inhibited by the activation of G_q-coupled M₁ muscarinic receptor (M₁R) (Dorofeeva et al., 2009), which leads to hydrolysis of both PI(4)P and PI(4,5)P₂ through the activation of PLCβ enzymes (Horowitz et al., 2005; Balla et al., 2008). However, Li *et al.* observed no decrease of ASIC1a currents during muscarinic receptor activation (Li et al., 2012). Therefore, it is necessary to further examine the dependence of ASICs on membrane phospholipids for their function.

We used recently developed translocatable pseudojanin (PJ) system (Hammond et al., 2012) for investigating the sensitivities of ASICs to PM PI(4)P and PI(4,5)P₂. In addition, we generated a novel inducible 3-phosphatase that can specifically dephosphorylate PM phosphatidylinositol 3,4,5-trisphosphate [PI(3,4,5)P₃] and investigated PI(3,4,5)P₃ sensitivities of ASICs and TRPV1 channels in intact cells. Our studies demonstrate that the sensitivities of proton-sensitive ion channels toward PM phospholipids differ significantly depending on the type of channels.

1. 2. Surface trafficking mechanisms of acid-sensing ion channels (ASICs)

ASIC2a and ASIC2b have different amino acid sequences in the N-terminus, the TM1 domain, and one-third of the extracellular loop region, while the rest of the sequences are identical. Several studies have exploited the difference in sequences of two subunits to find proton-binding sites present in ASIC2a, and identified five amino acids (H72, D77, E78, H109, and H180), which are absent in ASIC2b, as putative proton-binding sites (Baron et al., 2001; Smith et al., 2007b; Schuhmacher et al., 2015). They reported that single amino acid change in these five residues produced a proton-insensitive channel that trafficked normally to the cell surface like ASIC2b in Chinese hamster ovary (CHO) cells (Baron et al., 2001; Smith et al., 2007b). However, surface expression of these mutated channels as well as ASIC2b needs to be further studied.

In cultured hippocampal neurons, ASIC2a displays somatodendritic distribution primarily in dendrites and dendritic spines (Zha et al., 2009). When ASIC2a was heterologously expressed in human embryonic kidney (HEK) 293 cells, it was mostly detected in the plasma membrane and other intracellular locations (Chai et al., 2007). However, according to the previous study, ASIC2b has a reticular distribution in COS-7 cells (Hruska-Hageman et al., 2002). Additionally, one research group has observed that ASIC2 proteins display a perinuclear-staining pattern in vascular smooth muscle cells (VSMCs) (Grifoni et al., 2008). Quite recently, Wu *et al.* has reported that ASIC2a and ASIC2b show differential surface trafficking in NIH 3T3 cells (Wu et al., 2016). Here, we confirmed dramatically different subcellular localization of ASIC2a and ASIC2b, and further investigated underlying mechanisms for this differential surface trafficking of ASIC2 proteins.

Delivery of ion channels and receptors to the cell surface requires efficient transport between secretory apparatus, the ER, the Golgi, and the plasma membrane (Ma

and Jan, 2002; Cunningham et al., 2012). From the perspective of trafficking mechanisms, surface expression of ion channels is largely dependent on discrete motifs that reside in proteins, such as ER retention or export signals. Synthesized proteins containing arginine-based ER retention signals (RXR) or physiologically misfolded and improperly assembled proteins are retained in the ER via the quality control mechanism (Chang et al., 1999; Zerangue et al., 1999; Bichet et al., 2000; Standley et al., 2000; Margeta-Mitrovic et al., 2002; Michelsen et al., 2005). In these cases, ER retention can be antagonized by proper heteromultimeric assembly. In addition to ER retention signals, ER export signals can be utilized to regulate the surface composition of some membrane proteins. Even though the channel proteins are properly folded and assembled, exit from the ER can require specific anterograde ER export signals (Nishimura and Balch, 1997; Sevier et al., 2000; Bermak et al., 2001; Ma et al., 2001; Ma and Jan, 2002; Ma et al., 2002; Otsu et al., 2013).

In the current study, by constructing a series of ASIC2 chimeras, we found that the TM1 and the proximal post-TM1 domain of ASIC2a are critical for surface trafficking of ASIC2 channels. Further analysis of chimeras has supported that the proximal post-TM1 domain of ASIC2a is essential for generating proton-activated currents, in accordance with the previous reports (Baron et al., 2001; Smith et al., 2007b; Schuhmacher et al., 2015). Finally, our data show that ASIC2b can be delivered to the cell surface from the ER by heteromeric assembly with ASIC2a, and that the N-terminal region of ASIC2a is additionally necessary for the ASIC2a-dependent membrane targeting of ASIC2b.

II. MATERIALS AND METHODS

Cell culture and transfection

TsA201 (HEK293T) cells, derived from human embryonic kidney 293 cells (293tsA1609neo) by stably transfecting with the SV40 T-antigen (DuBridge et al., 1987) were obtained from Bertil Hille (University of Washington School of Medicine, Seattle, Washington). SH-SY5Y cells were obtained from Korean Cell Line Bank (Seoul National University, Seoul). Cells were cultured in DMEM supplemented with 10% FBS and 0.2% penicillin/streptomycin at 37°C with 5% CO₂, and plated in 35-mm culture dishes at 50–60% confluency a day before transfection. The cells were transiently transfected using Lipofectamine 2000 (Invitrogen) according to the manufacturer's protocol. For the expression of homomeric ASICs, cells were transfected with various cDNAs. For the expression of heteromeric ASICs, cells were transfected with different ASIC subunits in a 1:1 molar ratio. For TRPV1 expression, cells were transfected with cDNA encoding TRPV1 with or without GFP. When needed, 0.2 µg of cDNA encoding tetrameric red fluorescence protein (DsRed) was co-transfected with TRPV1 as a marker for successfully transfected cells. The next day, transfected cells were plated onto poly-L-lysine (0.1 mg/ml, Sigma) coated chips, and the fluorescent cells were studied 2 days after transfection. Rapamycin (LC Laboratories) was dissolved in DMSO (Sigma) to make 1 mM of stock solution. Arachidonic acid (Sigma) was dissolved in DMSO to make 10 mM of stock solution. Stock solutions were diluted in Ringer's solution before use.

Trigeminal ganglion neuron preparation

Sprague Dawley rats (5–6 weeks old, either sex) were decapitated under ketamine anesthesia (100 mg/kg, ip). Their trigeminal ganglia were dissected and treated with standard external

solution (in mM; 150 NaCl, 3 KCl, 2 CaCl₂, 1 MgCl₂, 10 Glucose, and 10 HEPES, a pH of 7.4 with Tris-base) containing 0.3% collagenase (type I) and 0.3% trypsin (type I) for 30–40 min at 37°C. Thereafter, the neurons were dissociated mechanically by trituration with fire-polished Pasteur pipettes in a culture dish. Isolated neurons were used for electrophysiological experiments 1–6 h after preparation.

Plasmids

Mouse cDNA clones of ASIC1a (GenBank accession no. NM_009597.1), ASIC2a (GenBank accession no. NM_001034013.2), ASIC2b (GenBank accession no. NM_007384.3), and ASIC3 (GenBank accession no. NM_183000.2) were generously donated by Michael J. Welsh (University of Iowa, Iowa city, Iowa). The cDNA encoding mouse ASIC1a was amplified by PCR and cloned into pEGFP-N1 (Clontech) using EcoRI and BamHI sites. The cDNA encoding mouse ASIC2a was amplified by PCR and cloned into pEGFP-N1 (Clontech) using EcoRI and BamHI sites, pEGFP-C1 (Clontech) using EcoRI and KpnI sites, mCherry-C1 (Clontech) using EcoRI and KpnI sites, or pcDNA3.1(+) (Invitrogen) using HindIII and KpnI sites. The cDNA encoding mouse ASIC2b was amplified by PCR and cloned into pEGFP-N1 (Clontech) or pEGFP-C1 (Clontech) using EcoRI and KpnI sites. The cDNA encoding mouse ASIC3 was amplified by PCR and cloned into pEGFP-N1 (Clontech) using EcoRI and KpnI sites. The plasmids Lyn-mCherry and mCherry-Cb5 were kind gifts from Takanari Inoue (Johns Hopkins University School of Medicine, Baltimore, Maryland).

Molecular cloning

For the generation of CF-PTEN chimera, the DNA fragment encoding codons 22–403 was amplified by the PCR from Ci-VSPTEN21 (Lacroix et al., 2011), a kind gift from Carlos A.

Villalba-Galea (Virginia Commonwealth University, Richmond, Virginia), using forward primer, 5'-aagcttcggacttagacttgacctata-3', reverse primer, 5'-ggatccgacttttgaatttgtaa-3', and fused to the C-terminus of CFP-FKBP. The following plasmids were generously given to us: Pseudojanin (PJ), PJ-Dead, PJ-Sac, INPP5E, LDR, PLC δ 1-PH-GFP (from Bertil Hille, University of Washington School of Medicine, Seattle, Washington); Osh1-PH-GFP (from Deok-Jin Jang, Kyungpook National University, Sangju, Korea); rat TRPV1 with internal ribosome entry site EGFP and rat TRPV1 without GFP (from Jae-Yong Park, Korea University, Seoul, Korea); and Btk-PH-GFP (from Carlos A. Villalba-Galea, Virginia Commonwealth University, Richmond, Virginia).

For the generation of ASIC2 chimeras, we used the overlap extension PCR strategy (Lee et al., 2010). The first PCRs were performed on two flanking regions using the primers containing the overlapping sequence of desired junction between ASIC2a and ASIC2b, and then the second PCR was performed using a mixture of the two PCR fragments from the first PCRs. The PCRs were carried out using the high-fidelity DNA polymerase, and products were subcloned into pEGFP-C1 (Clontech) or pcDNA3.1(+) (Invitrogen) for expression. Primers used for chimera construction are shown in Table 1.

For the single amino acid mutation or deletion mutation, we used a QuikChange Site-Directed Mutagenesis kit (Agilent). For the generation of single amino acid mutated Ch3, the following primers were used; sense, 5'-atcctactatttctcatatcaggctgttaccagggtggatgaagtg-3', antisense, 5'-cacttcatccaccttgtaacagcctgatatgagaaatagtaggat-3' for Ch3(H72A); sense, 5'-catgttaccagggtggctgaagtggggcccag-3', antisense, 5'-ctgggccaccacttcagccaccttgtaacatg-3' for Ch3(D77A); sense, 5'-ttaccaaggtggatgcagtggtggcccagag-3', antisense, 5'-ctctgggccaccactgcacccaccttggttaa-3' for Ch3(E78A). For the generation of N-terminal deleted ASIC2b, we used sense, 5'-gcgctgtgggtgctggccttc-3' and antisense, 5'-catgaattcgaagcttgagctcga-3'. For the generation of N- or C-terminal deleted ASIC3, we used a

QuikChange Site-Directed Mutagenesis kit (Agilent). The following primers were used for mutagenesis: sense, 5'-gggctgtgggccacagctgta-3', antisense, 5'-catgaattcgaagcttgagctcga-3' for ASIC3(Δ N); sense, 5'-acggtagccggggcccgggat-3', antisense, 5'-ccagaagtaccccaggactct-3' for ASIC3(Δ C). For the generation of N- and C-terminal deleted ASIC3, cDNA encoding 44–472 amino acids of ASIC3 was amplified by PCR and inserted into pEGFP-N1 (Clontech) using EcoRI and KpnI sites. All the chimeras and mutations were verified by DNA sequencing (Macrogen).

Plasma membrane fraction and Western blotting

Plasma membrane fraction was isolated using a Plasma Membrane Protein Extraction kit (abcam, ab65400) following the manufacturer's instructions. In brief, cells were lysed by homogenize buffer with a protease inhibitor cocktail. Homogenates were centrifuged at 700 x g for 10 min at 4°C. Pellets containing plasma membrane and organelle membranes were isolated from the cytosol fraction by high-speed centrifugation of the supernatants at 10,000 x g for 30 min at 4°C. To isolate the plasma membrane fraction further, pellets were re-suspended in Upper Phase buffer and were extracted in Lower Phase buffer. This was followed by centrifugation to pellet the plasma membrane fraction. Plasma membrane pellets were solubilized with 0.5% Triton X-100 in PBS for Western blotting.

For immunoblotting, protein samples were separated by SDS-PAGE using 8–10% gels. The separated proteins were transferred to polyvinylidene fluoride membranes, and blotted with anti-GFP (ThermoFisher Scientific; 4B10B2, 1:2,000), anti-calnexin (Enzo; ADI-SPA-860, 1:2,000), anti-E-Cadherin (NOVUS; NBP1-42793, 1:1,000), anti-GAPDH (Cell Signaling; #2118, 1:10,000), or anti-HA (Bethyl; A190-108A, 1:1,000) antibodies. After washing blots, proteins were visualized using an ECL detection system (Bio-Rad).

Co-Immunoprecipitation (Co-IP) and Western blotting

HEK293T cells were lysed with HEPES buffer (20 mM HEPES, pH 7.5, 150 mM NaCl, 1% NP-40, 0.1% SDS, and 1 mM NaF) containing a protease inhibitor cocktail. Whole-cell lysates were incubated on ice for 30 min and then cleared at 13,000 rpm for 30 min at 4°C. For Co-IP, the supernatants were incubated overnight at 4°C with 1 µg/ml anti-FLAG (Sigma; M2) antibody, followed by incubation with protein A/G PLUS-agarose beads for 1 h. For immunoblotting, protein samples were separated by SDS-PAGE using 10% gels. The separated proteins were transferred to polyvinylidene fluoride membranes. The blots were incubated overnight at 4°C with anti-HA antibody (Roche Applied Science; 3F10, 1:1,000) or anti-FLAG antibody (Sigma; F1804, 1:1,000). After washing blots, they were incubated with horseradish peroxidase-conjugated secondary antibody for 1 h at room temperature and visualized using an ECL detection system (Bio-Rad).

BiFC assay

For BiFC assay for ASIC2a and ASIC2b, ASIC2a and ASIC2b were cloned into bimolecular fluorescence complement (pBiFC)-VN173 and pBiFC-VC155 vectors. HEK293T cells were co-transfected with cloned BiFC vectors in all possible pairwise combinations. After 24 h, these cells were fixed with 4% paraformaldehyde for 20 min at room temperature and mounted with Dako Fluorescence Mounting Medium. Venus fluorescence signals were observed with an Olympus Fluoview FV1000 confocal microscope (Olympus) at room temperature. For BiFC assay for ASIC2a and ASIC3, ASIC2a and ASIC3 were cloned into bimolecular fluorescence complement (pBiFC)-VC155 and pBiFC-VN173 vectors, respectively, using EcoRI and KpnI sites. HEK293T cells were co-transfected with cloned BiFC vectors, and Venus fluorescence signals were observed by a Carl Zeiss LSM 700 confocal microscope (Carl Zeiss) at room temperature.

Duolink proximity ligation assay

Interaction was detected by a Duolink Proximity Ligation Assay kit (Olink Bioscience, Uppsala, Sweden: PLA Probe anti-Mouse MINUS; PLA Probe anti-Rabbit PLUS; Detection Kit 563). The PLA Probe anti-Mouse MINUS binds to the HA antibody (Cell Signaling; #2367), whereas the PLA Probe anti-Rabbit PLUS binds to the FLAG antibody (Cell Signaling; #2368). After preincubation with a blocking agent for 1 h, the fixed HEK293T cells were incubated overnight with the primary antibodies to anti-HA (Cell Signaling, 1:100) and anti-FLAG (Cell Signaling, 1:100). Duolink PLA probes detecting mouse or rabbit antibodies were diluted in the blocking agent to a concentration of 1:5 and applied to the slides, followed by incubation for 1 h in a pre-heated humidity chamber at 37°C. Unbound PLA probes were removed by washing. The slides were then incubated in a ligation solution consisting of Duolink Ligation stock (1:5) and Duolink Ligase (1:40) for 30 min at 37°C. Detection of the amplified probe was performed with the Duolink Detection kit. Duolink Detection stock was diluted at 1:5 and applied for 100 min at 37°C. Final washing steps were carried out in saline sodium citrate buffer. Duolink PLA signals were observed with an Olympus Fluoview FV1000 confocal microscope (Olympus) at room temperature.

Patch clamp recording

Patch clamp recording using the whole-cell configuration was performed at room temperature (22–25°C). Electrodes pulled from glass micropipette capillaries (Sutter Instrument) had resistances of 2–3 MΩ, and series resistance errors were compensated by > 60%. Fast and slow capacitances were compensated before the application of test-pulse. We used a HEKA EPC-10 amplifier with pulse software (HEKA Elektronik) for recordings. The external Ringer's solution used for recording ASIC currents contained 160 mM NaCl,

5 mM KCl, 1 mM MgCl₂, 2 mM CaCl₂, and 10 mM HEPES, adjusted to pH 7.4 with tetramethylammonium hydroxide. For acidic solutions below pH 6.0, HEPES was replaced with MES. The pipette solution contained 140 mM KCl, 5 mM MgCl₂, 10 mM HEPES, 0.1 mM 1,2-bis(2-aminophenoxy)ethane-*N,N,N',N'*-tetraacetic acid (BAPTA), 3 mM Na₂ATP, and 0.1 mM Na₃GTP, adjusted to pH 7.4 with KOH. ASIC currents were recorded by holding the cell at -70 mV. The pH pulses were applied every 2 min for a complete recovery from desensitization. The external Ringer's solution used for recording TRPV1 currents contained 150 mM NaCl, 5 mM KCl, 1 mM MgCl₂, 2 mM EGTA, 10 mM Glucose, and 10 mM HEPES, adjusted to pH 7.4 with NaOH. The pipette solution contained 135 mM CsCl, 5 mM MgCl₂, 10 mM HEPES, 5 mM EGTA, 5 mM Na₂ATP, and 10 mM Glucose, adjusted to pH 7.4 with CsOH. TRPV1 currents were recorded by holding the cell at -80 mV. The following reagents were obtained: BAPTA, Na₂ATP, Na₃GTP, EGTA, CsOH and tetramethylammonium hydroxide (Sigma), HEPES (Calbiochem), MES (Alfa Aesar), and other chemicals (Merck).

For measuring the currents from the trigeminal ganglion neurons, we used an Axopatch 200B amplifier (Molecular Devices). The neurons were voltage-clamped at a holding potential of -60 mV. Patch pipettes were made from borosilicate capillary glass (Narishige) by use of a pipette puller (Sutter Instrument). The resistance of the recording pipettes filled with the internal solution (in mM; 140 CsF, 10 CsCl, 2 EGTA, 2 ATP-Na₂, and 10 HEPES with a pH adjusted to 7.2 with Tris-base) was 0.8–1.5 MΩ. The membrane currents were filtered at 1 kHz, digitized at 4 kHz, and stored on a computer equipped with pCLAMP 10.3 (Molecular Devices). During recordings, 10-mV hyperpolarizing step pulses (30 ms in duration) were periodically applied to monitor the access resistance, and the recordings were discontinued if the access resistance changed by more than 15%. All the extracellular solutions were applied using the “Y-tube system” for rapid solution exchange

(Murase et al., 1989).

For the acquisition and analysis of data, we used Pulse/Pulse Fit software in combination with an EPC-10 patch clamp amplifier (HEKA Elektronik) and Igor Pro (WaveMetrics, Inc.). The pH-dependency curve was fitted with a Hill equation. For measuring the desensitization time constant, a single or double exponential function was used. When a double exponential function was used, relative areas of time constants were calculated by integrating the functions, $y_1=A_1\exp\{-(x-x_0)/\tau_1\}$ and $y_2=A_2\exp\{-(x-x_0)/\tau_2\}$ (A , coefficient; x , time; τ , tau). Further data processing was performed with Excel 2012 (Microsoft) and Igor Pro (WaveMetrics, Inc.).

Confocal imaging

The living cells were imaged 2 days after transfection on poly-L-lysine coated chips with a Carl Zeiss LSM 700 confocal microscope (Carl Zeiss) at room temperature. The external Ringer's solution contained 160 mM NaCl, 2.5 mM KCl, 2 mM CaCl₂, 1 mM MgCl₂, 10 mM HEPES, and 8 mM Glucose, adjusted to pH 7.4 with NaOH. Images were scanned with a 40 X (water) objective lens at 1024 X 1024 pixels using a digital zoom. For time courses, cell images were scanned at 512 X 512 pixels using a digital zoom. During time course experiments, images were taken every 5 s. All confocal images were transferred from LSM5 to JPEG or TIFF format, and raw data from time courses was processed with Microsoft Office Excel 2012 (Microsoft) and Igor Pro (WaveMetrics, Inc.).

Quantitative analysis of fluorescent images

Quantitative analysis of confocal images was carried out using ZEN2011 software (Carl Zeiss) and ImageJ. Pearson's correlation coefficients of multiple sets of images were quantified by the 'Colocalization' tool in the ImageJ. The values are between 0 and 1; a

value of 1 means complete co-localization, while a value of 0 means no co-localization. Overlap coefficients of multiple sets of images were quantified by the following equation: $\text{Overlap coefficient} = \frac{\sum(\text{Ch1}_i)(\text{Ch2}_i)}{\sqrt{(\sum(\text{Ch1}_i)^2)(\sum(\text{Ch2}_i)^2)}}$, where Ch1_i and Ch2_i signify the intensities of Channel 1 (GFP) and Channel 2 (mCherry), respectively. The values are between 0 and 1; a value of 1 means complete co-localization, while a value of 0 means no co-localization. Cytosolic fluorescence intensity was measured using the ‘Measure’ tool for the region of interest. Line scanning of fluorescent images was processed by using the ‘Profile’ tool in ZEN2011 software (Carl Zeiss).

To determine the percentages of cells showing each construct in specific subcellular localizations, we manually counted cells co-transfected with a specific organelle probe. For each condition, we counted 250 cells from five independent experiments. The raw data were processed with Excel 2012 (Microsoft) and Igor Pro (WaveMetrics, Inc.).

Statistical analysis

All quantitative data are represented as mean \pm SEM. Comparisons between two groups were analyzed using Student’s two-tailed unpaired *t*-test. The significance of data among more than two groups was assessed by one-way ANOVA followed by Bonferroni post-hoc test. Comparisons among more than two groups with two independent variables were analyzed using two-way ANOVA followed by Bonferroni post-hoc test. Differences were considered significant at the * $P < 0.05$, ** $P < 0.01$, and *** $P < 0.001$ levels, as appropriate.

Table 1. Primers and templates used for chimera construction.

| | Fragment 1 | | Fragment 2 | | Template | |
|---------------|--------------------------------------|--------------------------------------|-------------------------------------|----------------------------|------------|------------|
| | FP (5'-3') | RP (5'-3') | FP (5'-3') | RP (5'-3') | Fragment 1 | Fragment 2 |
| Ch1 | tcgaattctatggacctcaaggagagc | ggccagcaccacagcgcacccggatggtcagcgg | ccgctgacctccggcgtgcgctgtgggtgctggcc | gcggtacctcagcaggcaatctcctc | ASIC2a | ASIC2b |
| Ch2 | tcgaattctatggacctcaaggagagc | tcgctgtgtgacgggaatgagaaatagtaggatac | gtatcctactatftcattcccgtcacacacgcga | gcggtacctcagcaggcaatctcctc | ASIC2a | ASIC2b |
| Ch3 | tcgaattctatggacctcaaggagagc | ggggtgtgtgacacaggtcacagctgggaagac | gtcttccagctgtgacctgtgcaacaacaacccc | gcggtacctcagcaggcaatctcctc | ASIC2a | ASIC2b |
| 2a-P | tcgaattctatggacctcaaggagagc | gagggtcacagctgggaacggcagctggcggctcca | tggagccgccagctgccgttccagctgtgacctc | gcggtacctcagcaggcaatctcctc | Ch2 | ASIC2a |
| 2a-T | tcgaattctatggacctcaaggagagc | ggtaacatgctgatatgagagccagtagagcagcgg | cgctgctctactggctctcatatcagcatgttacc | gcggtacctcagcaggcaatctcctc | Ch1 | ASIC2a |
| 2a-N | tcgaattctatgagccggagcggcggagcccggctg | ggccactgccaaagcaccgccgctgaaagagcc | ggctcttccagcggcgggtgcttgggcagtggcc | gcggtacctcagcaggcaatctcctc | ASIC2b | ASIC2a |
| 2a-NTP | tcgaattctatgagccggagcggcggagcccggctg | gccattgaggtgacaggggtgacagcggggaacgg | ccgttccccgctgtcacctctgcaacctcaatggc | gcggtacctcagcaggcaatctcctc | ASIC2b | ASIC2a |
| 2b-P | tcgaattctatgagccggagcggcggagcccggctg | ggtaacatgctgatatgagagccagtagagcagcgg | cgctgctctactggctctcatatcagcatgttacc | gcggtacctcagcaggcaatctcctc | ASIC2b | Ch3 |
| 2b-T | tcgaattctatgagccggagcggcggagcccggctg | cgtgtgtgacgggaaactgaaatagtaggatactct | agagtatcctactatftcagtttcccgtcacacag | gcggtacctcagcaggcaatctcctc | 2b-TP | ASIC2b |
| 2b-TP | tcgaattctatgagccggagcggcggagcccggctg | ggccactgccaaagcaccgccgctgaaagagcc | ggctcttccagcggcgggtgcttgggcagtggcc | gcggtacctcagcaggcaatctcctc | ASIC2b | Ch3 |

III. RESULTS

3. 1. Regulation of acid-sensing ion channels (ASICs) by membrane phospholipids

The Activities of TRPV1 Channels are Dependent on Membrane Phosphoinositides

To assess the requirement of PM phosphoinositides for the activities of proton-sensitive ion channels, we employed the chemically-inducible dimerization (CID) system. Rapamycin-induced dimerization of FKBP (FK506 binding protein) and FRB (FKBP-rapamycin binding domain of mTOR) can be used to rapidly and irreversibly recruit the enzyme of interest to the target region inside the cell (DeRose et al., 2013). We applied the recently described fusion protein mRFP-FKBP-Pseudojanin (PJ), which contains both inositol polyphosphate-5-phosphatase E (INPP5E) and sac1 phosphatase, and thus, the recruitment of which to the PM leads to simultaneous depletion of PI(4,5)P₂ and PI(4)P (Hammond et al., 2012). First, we tested the activity of the PJ construct by using the pleckstrin homology (PH) domain of PLCδ1 (PLCδ1-PH-GFP) and oxysterol-binding protein homologues (Osh1-PH-GFP) as indicators for PM PI(4,5)P₂ and PI(4)P, respectively. PJ was localized to the cytoplasm when expressed in tsA201 cells. Recruiting PJ to the PM anchor LDR (N-terminal myristoylation and palmitoylation modification sequence of a Lyn kinase coupled to FRB domain) by the addition of 1 μM of rapamycin for 60 s resulted in the release of both Osh1-PH and PLCδ-PH to the cytoplasm in each separate confocal experiment (Fig. 2A, *bottom*). The cytosolic fluorescence intensity of PJ rapidly declined upon rapamycin addition, while that of Osh1-PH or PLCδ-PH increased (Fig. 2B, *bottom*). We also confirmed that the recruitment of PJ-Sac (INPP5E domain is inactivated by mutation to specifically dephosphorylate PI(4)P (Hammond et al., 2012)) resulted in the release of Osh1-PH from the PM and increase in the cytosolic fluorescence intensity of Osh1-PH (Fig. 2, A and B, *middle*). Recruitment of INPP5E to the PM decreased

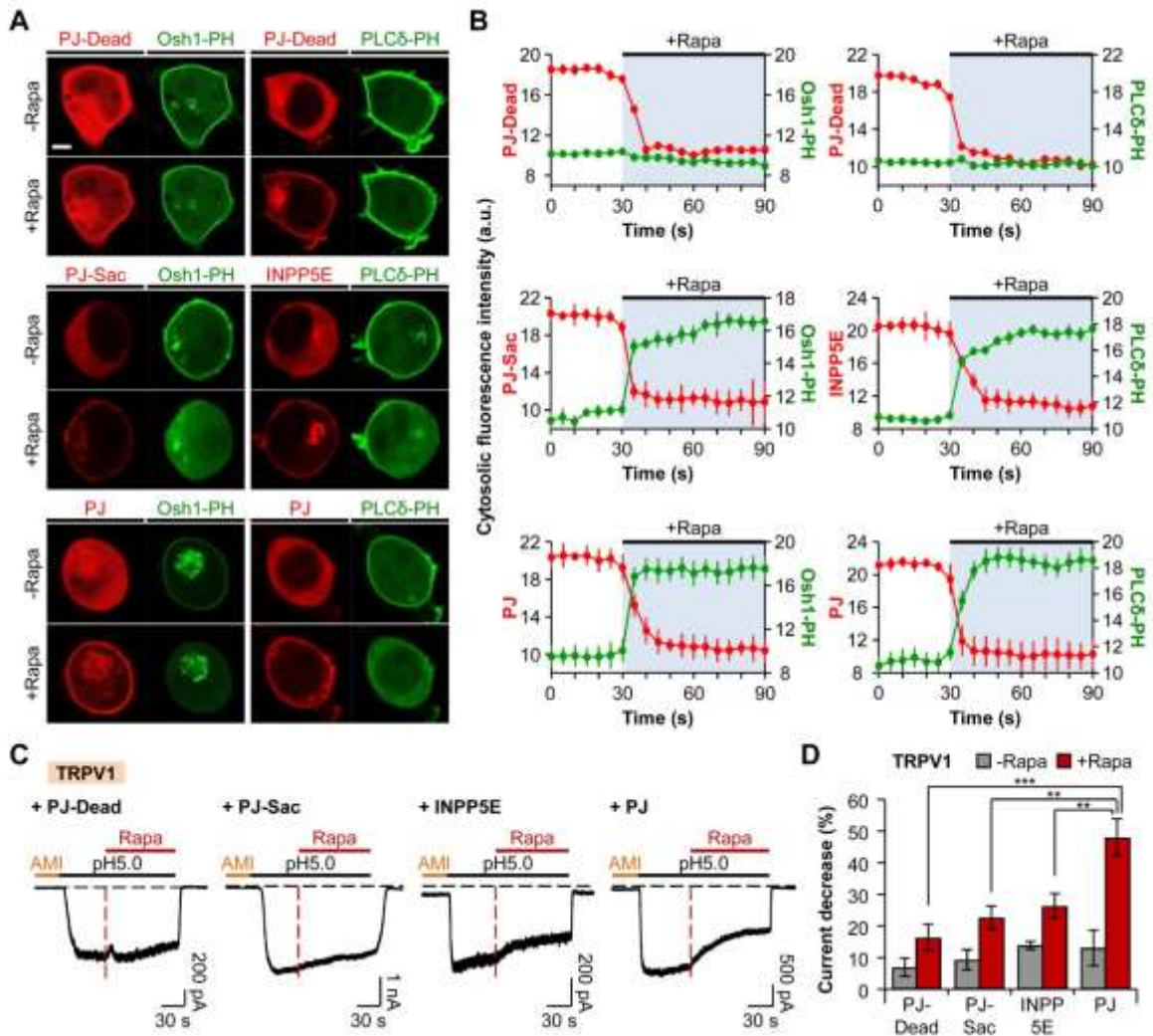


Fig. 2. The activity of TRPV1 is dependent on phosphoinositides. (A) Confocal images of cells expressing PJ-Dead (*top*), PJ-Sac (*middle*), INPP5E (*middle*), or PJ (*bottom*) with LDR and respective biosensors for PI(4)P (Osh1-PH-GFP) or PI(4,5)P₂ (PLCδ1-PH-GFP). Images before and after the addition of rapamycin (1 μM) for 60 s (Scale bar, 5 μm). (B) Cytosolic fluorescence intensities of RFP (*red*) and GFP (*green*) for the cells in (A). The values of the Y-axis use an arbitrary unit. Cells expressing PJ-Dead (*top*), PJ-Sac (*middle*), INPP5E (*middle*), or PJ (*bottom*) (n=3, respectively). (C) TRPV1 currents triggered by prolonged extracellular pH drop to 5.0 for 150 s. Rapamycin (1 μM) was co-applied for 90 s during the acid stimuli. Amiloride (300 μM) was pretreated for 30 s before the pH pulse. Black dashed line indicates the zero current level. Red dashed line indicates the point of rapamycin application. (D) Percentage of current decrease in (C) during 45 s of acidification before (*grey*) and after (*red*) rapamycin addition (n=12 for PJ-Dead; n=14 for PJ-Sac; n=12 for INPP5E; n=10 for PJ). ** *P* < 0.01 and *** *P* < 0.001, with two-way

ANOVA followed by Bonferroni post-hoc test and one-way ANOVA followed by Bonferroni post-hoc test. Data are mean \pm SEM. Abbreviations: Rapa, Rapamycin; AMI, Amiloride.

the PI(4,5)P₂ level, which was confirmed by the translocation of PI(4,5)P₂ probe to the cytoplasm with the increase in the cytosolic intensity of PLC δ -PH (Fig. 2, A and B, *middle*). However, recruiting the cytosolic PJ-Dead, a chimera with inactivated sac1 and INPP5E (Hammond et al., 2012), to the PM had no effects on the localization of Osh1-PH or PLC δ -PH (Fig. 2A, *top*). Consequently, the cytosolic fluorescence intensities of Osh1-PH and PLC δ -PH remained unchanged following the addition of rapamycin (Fig. 2B, *top*).

We applied this system on acid-evoked TRPV1 currents to test the regulatory aspects of phosphoinositides reported by previous studies (Chuang et al., 2001; Liu et al., 2005; Stein et al., 2006; Lukacs et al., 2007; Klein et al., 2008; Cao et al., 2013; Lukacs et al., 2013a, Lukacs et al., 2013b, Senning et al., 2014). Since tsA201 cells have been reported to have endogenous ASIC currents (Donier et al., 2008), the cells transiently expressing TRPV1 and respective PJ system constructs were preincubated by amiloride, a general inhibitor of ASICs, before the acid stimulation to selectively measure the TRPV1 currents. After the preincubation of cells with extracellular solution containing 300 μ M of amiloride for 30 s, the cells were stimulated by pH 5.0 solution for 60 s; then, 1 μ M of rapamycin was co-applied with pH 5.0 solution for 90 s. Since we observed variable desensitization among the cells during prolonged acidification before the addition of rapamycin, we first compared how much the currents decrease during acidification in the absence of rapamycin among four groups (PJ-Dead, PJ-Sac, INPP5E, and PJ). TRPV1 currents usually reached the maximum current amplitude within 15 s after the currents were activated; thus, we compared the current decrease during 45 s of acidification after reaching the maximum current amplitude. The currents of TRPV1 in cells expressing PJ-

Dead or PJ-Sac were desensitized by $7 \pm 3\%$ (n=12) or $9 \pm 3\%$ (n=14), respectively (Fig. 2, C and D). When the cells were transfected with INPP5E or PJ, the currents were decreased by $14 \pm 1\%$ (n=12) or $13 \pm 6\%$ (n=10), respectively (Fig. 2, C and D). Desensitization rates of currents showed no statistically significant differences among the four groups before the application of rapamycin. The currents in cells expressing PJ-Dead, PJ-Sac, and INPP5E were decreased by $16 \pm 4\%$ (n=12), $23 \pm 4\%$ (n=14), and $26 \pm 4\%$ (n=12), respectively, during 45 s of acidification right after rapamycin addition (Fig. 2, C and D). However, translocation of PJ to the PM by the application of rapamycin decreased TRPV1 currents by $48 \pm 6\%$ (n=10) during 45 s of acidification (Fig. 2, C and D). These results suggest that the activities of TRPV1 channels are diminished by simultaneous breakdown of both PM PI(4)P and PI(4,5)P₂, as previously reported (Hammond et al., 2012; Lukacs et al., 2013b).

The Activities of ASICs are Independent from PI(4)P and PI(4,5)P₂

Next, we examined whether ASICs also require phosphoinositides for their function as TRPV1 channels. ENaC belongs to the same superfamily of ion channels as ASICs and is known to be regulated by PM PI(4,5)P₂ and PI(3,4,5)P₃ (Yue et al., 2002; Pochynyuk et al., 2006; Pochynyuk et al., 2007). That means, ASICs could have sensitivities toward phosphoinositides. To test this, we employed the PJ system and observed the activities of homomeric and heteromeric ASICs. The cells transiently expressing each GFP-tagged ASIC subunit (ASIC1a, or ASIC2a, or ASIC3) and respective PJ systems were repetitively activated by extracellular acidification from pH 7.4 to pH 6.0 (ASIC1a or ASIC3) or to pH 4.5 (ASIC2a) for 10 s with 2 min time intervals. As previously reported, GFP fusion to the C-terminus of ASIC subunit did not affect the electrophysiological properties of wild-type ASIC currents expressed in tsA201 cells (Chai et al., 2007). For recruiting the interested enzyme to the PM, 1 μ M of rapamycin was perfused for 60 s before the second pH pulse.

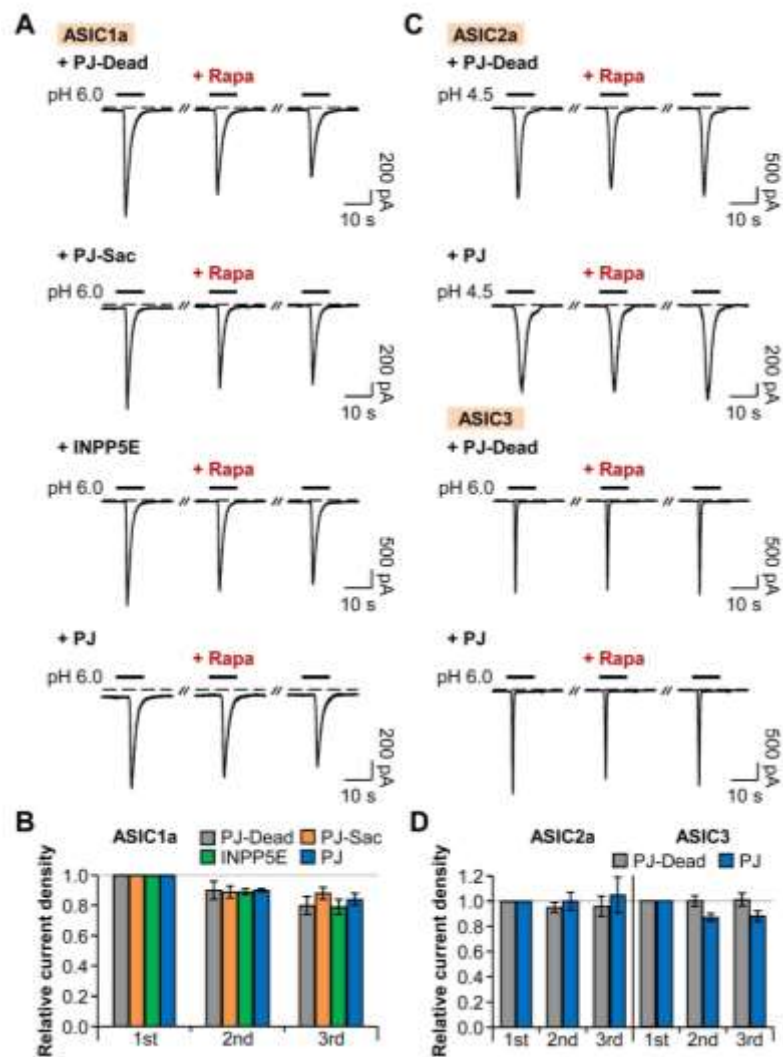


Fig. 3. Homomeric ASIC currents are insensitive to PI(4)P and PI(4,5)P₂. (A) ASIC1a currents evoked by repetitive rapid extracellular pH change from 7.4 to 6.0 for 10 s with time intervals of 120 s in cells expressing LDR and either PJ-Dead, PJ-Sac, INPP5E, or PJ. Rapamycin (1 μ M) was bath-applied for 60 s, and then normal extracellular solution was perfused for 10 s right before the second pulse to minimize possible side effects of rapamycin. Dashed line indicates the zero current level. (B) Relative current density measured for the cells in (A) (n=6, respectively). Current density of each pulse was divided by that of the first pulse. There is no statistical significance with two-way ANOVA followed by Bonferroni post-hoc test. (C) ASIC2a or ASIC3 current traces evoked by pH drop to 4.5 or 6.0 for 10 s. (D) Relative current density measured for the cells in (C) (n=6, respectively). There is no statistical significance with two-way ANOVA followed by Bonferroni post-hoc test. Data are mean \pm SEM. Abbreviations: Rapa, Rapamycin.

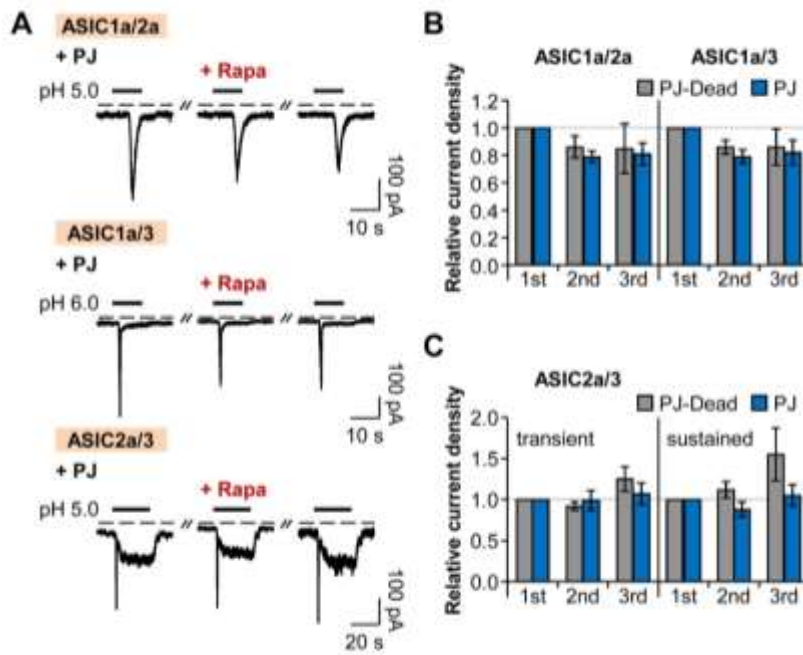


Fig. 4. Heteromeric ASIC currents are insensitive to PI(4)P and PI(4,5)P₂. (A) Current traces from ASIC1a/2a, ASIC1a/3, and ASIC2a/3 heteromeric channels evoked by extracellular acidification in cells expressing LDR and PJ. Rapamycin (1 μ M) was bath-applied for 60 s, and then normal extracellular solution was perfused for 10 s right before the second pulse to minimize possible side effects of rapamycin. Dashed line indicates the zero current level. (B) Relative current density measured for the currents of ASIC1a/2a and ASIC1a/3 in (A) (n=3, respectively). Current density of each pulse was divided by that of the first pulse. There is no statistical significance with two-way ANOVA followed by Bonferroni post-hoc test. (C) Relative current density measured for the transient and sustained currents of ASIC2a/3 in (A) (n=3 for PJ-Dead; n=5 for PJ). There is no statistical significance with two-way ANOVA followed by Bonferroni post-hoc test. Data are mean \pm SEM. Abbreviations: Rapa, Rapamycin.

To minimize possible side effects of rapamycin, normal extracellular solution was perfused right after the application of rapamycin for 10 s just before the second pH pulse. First, we confirmed that, as a control, the recruitment of PJ-Dead to the PM anchor does not affect the repetitive proton-activated ASIC1a currents except for tachyphylaxis (reduction in current amplitude with repeated stimulation), a unique property of homomeric ASIC1a

channels (Chen et al., 2007) (Fig. 3, A and B). Then, we observed that translocation of PJ-Sac or INPP5E to the PM to specifically deplete PM PI(4)P or PI(4,5)P₂, respectively, had no effects on the relative current density of homomeric ASIC1a channels (Fig. 3, A and B). Simultaneous depletion of both PI(4)P and PI(4,5)P₂ by PJ also had no significant effect on the successively triggered ASIC1a currents (Fig. 3, A and B). We found that neither ASIC2a nor ASIC3 homomeric channels were affected by the recruitment of PJ to the PM (Fig. 3, C and D), allowing us to conclude that unlike proton-sensitive TRPV1 channels, the activities of homomeric ASICs are independent of PM PI(4)P and PI(4,5)P₂.

We also tested whether heteromeric ASICs have dependence on phosphoinositides for their function, since most ASICs exist as heteromeric channels in physiological conditions (Askwith et al., 2004; Hattori et al., 2009; Sherwood et al., 2011). The current traces from heteromeric channels of ASIC1a/2a, ASIC1a/3, and ASIC2a/3 were similar to those of a previous study (Hesselager et al., 2004). Recruitment of PJ to the PM had no significant effects on either ASIC1a/2a or ASIC1a/3 heteromeric channels (Fig. 4, A and B), and transient and sustained currents of ASIC2a/3 heteromeric channels were not significantly affected by the application of rapamycin (Fig. 4, A and C). In conclusion, neither homomeric ASICs nor heteromeric ASICs require phosphoinositides for their activities.

Neither ASICs nor TRPV1 Activities are Affected by Depletion of PI(3,4,5)P₃

Even though the PJ system is a powerful tool for probing the role of phosphoinositides for the function of ion channels, it has a limitation in terms of investigating the specific effect of PI(3,4,5)P₃ on the channels. Therefore, we generated a novel chimeric protein to further investigate the role of PI(3,4,5)P₃ in the activities of proton-sensitive ion channels. One of the tumor suppressor genes, PTEN (phosphatase and tensin homologue deleted on chromosome 10)

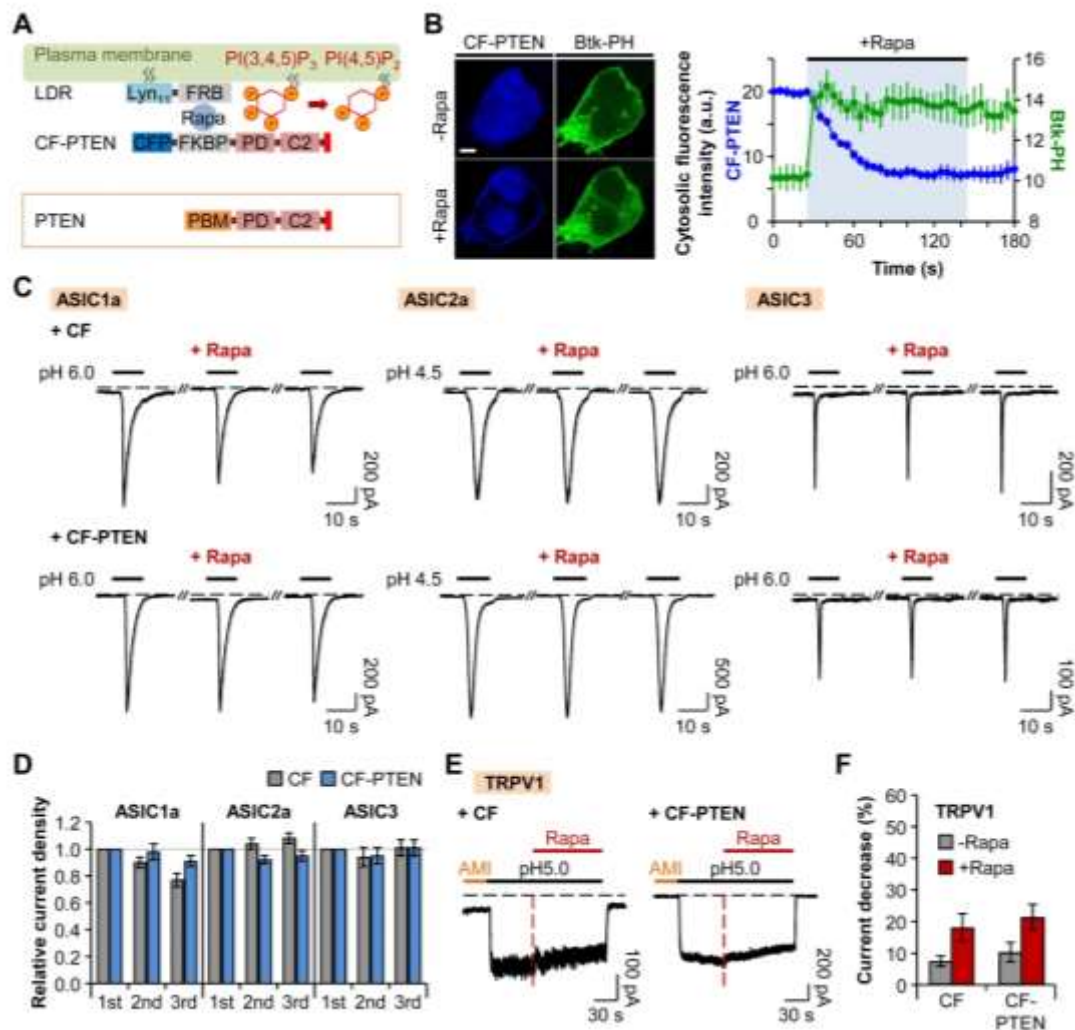


Fig. 5. Neither ASICs nor TRPV1 activities are affected by depletion of PI(3,4,5)P₃. **(A)** CF-PTEN is rapidly recruited to the plasma membrane anchor LDR by dimerization of FRB and FKBP upon addition of rapamycin, and the PD domain of CF-PTEN specifically dephosphorylates PI(3,4,5)P₃ to PI(4,5)P₂. Red bar in the C-terminal tail of PTEN indicates PDZ-binding domain. **(B)** Confocal images of cells expressing LDR, CF-PTEN, and Btk-PH-GFP before and after the addition of rapamycin (1 μM) for 120 s (Scale bar, 5 μm) and cytosolic fluorescence intensities of CFP (*blue*) and GFP (*green*) (n=3). The values of the Y-axis use an arbitrary unit. **(C)** ASIC current traces triggered by extracellular acidification in cells expressing LDR and CF (lacking PTEN) or CF-PTEN. Rapamycin (1 μM) was bath-applied for 60 s, and then normal extracellular solution was perfused for 10 s right before the second pulse to minimize possible side effects of rapamycin. Dashed line indicates the zero current level. **(D)** Relative current density measured for the cells in **(C)** (CF (n=8), CF-PTEN (n=7) for ASIC1a; CF (n=8), CF-PTEN (n=8) for ASIC2a; and CF (n=10), CF-

PTEN (n=10) for ASIC3). Current density of each pulse was divided by that of the first pulse. There is no statistical significance with two-way ANOVA followed by Bonferroni post-hoc test. **(E)** TRPV1 currents in response to pH drop in the cells expressing LDR and CF or CF-PTEN. Rapamycin (1 μ M) was co-applied for 90 s during the acid stimuli. Amiloride (300 μ M) was pretreated for 30 s before the pH pulse. Black dashed line indicates the zero current level. Red dashed line indicates the point of rapamycin application. **(F)** Percentage of current decrease in **(E)** during 45 s of acidification before (*grey*) and after (*red*) rapamycin addition (n=9 for CF; n=10 for CF-PTEN). Data are mean \pm SEM. Abbreviations: CF, CFP-FKBP; CF-PTEN, CFP-FKBP-PTEN; PD, Phosphatase domain; PBM, Phosphoinositide-binding motif; Rapa, Rapamycin; AMI, Amiloride.

codes a cytosolic 3-phosphatase that degrades PI(3,4,5)P₃ by removing the phosphate at the D3 position of the inositol ring (Das et al., 2003; Vazquez et al., 2006; Rahdar et al., 2009). PTEN has a substrate specificity toward PI(3,4,5)P₃ (Iwasaki et al., 2008) and is composed of N-terminal phosphoinositide-binding motif (PBM) that contributes to the recruitment of PTEN to the PM, phosphatase domain (PD), C2 domain (C2) that binds to PM phosphatidylserine (PS), and C-terminal tail PDZ-binding domain (Das et al., 2003; Vazquez et al., 2006; Rahdar et al., 2009; Lacroix et al., 2011) (Fig. 5A). We inserted the region from PD to C-terminal tail of PTEN to the C-terminus of CFP-FKBP (Fig. 5A). CFP-FKBP-PTEN (CF-PTEN) was translocated to the PM anchor LDR upon addition of 1 μ M rapamycin; in turn, PI(3,4,5)P₃ was depleted as shown by the specific PI(3,4,5)P₃ probe, PH domain of Bruton tyrosine kinase (Btk) (Btk-PH-GFP) (Fig. 5B). The cytosolic fluorescence intensity of Btk-PH rapidly increased while that of CF-PTEN gradually declined by rapamycin addition (Fig. 5B), indicating the successful development of a novel translocatable 3-phosphatase tool.

Using this tool, we tested the sensitivities of homomeric ASICs and TRPV1 channels to PM PI(3,4,5)P₃. Although the membrane PI(3,4,5)P₃ was depleted following the addition of rapamycin, the repetitively activated currents of homomeric ASIC1a, ASIC2a, and ASIC3 channels remained unchanged (Fig. 5, C and D). These results suggest that ASICs are insensitive to

the depletion of PI(3,4,5)P₃ in intact cells. Next, we investigated whether the depletion of membrane PI(3,4,5)P₃ in an intact cell affects the proton-activated TRPV1 currents. The current decrease during 45 s of acidification right before the addition of rapamycin was not significantly different between two groups (CF: 8 ± 2% (n=9) and CF-PTEN: 10 ± 3% (n=10)) (Fig. 5, E and F). In the presence of rapamycin, TRPV1 currents were decreased by 18 ± 4% (n=9) or 21 ± 4% (n=10) in cells expressing CF or CF-PTEN, respectively, during 45 s of acidification (Fig. 5, E and F). Difference in current decrease ratio between the two groups was not statistically significant. These results indicate that the depletion of PI(3,4,5)P₃ has no effects on the activities of TRPV1 channels, although TRPV1 currents are inhibited by simultaneous depletion of both PI(4)P and PI(4,5)P₂. This result is supported by the previous reports suggesting that PI(3,4,5)P₃ is not an endogenous regulatory factor of TRPV1 currents (Klein et al., 2008; Cao et al., 2013). In inside-out patches, the application of pH domain of the general receptor of phosphoinositides 1 (GRP1) which selectively binds to PI(3,4,5)P₃ did not inhibit the TRPV1 currents, while the application of PLCδ1-PH produced the decrease of the currents (Klein et al., 2008). Moreover, in a reconstituted liposome, PI(3,4,5)P₃ did not have any effect on the TRPV1 currents, unlike other phosphoinositides (Cao et al., 2013). Taken together, neither ASICs nor TRPV1 activities are altered by depletion of PI(3,4,5)P₃.

ASICs and TRPV1 Channels are Differentially Regulated by AA

In the data above, we investigated the regulatory effects of PM phosphoinositides on proton-sensitive ion channels, ASICs and TRPV1, and discovered a difference in their sensitivities toward phosphoinositides. We next asked how these proton-sensitive ion channels are regulated by arachidonic acid (AA), which is liberated from the membrane phospholipids by phospholipase A₂ (PLA₂) activity (Ghosh et al., 2006; Burke et al., 2009). A pro-inflammatory mediator, AA is a polyunsaturated fatty acid acting as a lipid second

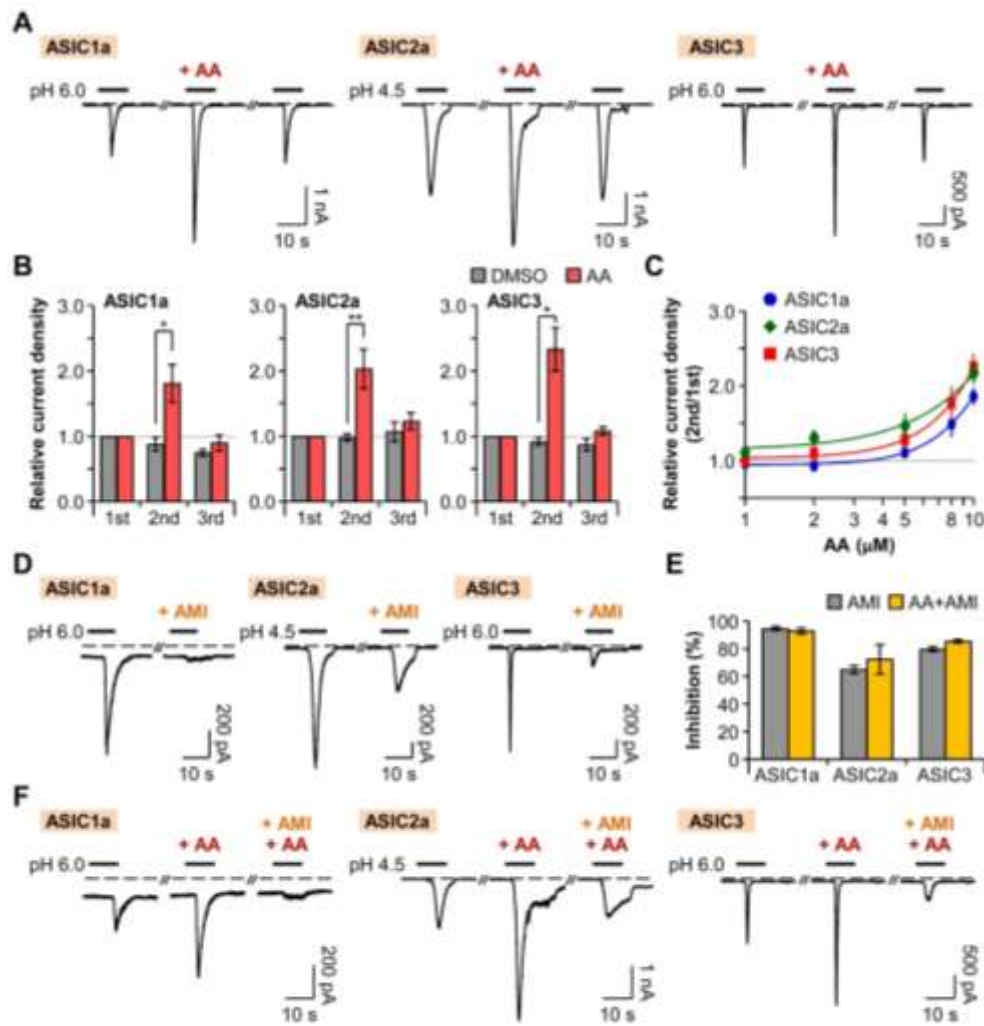


Fig. 6. Potentiation of ASICs by AA. (A) ASIC current traces activated by rapid extracellular pH changes. AA (10 μ M) was bath-applied for 20 s before the second pulse. Dashed line indicates the zero current level. (B) Relative current density was measured for the cells expressing ASIC1a (n=5 for DMSO; n=6 for AA), ASIC2a (n=5 for DMSO; n=10 for AA), and ASIC3 (n=5 for DMSO; n=12 for AA). Current density of each pulse was divided by that of the first pulse. * $P < 0.05$ and ** $P < 0.01$, with two-way ANOVA followed by Bonferroni post-hoc test and student's t -test. (C) Dose-dependent relative current density of ASIC1a (blue) (n=5–20), ASIC2a (green) (n=5–25), and ASIC3 (red) (n=5–23). (D) ASIC1a and ASIC3 currents were inhibited by preincubation of cells with pH 7.4 solution containing amiloride (300 μ M) for 20 s before the second pulse. In the case of ASIC2a, 600 μ M of amiloride was applied for 30 s before and during the second pulse. (E) Percentage of inhibition by amiloride in the absence (grey) or the presence (yellow) of AA (AMI (n=7) and AA+AMI (n=4) for ASIC1a; AMI (n=4) and AA+AMI (n=3) for ASIC2a; and AMI (n=6) and AA+AMI (n=6) for ASIC3). (F) The potentiating effect of AA (10 μ M) on ASIC currents was inhibited by amiloride. Data are mean \pm SEM. Abbreviations: AA, Arachidonic acid; AMI, Amiloride.

messenger (Meves, 2008; Kweon and Suh, 2013). Several ion channels, including ASICs (Allen and Attwell, 2002; Smith et al., 2007a) and TRP channels (Chyb et al., 1999; Cao et al., 2013), are known to be regulated by AA either by a direct or indirect action (Meves, 2008). Here, we investigated whether AA also differentially regulates the activities of ASICs and TRPV1 channels as do phosphoinositides. When the extracellular solution containing 10 μ M of AA was perfused for 20 s right before the second pH pulse, the peak current density of the second pulse in cells transiently expressing homomeric ASIC1a channels was increased by $81 \pm 29\%$ (n=6) compared to that of the first pulse (Fig. 6, A and B). On the other hand, the peak current density of the second pulse was slightly decreased in the control group (Fig. 6B). We observed that the potentiating effect of AA is reversible, and the peak current density was recovered to the initial level after washout of AA (Fig. 6, A and B). In the cells expressing ASIC2a homomeric channels, the peak current density of the second pulse was reversibly increased by $103 \pm 30\%$ (n=10) compared to that of the first pulse, whereas, in the control group, the difference in the current density between the first and the second pulses was negligible (Fig. 6, A and B). Similarly, the peak current density of the second pulse in cells expressing ASIC3 homomeric channels was reversibly increased by $133 \pm 33\%$ (n=12) compared to that of the first pulse (Fig. 6, A and B). AA increased the respective ASIC currents in a dose-dependent manner (Fig. 6C). ASIC1a, ASIC2a, and ASIC3 homomeric channels displayed similar dose-dependent curves.

Next, we also tested whether the potentiated currents by AA are attributable to other non-specific currents in tsA201 cells. First, we observed that respective ASIC currents were inhibited by amiloride. ASIC1a currents were inhibited by $95 \pm 1\%$ (n=7) when the extracellular solution containing 300 μ M of amiloride was perfused for 20 s right before the second pH pulse (Fig. 6, D and E). AA (10 μ M)-induced increased ASIC1a currents were also inhibited by $93 \pm 2\%$ (n=4) by co-application of AA and amiloride before the second pH

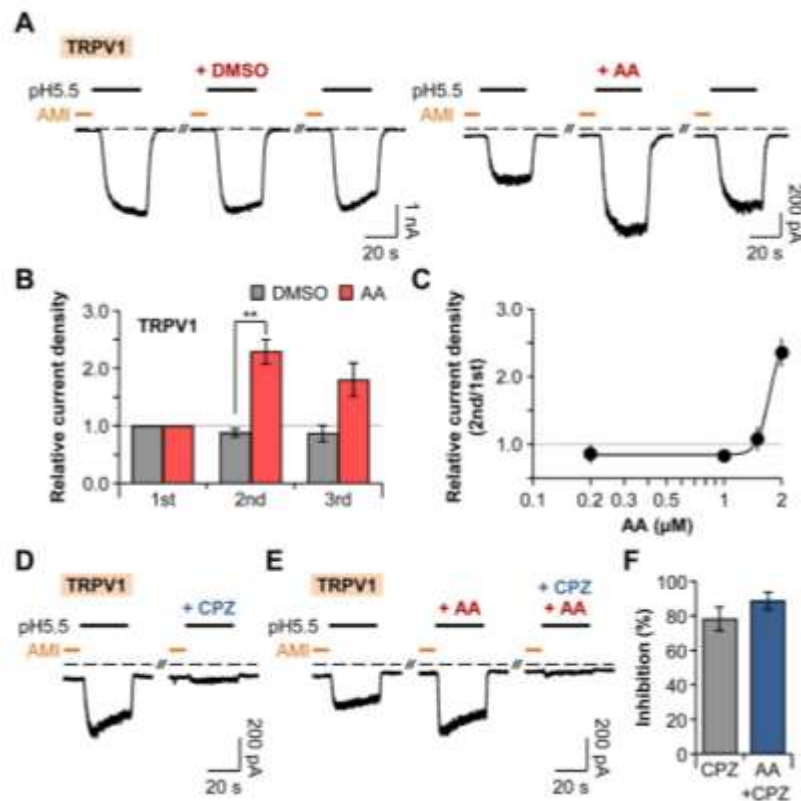


Fig. 7. Potentiation of TRPV1 by AA. (A) TRPV1 current traces repetitively activated by extracellular pH drop to 5.5 for 30 s with time intervals of 300 s. Amiloride (300 μM) was pretreated for 10 s before the pH pulses. AA (2 μM) was applied for 20 s before the second amiloride treatment. Dashed line indicates the zero current level. (B) Relative current density was measured for the cells in (A) (n=4 for DMSO; n=9 for AA). Current density of each pulse was divided by that of the first pulse. ** $P < 0.01$, with two-way ANOVA followed by Bonferroni post-hoc test and student's t -test. (C) Dose-dependent relative current density of TRPV1 (n=5–17). (D) TRPV1 currents were inhibited by preincubation of cells with pH 7.4 solution containing capsazepine (10 μM) for 20 s before the second amiloride treatment. (E) The potentiating effect of AA (2 μM) on TRPV1 currents was inhibited by capsazepine. (F) Percentage of inhibition by capsazepine in the absence (grey) or the presence (blue) of AA (n=6 for CPZ; n=6 for AA+CPZ). Data are mean \pm SEM. Abbreviations: AA, Arachidonic acid; AMI, Amiloride; CPZ, Capsazepine.

pulse (Fig. 6, E and F). In the case of ASIC2a homomeric channels, the currents were inhibited by $65 \pm 3\%$ (n=4) when amiloride (600 μM) was applied for 30 s before and during the second pH pulse (Fig. 6, D and E). The potentiating effects of AA (10 μM) on ASIC2a

currents were inhibited by $72 \pm 11\%$ (n=3) by amiloride (Fig. 6, E and F). ASIC3 currents were inhibited by $80 \pm 2\%$ (n=6) by preincubation of cells with extracellular solution containing 300 μM of amiloride for 20 s before the second pH pulse (Fig. 6, D and E), and the potentiating effects of AA (10 μM) were similarly inhibited by $85 \pm 1\%$ (n=6) (Fig. 6, E and F). Collectively, our results suggest that AA reversibly potentiates homomeric ASIC currents.

At this time, we investigated the effect of AA on proton-activated TRPV1 currents. The bath-application of AA (2 μM) for 20 s right before the second addition of amiloride increased the current density of the second pulse by $129 \pm 21\%$ (n=9) compared to that of the first pulse, whereas the difference in the current density between the first and the second pulses were insignificant (Fig. 7, A and B). Unlike ASIC currents, AA-induced potentiated TRPV1 currents were not fully recovered to the initial level (Fig. 7, A and B). AA potentiated the TRPV1 currents in a dose-dependent manner (Fig. 7C). We also tested whether these potentiated currents are indeed attributable to TRPV1 channels. TRPV1 currents were inhibited by $78 \pm 7\%$ (n=4) by bath-application of capsazepine (10 μM), a specific TRPV1 inhibitor for 20 s (Fig. 7, D and F). Co-application of capsazepine and AA (2 μM) before the second amiloride treatment inhibited the potentiating effect of AA on TRPV1 currents by $89 \pm 5\%$ (n=4) (Fig. 7, E and F). Taken together, AA enhances the activities of TRPV1 channels, although the recovery aspect differs from that of ASICs (Figs. 6B and 7B).

3. 2. Surface trafficking mechanisms of acid-sensing ion channels (ASICs)

Different subcellular localization and proton-sensitivity between ASIC2a and ASIC2b in HEK293T cells

ASIC2a and ASIC2b differ in the N-terminus, the TM1 domain, and one-third of the extracellular

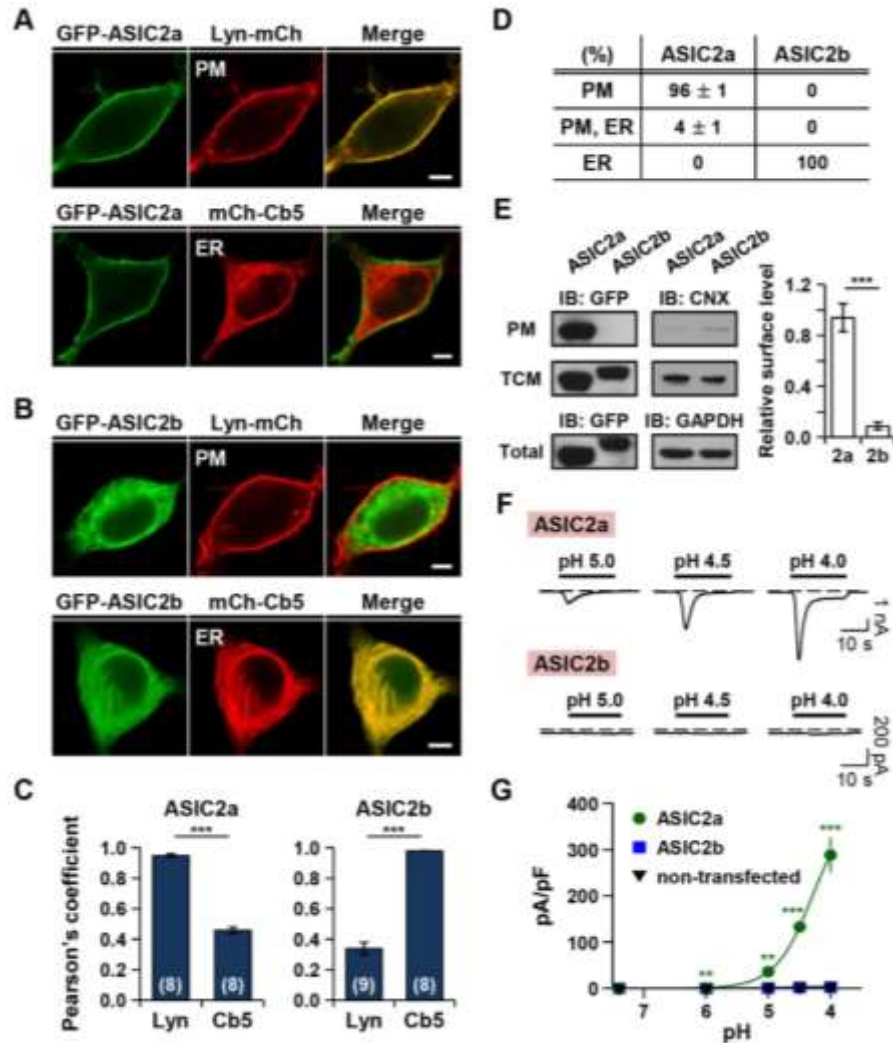


Fig. 8. Different subcellular localization and proton-sensitivity between ASIC2a and ASIC2b in HEK293T cells. (A and B) Representative confocal images of HEK293T cells expressing (A) ASIC2a or (B) ASIC2b with a plasma membrane (Lyn-mCh) or ER (mCh-Cb5) probe. ASIC2a is co-localized with the plasma membrane marker, while ASIC2b is co-localized with the ER marker. The scale bar represents 5 μm . (C) Pearson's correlation coefficient denoting co-localization of fluorescent images was calculated (mean \pm SEM, *** $P < 0.001$, with Student's two-tailed unpaired t -test). The number on each bar indicates n for each condition from three independent experiments. (D) Percentage of cells showing each subunit in specific subcellular localizations was obtained by manually counting cells co-transfected with a plasma membrane or ER probe (mean \pm SEM). For each subunit, 250 cells were counted from five independent experiments. (E) Left, Western blotting on the plasma membrane (PM) fraction, total cellular membrane (TCM) fraction, and total lysate of cells expressing GFP-tagged ASIC2a or ASIC2b was performed using anti-GFP antibody. As

controls, the PM and the TCM fractions were blotted using anti-calnexin (CNX) antibody, and total lysate was blotted using anti-GAPDH antibody. Right, the PM expression was normalized to the TCM expression (n=5 for each, mean \pm SEM, *** $P < 0.001$, with Student's two-tailed unpaired t -test). (F) Proton-activated currents in HEK293T cells expressing ASIC2a (*top*) or ASIC2b (*bottom*). Rapid extracellular pH drop to indicated values from 7.4 generated the currents in cells expressing ASIC2a, while the cells expressing ASIC2b generated no currents. The time interval between pH applications is 2 min for a complete recovery from desensitization. Dashed line indicates the zero current level. (G) pH-dependent peak current density (mean \pm SEM, ** $P < 0.01$, *** $P < 0.001$, with Student's two-tailed unpaired t -test compared to non-transfected). The current density of ASIC2a is increased with decreasing pH value of extracellular solution. (ASIC2a, n=5; ASIC2b, n=5; non-transfected, n=6).

loop region. For the determination of their subcellular localization in HEK293T cells, we fused GFP to N-termini of ASIC2a or ASIC2b (GFP-ASIC2a and GFP-ASIC2b, respectively), and transiently transfected into cells with a plasma membrane or ER marker. Subcellular distribution of ASIC2a and ASIC2b was examined by a confocal laser scanning microscopy 2 days after transfection. ASIC2a was predominantly localized in the cell surface, as evidenced by a yellow color in the merged image of ASIC2a and the plasma membrane marker, Lyn (N-terminal myristoylation and palmitoylation signal sequence from Lyn kinase) (Fig. 8A). A high expression of ASIC2a in the cell surface was indicated by a high value of Pearson's correlation coefficient between ASIC2a and Lyn, compared with that measured between ASIC2a and the ER marker, Cb5 (cytochrome b5) (Fig. 8C, *left*). By contrast, ASIC2b was accumulated in the ER, as evidenced by the overlay image of ASIC2b and Cb5 (Fig. 8B) and a high value of Pearson's correlation coefficient between ASIC2b and Cb5 (Fig. 8C, *right*). Among 250 cells transfected with ASIC2a, most cells displayed a high expression of ASIC2a in the plasma membrane 2 days after transfection (Fig. 8D). However, all of the cells transfected with ASIC2b showed its expression in the ER (Fig. 8D). We examined subcellular localization of ASIC2a and ASIC2b after different days

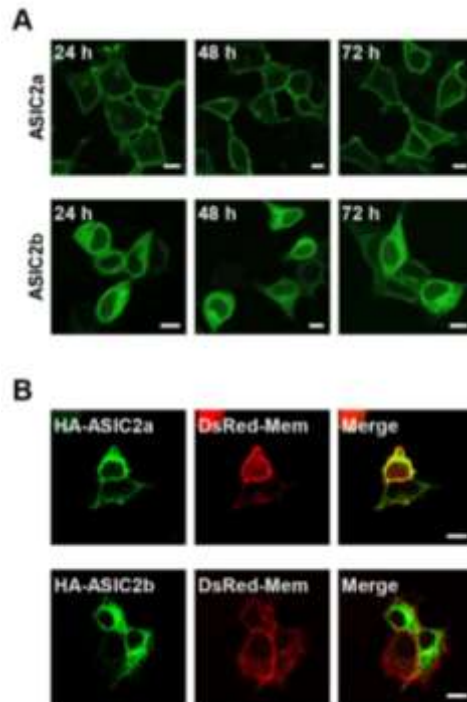


Fig. 9. Differential subcellular localization of ASIC2a and ASIC2b. (A) Subcellular localization of GFP-tagged ASIC2a or ASIC2b was examined after different days of transfection. ASIC2a is localized in the plasma membrane already 1 day after transfection, while ASIC2b remained in the ER even 3 days after transfection. (B) Immunocytochemistry on HEK293T cells co-expressing the plasma membrane marker DsRed-Mem and HA-ASIC2a (*top*) or HA-ASIC2b (*bottom*) by anti-HA antibody. The scale bar represents 10 μ m.

of transfection (1 day, 2 days, and 3 days) (Fig. 9A). ASIC2a was localized in the plasma membrane already 1 day after transfection. However, ASIC2b remained in the ER even 3 days after transfection. In addition, immunostaining cells expressing HA-ASIC2a or HA-ASIC2b with anti-HA antibody revealed an identical subcellular distribution (Fig. 9B), excluding the possibility of that GFP-tagging leads to mislocalization of proteins.

Their subcellular localization was also confirmed by Western blotting. As shown in Fig. 8E, ASIC2a and ASIC2b were strongly detected in the total cellular membrane (TCM) fraction. However, in the plasma membrane (PM) fraction, ASIC2a was solely detected at

predicted size, and we obtained no evidence for surface expression of ASIC2b. We also performed immunoblotting on the TCM and the PM fractions with an anti-calnexin (CNX) antibody to test a purity of the PM fraction. While calnexin was strongly detected in the TCM fraction, it was barely detected in the PM fraction (Fig. 8E).

ASIC2a and ASIC2b also have differential sensitivity to extracellular protons. Extracellular acidification triggered inward currents in cells expressing ASIC2a, and the peak current density was increased with decreasing pH value of extracellular solution (n=5) (Fig. 8, F and G). However, ASIC2b generated no currents to extracellular pH drop, as previously known as a non-functional homomeric channel (n=5) (Fig. 8, F and G). There was no statistically significant difference between proton-activated currents measured from non-transfected cells (n=6) and ASIC2b-transfected cells (Fig. 8, F and G).

Replacement of the first 129 amino acids in ASIC2b by corresponding regions of ASIC2a conferred surface expression and proton-sensitivity

We created a series of chimeras of ASIC2a and ASIC2b to identify the critical regions required for membrane targeting of ASIC2a. Firstly, the N-terminus of ASIC2b was replaced by the equivalent sequences of ASIC2a (Fig. 10, A and B, cf. Ch1). However, this Ch1 also resided in the ER, as indicated by a low value of Pearson's correlation coefficient between Ch1 and Lyn (Fig. 10, C–E). Like ASIC2b, Ch1 generated no proton-activated currents (n=5) (Fig. 10, C and F). When the TM1 domain was more replaced by that of ASIC2a (Fig. 10, A and B, cf. Ch2), more than 70% of cells showed that Ch2 is expressed in the plasma membrane with partial accumulation in the ER (Fig. 10, C–E). However, we could not detect any proton-activated currents in cells expressing Ch2, even though it was expressed in the cell surface (n=6) (Fig. 10, C and F). When 17 more amino acids were replaced (Fig. 10, A and B, cf. Ch3), this chimera dramatically trafficked to the cell surface,

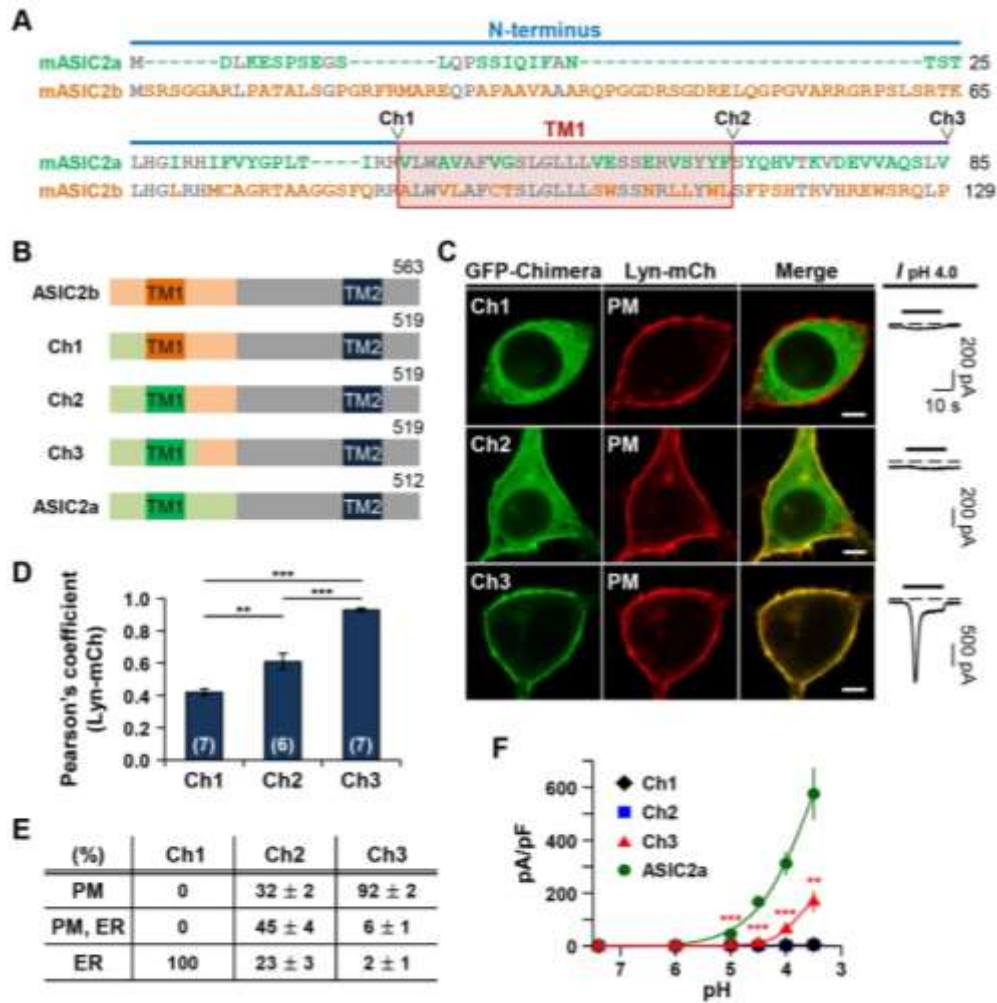


Fig. 10. Replacement of the first 129 amino acids in ASIC2b by corresponding regions of ASIC2a conferred surface expression and proton-sensitivity. (A) Sequence alignment of ASIC2a (1–85 amino acids) and ASIC2b (1–129 amino acids). Blue and purple lines indicate the N-terminus and the extracellular loop region, respectively. The TM1 domain is denoted by a red box. Conserved residues between two subunits are in gray. In ASIC2b, 1–86 amino acids (aa) were replaced by 1–42 aa of ASIC2a (Ch1), 1–112 aa were replaced by 1–68 aa of ASIC2a (Ch2), and 1–129 aa were replaced by 1–85 aa of ASIC2a (Ch3). (B) Schematic diagram of constructed chimeras. (C) Left, representative confocal images of HEK293T cells expressing each chimera with the PM marker, Lyn-mCh. The scale bar represents 5 μ m. Right, pH 4.0-induced currents measured from the cells expressing each chimera. Dashed line indicates the zero current level. (D) Pearson's correlation coefficient between the PM marker and each chimera (mean \pm SEM, ** $P < 0.01$, *** $P < 0.001$, with one-way ANOVA followed by Bonferroni post-hoc test). The number on each bar indicates n for each condition from three independent experiments. (E) Percentage of cells showing each

chimera in specific subcellular localizations (mean \pm SEM). For each chimera, 250 cells were counted from five independent experiments. (F) pH-dependent peak current density of each channel (mean \pm SEM, ** $P < 0.01$, *** $P < 0.001$, with Student's two-tailed unpaired t -test compared to ASIC2a). The time interval between pH applications is 2 min for a complete recovery from desensitization (Ch1, n=5; Ch2, n=6; Ch3, n=5; ASIC2a, n=5).

as indicated by a high value of Pearson's correlation coefficient between Ch3 and Lyn (Fig. 10, C–E). Furthermore, Ch3 generated inward currents in response to protons, although the current density was smaller than that of ASIC2a (n=5) (Fig. 10, C and F). Collectively, these results suggest that the TM1 and the proximal post-TM1 domain of ASIC2a are critical for membrane targeting and generating proton-activated currents.

The TM1 and the proximal post-TM1 domain of ASIC2a are critical regions for surface trafficking of ASIC2

Based on our observation in Fig. 10, we constructed more chimeras to verify the importance of the TM1 and the proximal post-TM1 domain in surface trafficking of ASIC2a. When the proximal post-TM1 domain in ASIC2a was replaced by that of ASIC2b (Fig. 11A, cf. 2a-P), this chimeric channel was still localized on the cell surface (Fig. 11, B–D). However, it had lost proton-sensitivity (Fig. 11B). In the reverse chimera (Fig. 11A, cf. 2b-P), we observed that exchange of the proximal post-TM1 domain in ASIC2b to that of ASIC2a is not sufficient for exit of ASIC2b from the ER (Fig. 11, B–D). This 2b-P also generated no currents in response to protons (n=5) (Fig. 11B). However, when the TM1 domain was further replaced, this 2b-TP efficiently targeted the cell surface (Fig. 11, B–D). We could also measure the proton-induced currents in cells expressing 2b-TP (n=6) (Fig. 11B). To investigate the importance of the TM1 domain in membrane targeting, we exchanged the TM1 domain in ASIC2a with that of ASIC2b (Fig. 11A, cf. 2a-T). Interestingly, this

chimeric channel displayed poor membrane localization despite retaining proton-sensitivity (n=6) (Fig. 11, B–D). Next, we examined whether the insertion of the TM1 domain of ASIC2a into ASIC2b can lead to exit of ASIC2b from the ER (Fig. 11A, cf. 2b-T). The replacement of the TM1 domain of ASIC2b by that of ASIC2a promoted forward trafficking

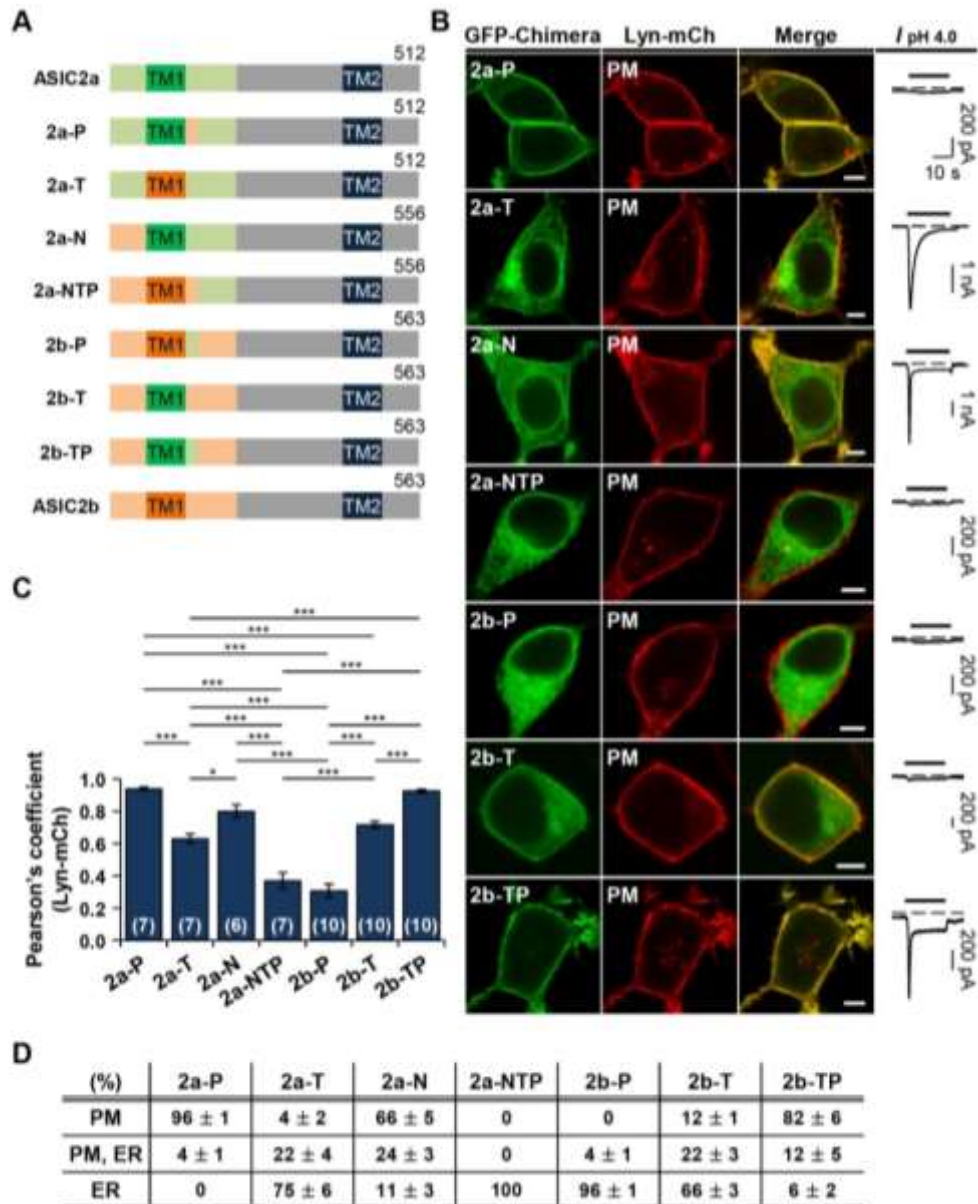


Fig. 11. The TM1 and the proximal post-TM1 domain of ASIC2a are critical regions for surface trafficking of ASIC2. **(A)** Schematic diagram of constructed chimeras. **(B)** Left, representative confocal images of HEK293T cells expressing each chimera with the PM marker, Lyn-mCh. The scale bar represents

5 μ m. Right, pH 4.0-induced currents measured from the cells expressing each chimera. Dashed line indicates the zero current level. (C) Pearson's correlation coefficient between the PM marker and each chimera (mean \pm SEM, * $P < 0.05$, *** $P < 0.001$, with one-way ANOVA followed by Bonferroni post-hoc test). The number on each bar indicates n for each condition from three independent experiments. (D) Percentage of cells showing each chimera in specific subcellular localizations (mean \pm SEM). For each chimera, 250 cells were counted from five independent experiments.

of ASIC2b, as evidenced by a yellow color at the cell surface in the merged image of 2b-T and Lyn (Fig. 11, B–D). However, 2b-T generated no currents in response to extracellular protons even at the cell surface (n=5) (Fig. 11B). These results suggest that the TM1 domain of ASIC2a is important for surface trafficking of ASIC2, although the proximal post-TM1 domain of ASIC2a is also necessary for the efficient membrane targeting and proton-sensitivity of ASIC2.

We also tested whether the N-terminus is involved in surface trafficking of ASIC2a. When the N-terminus of ASIC2a was replaced by that of ASIC2b (Fig. 11A, cf. 2a-N), membrane localization was partially disrupted (Fig. 11, B–D). When the N-terminus, the TM1, and the proximal post-TM1 domain were all replaced in ASIC2a (Fig. 11A, cf. 2a-NTP), this chimera completely lost both membrane localization and proton-sensitivity (n=5) (Fig. 11, B–D). These results suggest that orchestrated work of the TM1 domain and neighboring regions such as the N-terminus and the proximal post-TM1 domain is necessary for the efficient surface trafficking of ASIC2a. However, according to the results, replacement of the TM1 and the proximal post-TM1 domain is sufficient for conferring surface expression and proton-sensitivity on ASIC2b (Fig. 11, cf. 2b-TP).

The N-terminus and the TM1 domain regulate the channel properties

While we performed the electrophysiological experiments with chimeras, we noticed that

proton-activated currents produced by each chimeric channel have different shapes (Fig. 12A). Therefore, we further analyzed the biophysical properties of the currents by measuring the time constant (τ) for desensitization at pH 4.0. To calculate the desensitization time constant, we used a single exponential function for ASIC2a and Ch3 currents, and a double exponential function for 2a-N, 2b-TP, and 2a-T currents. First, the desensitization time constant of ASIC2a (1.06 ± 0.08 s, $n=7$) was similar to the value previously reported by others (Hattori et al., 2009) (Fig. 12B). We then characterized the currents from Ch3 to determine whether Ch3 replicates the properties of ASIC2a. The desensitization time constant of Ch3 at pH 4.0 were 0.86 ± 0.05 s ($n=6$) (Fig. 12B), demonstrating that desensitizing kinetics of Ch3 is not significantly different from those of ASIC2a. However, the peak current density of Ch3 at pH 3.5 was significantly smaller than that of ASIC2a (Fig. 12E), and pH-dependent response curve of Ch3 was shifted to the right compared with ASIC2a (Fig. 12F).

When the N-terminus in ASIC2a was replaced by that of ASIC2b (Fig. 11A, cf. 2a-N), desensitizing kinetics was significantly altered. At pH 4.0, the desensitization time constants of 2a-N currents were 0.30 ± 0.03 s ($n=6$) for τ_1 and 2.8 ± 0.1 s ($n=6$) for τ_2 (Fig. 12C). In addition, 2a-N elicited readily desensitized currents. The cells expressing 2a-N produced only sustained currents to consecutive acid stimuli, and transient currents were eliminated; thus, we could not measure the pH-dependent peak current density in a single cell. Therefore, we plotted a pH-dependency curve by measuring the currents in individual cells. The peak current density of 2a-N was significantly decreased at pH 3.5 (Fig. 12E).

These alterations in biophysical properties of the currents were similarly observed when the N-terminus in Ch3 was exchanged to that of ASIC2b (Fig. 11A, cf. 2b-TP). At pH 4.0, the desensitization time constants of 2b-TP currents was 0.42 ± 0.03 s ($n=6$) for τ_1 and 5.1 ± 0.7 s ($n=6$) for τ_2 (Fig. 12C), and 2b-TP also triggered desensitized currents to

successive stimuli, suggesting a role of ASIC2a N-terminus in stabilizing the transient component of the currents. In addition, the peak current density of 2b-TP at pH 3.5 was significantly smaller than that of ASIC2a (Fig. 12E).

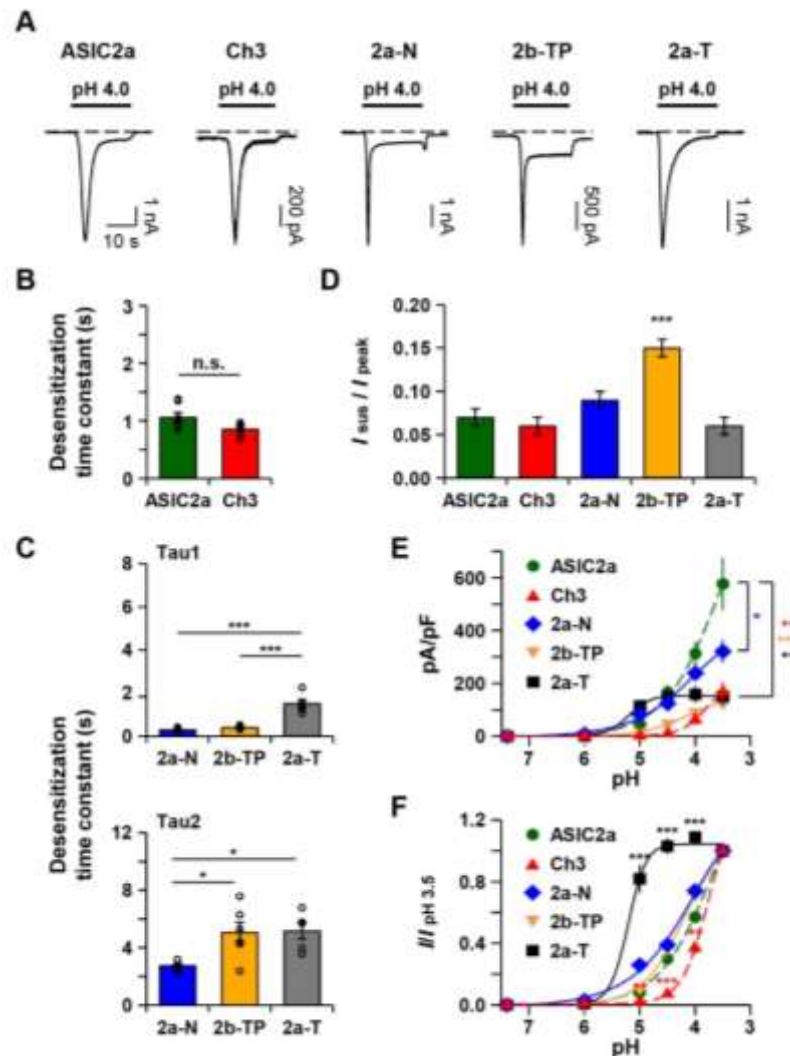


Fig. 12. The N-terminus and the TM1 domain regulate the channel properties. (A) Representative current traces from cells expressing each channel. Dashed line indicates the zero current level. (B) Time constant (τ) for desensitization at pH 4.0 was calculated by fitting the current in a single exponential function (mean \pm SEM, n.s.; not significant). (C) Time constants (τ) for desensitization at pH 4.0 were calculated by fitting the current in a double exponential function (mean \pm SEM, * $P < 0.05$, *** $P < 0.001$, with one-way ANOVA followed by Bonferroni post-hoc test). When Area1 and Area2 represent the area of τ_1 and τ_2 , respectively, Area1/Area2 values were 0.91 ± 0.11 ($n=6$) for 2a-N, 1.40 ± 0.10 ($n=6$) for 2b-TP, and 0.26 ± 0.06 ($n=5$) for 2a-T. (D) Ratio of sustained current to peak current at pH 4.0 (mean \pm SEM, *** $P < 0.001$,

with Student's two-tailed unpaired *t*-test compared to ASIC2a). (E) pH-dependent peak current density of each channel (mean \pm SEM, * $P < 0.05$, ** $P < 0.01$, *** $P < 0.001$, with Student's two-tailed unpaired *t*-test compared to ASIC2a). The time interval between pH applications is 2 min for a complete recovery from desensitization. For 2a-N and 2b-TP, pH-dependent response was measured from individual cells. pH-dependency curves of ASIC2a and Ch3 from Fig. 2f were plotted as controls (*dashed line*). (ASIC2a, n=5; Ch3, n=5; 2a-N, n=5 at each point; 2b-TP, n=6 at each point; 2a-T, n=6). (F) Normalized pH-dependency curves in Fig. 4E. Peak current at each pH was divided by pH 3.5-evoked peak current (mean \pm SEM, ** $P < 0.01$, *** $P < 0.001$, with Student's two-tailed unpaired *t*-test compared to ASIC2a).

When the TM1 domain in ASIC2a was switched to that of ASIC2b (Fig. 11A, cf. 2a-T), desensitization time constants of the currents were 1.51 ± 0.20 s (n=5) for τ_1 and 5.2 ± 0.6 (n=5) for τ_2 (Fig. 12C). The pH-dependent peak current density of 2a-T reached a plateau near at pH 4.5, whereas that of ASIC2a did not reach the maximum current, even at pH 3.5 as previously reported (Fig. 12E) (Harding et al., 2014). As shown in Fig. 12F, compared with ASIC2a, the relative currents of 2a-T significantly increased when the acidic stimuli (pH \leq 5.0) were applied. However, the peak current density of 2a-T at pH 3.5 was significantly smaller than that of ASIC2a (Fig. 12E). Even though 2a-T has poor plasma membrane localization, it should be emphasized that we cannot rule out small fraction of 2a-T in the plasma membrane that can generate the currents. A half-maximal pH (pH₅₀) value of 2a-T was 5.21 (Fig. 12F).

We also compared the ratio of sustained current to peak current ($I_{\text{sus}}/I_{\text{peak}}$) at pH 4.0. The ratio was significantly increased in 2b-TP (0.15 ± 0.01 , n=9) compared to ASIC2a (0.07 ± 0.01 , n=7) (Fig. 12D). There was no statistically difference in Ch3 (0.06 ± 0.01 , n=10), 2a-N (0.09 ± 0.01 , n=8), or 2a-T (0.06 ± 0.01 , n=5) compared with ASIC2a. Taken all the data together, these results suggest that the N-terminus and the TM1 domain contribute to the gating properties of ASIC2 channels.

H72 and E78 are critical for proton-sensitivity, whereas D77 is involved in determining subcellular localization and proton-sensitivity

In the study with chimeras, we observed that the proximal post-TM1 domain of ASIC2a is required for generating proton-activated currents, even though the channels are expressed in the cell surface (Figs. 10 and 11; Ch2, 2a-P, and 2b-T). This region contains histidine (H), aspartate (D), and glutamate (E), which are known to be putative proton-binding sites (Fig. 13A) (Baron et al., 2001; Smith et al., 2007b). To investigate the involvement

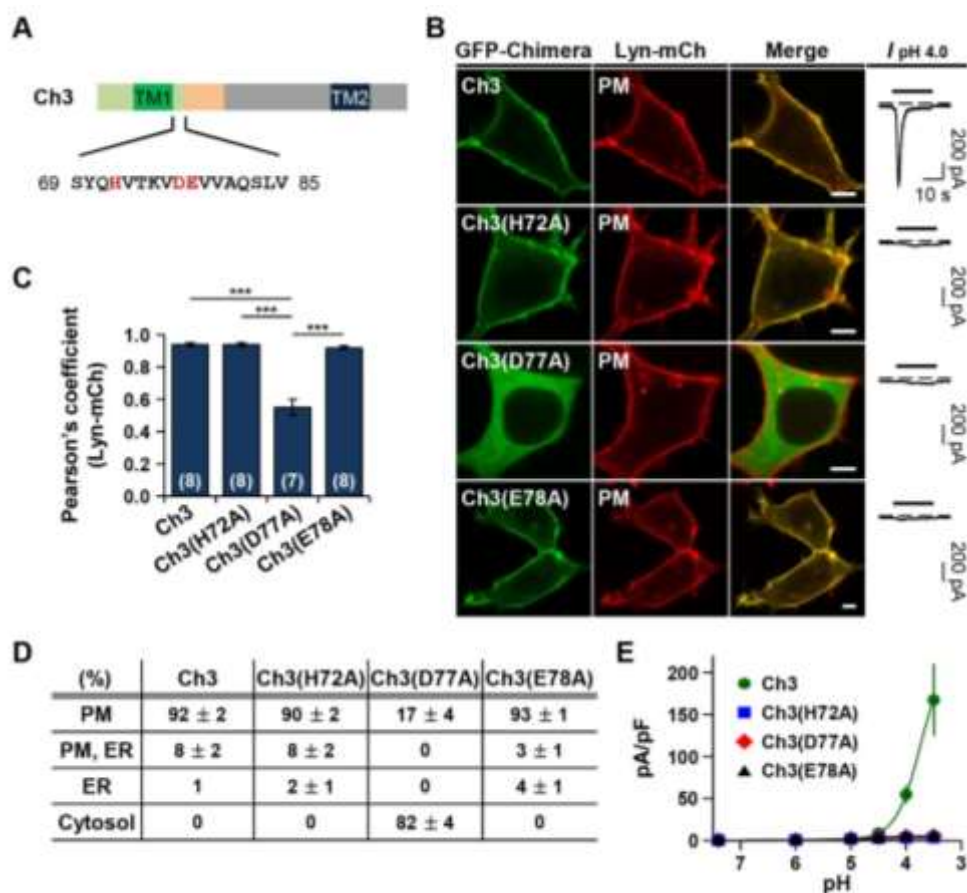


Fig. 13. H72 and E78 are critical for proton-sensitivity, whereas D77 is involved in determining subcellular localization and proton-sensitivity. (A) Putative proton-binding sites (H72, D77, and E78) located in the proximal post-TM1 domain of Ch3 were highlighted in red. (B) Left, representative confocal images of HEK293T cells expressing each chimera with the plasma membrane marker, Lyn-mCh. The scale bar represents 5 μ m. Right, pH 4.0-induced currents measured from the cells expressing each chimera. Dashed line indicates the zero current level. (C) Pearson's correlation coefficient between the plasma

membrane marker and each chimera (mean \pm SEM, *** $P < 0.001$, with one-way ANOVA followed by Bonferroni post-hoc test). The number on each bar indicates n for each condition from three independent experiments. (D) Percentage of cells showing each chimera in specific subcellular localizations (mean \pm SEM). For each chimera, 250 cells were counted from five independent experiments. (e) pH-dependent peak current density of each chimera (mean \pm SEM). The time interval between pH applications is 2 min for a complete recovery from desensitization (Ch3, n=5; Ch3(H72A), n=5; Ch3(D77A), n=6; Ch3(E78A), n=5).

of these residues in proton-sensitivity of Ch3, we made three single amino acid mutated channels (Ch3(H72A), Ch3(D77A), and Ch3(E78A)) and examined their subcellular distribution and proton-sensitivity. We observed that mutation at the position of H72 or E78 completely abolished proton-sensitivity, even though chimeric channels were still present in the cell surface (n = 5 for each) (Fig. 13, B–E). These results indicate that H72 and E78 are critical residues for responding to extracellular protons, as previously reported (Baron et al., 2001; Smith et al., 2007b). However, we found that Ch3(D77A) lost both surface expression and proton-sensitivity (n=6) (Fig. 13, B–E). It suggests that D77 has a role in determining subcellular localization as well as proton-sensitivity of the channel.

ASIC2b traffics to the cell surface by heteromeric assembly with ASIC2a

In physiological conditions, ASICs mostly exist as heteromeric channels (Askwith et al., 2004; Hesselager et al., 2004; Hattori et al., 2009; Sherwood et al., 2011). According to the previous study, ASIC2a and ASIC2b are co-localized in a subpopulation of rat taste cells (Ugawa et al., 2003). Based on this finding, we co-transfected fluorescent protein-tagged ASIC2a and ASIC2b in HEK293T cells. Strikingly, ASIC2b successfully targeted the cell surface when it was co-expressed with ASIC2a (Fig. 14A). In most of the cells, ASIC2b was co-localized with ASIC2a in the plasma membrane, as indicated by a high value of Pearson's correlation coefficient between two subunits (Fig. 14, B and C). Additionally, in

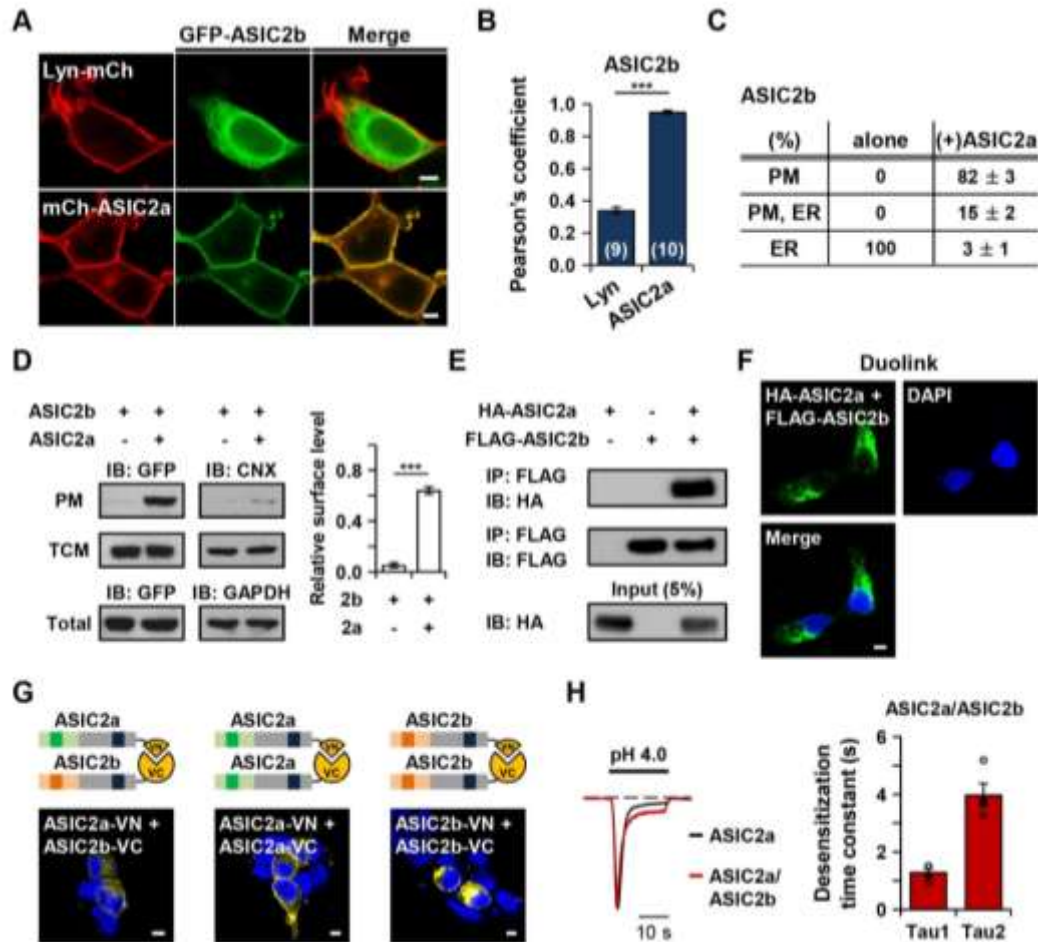


Fig. 14. ASIC2b traffics to the cell surface by heteromeric assembly with ASIC2a. **(A)** Representative confocal images of HEK293T cells co-expressing ASIC2b with the plasma membrane marker (*top*) or ASIC2a (*bottom*). **(B)** Pearson's correlation coefficient between ASIC2b and Lyn or ASIC2a (mean ± SEM, *** $P < 0.001$, with Student's two-tailed unpaired t -test). The number on each bar indicates n for each condition from three independent experiments. **(C)** Percentage of cells showing ASIC2b in specific subcellular localizations in the absence or presence of ASIC2a (mean ± SEM). For each experiment, 250 cells were counted from five independent experiments. **(D)** Left, Western blotting on the plasma membrane (PM) fraction, total cellular membrane (TCM) fraction, and total lysate of cells expressing GFP-tagged ASIC2b with or without ASIC2a in pcDNA3.1(+) was performed using anti-GFP antibody. As controls, the PM and the TCM fractions were blotted using anti-calnexin (CNX) antibody, and total lysate was blotted using anti-GAPDH antibody. Right, the PM expression was normalized to the TCM expression ($n=3$ for each, mean ± SEM, *** $P < 0.001$, with Student's two-tailed unpaired t -test). **(E)** Co-immunoprecipitation assay in HEK293T cells co-expressing HA-ASIC2a and FLAG-ASIC2b. **(F)** Duolink PLA. Intense PLA signal was

detected in HEK293T cells co-expressing HA-ASIC2a and FLAG-ASIC2b. **(G)** Schematic diagram of BiFC assay and confocal images of HEK293T cells expressing each combinatory construct. VN and VC are N- and C-terminal fragments of the Venus protein, respectively. Venus signals were examined for heteromerization of ASIC2a and ASIC2b, and homomerization of ASIC2a or ASIC2b. The fluorescent signals of BiFC were detected, as indicated by a yellow color. **(H)** Representative current traces of ASIC2a homomeric channel (*black*) and ASIC2a/ASIC2b heteromeric channel (*red*) were superimposed. Dashed line indicates the zero current level. Desensitization time constants (τ) of ASIC2a/ASIC2b current at pH 4.0 were calculated by fitting the current in a double exponential function (mean \pm SEM). When Area1 and Area2 represent the area of τ_1 and τ_2 , respectively, Area1/Area2 values were 1.39 ± 0.42 (n=4). The scale bar represents 5 μ m.

the biochemical experiment, we observed that the surface level of ASIC2b was significantly increased in the presence of ASIC2a (Fig. 14D). To investigate the heteromeric interaction between two subunits in HEK293T cells, we performed co-immunoprecipitation (Co-IP) using HA-tagged ASIC2a and FLAG-tagged ASIC2b. The cell lysates were immunoprecipitated with an anti-FLAG antibody and then blotted with an anti-HA antibody. As shown in Fig. 14E, ASIC2a strongly associates with ASIC2b. We also examined the heteromeric assembly of ASIC2a and ASIC2b by using a Duolink proximity ligation assay (PLA) (Fig. 14F). Duolink PLA signals are generated when the distance between interacting proteins is < 40 nm (Söderberg et al., 2006; Hwang et al., 2014). We detected a strong PLA signal from HA-ASIC2a and FLAG-ASIC2b in HEK293T cells (Fig. 14F).

The association between two subunits was further supported by a bimolecular fluorescence complementation (BiFC) assay, which allows visualization of subcellular localization of interacting proteins in living cells (Fig. 14G) (Shyu et al., 2006). To establish the Venus-based BiFC system, one complementary half of the Venus fluorescent protein, either the C-terminal fragment (VC) or the N-terminal fragment (VN), was fused to the C-terminus of ASIC2a or ASIC2b. The BiFC fluorescent signal was detected in the plasma membrane

when ASIC2a-VN and ASIC2b-VC were co-transfected in HEK293T cells (Fig. 14G). As a positive control, ASIC2a homomers (ASIC2a-VN + ASIC2a-VC) showed a strong BiFC signal in the plasma membrane (Fig. 14G). For investigating whether ASIC2b also assembles by itself in the ER, we co-transfected ASIC2b-VN and ASIC2b-VC in HEK293T cells. Interestingly, we observed a strong BiFC signal in the ER, suggesting that ASIC2b has the ability to assemble by itself (Fig. 14G). As a negative control, we tested a BiFC signal between ASIC2b and unrelated ion channel that resides in the ER. We employed TWIK-1 or TREK-1, a member of two-pore domain K⁺ (K2P) channels. According to the previous study, TWIK-1/TREK-1 heterodimerization is required for cell surface expression of two subunits (Hwang et al., 2014). We detected no BiFC signals when ASIC2b-VN was co- expressed

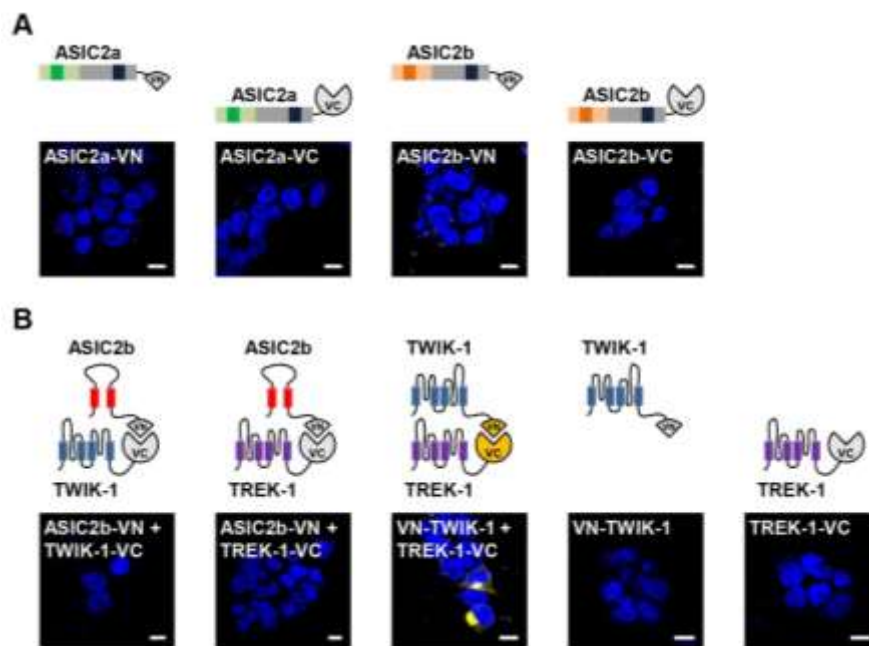


Fig. 15. Control experiments for BiFC assay. (A) For determination of specificity of BiFC, HEK293T cells were transfected with one half of split Venus protein. No fluorescence was detected when either ASIC2a or ASIC2b with one half of Venus protein was expressed alone. (B) ASIC2b-VN was tested with TWIK-1-VC or TREK-1-VC. BiFC signal was detected in cells co-expressing VN-TWIK-1 and TREK-1-VC. No fluorescence was detected when either TWIK-1 or TREK-1 with one half of Venus protein was expressed alone. The scale bar represents 10 μ m.

with TWIK-1-VC or TREK-1-VC in HEK293T cells, while co-expression of VN-TWIK-1 and TREK-1-VC showed a strong BiFC signal (Fig. 15B). No fluorescence was detected when ASIC2a, ASIC2b, TWIK-1, or TREK-1 with one half of Venus protein was expressed alone (Fig. 15). Taken together, these results strongly suggest that ASIC2b requires an association with ASIC2a for its successful membrane trafficking.

We also examined whether ASIC2b can modulate the properties of ASIC2a currents at the cell surface. In heterologous expression systems, several electrophysiological studies have demonstrated that co-expression of ASIC2b alters the biophysical properties of ASIC channels, which has provided evidence for heteromeric association between ASIC2b and other subunits (Lingueglia et al., 1997; Ugawa et al., 2003; Hesselager et al., 2004). We also measured the currents from ASIC2a/ASIC2b heteromeric channels by co-expressing two subunits in HEK293T cells. Unlike the currents from ASIC2a homomeric channels, ASIC2a/ASIC2b currents desensitized with biphasic kinetics, as previously reported (Fig. 14H) (Ugawa et al., 2003). We calculated the desensitization time constants for ASIC2a/ASIC2b currents using a double exponential function (1.29 ± 0.13 s ($n = 4$) for τ_1 and 4.0 ± 0.4 ($n = 4$) for τ_2 at pH 4.0) (Fig. 14H). The desensitization time constant for slow component of the currents was significantly increased in ASIC2a/ASIC2b currents compared to ASIC2a homomeric currents (*** $P < 0.001$, with Student's two-tailed unpaired t -test).

Surface expression of ASIC2b is increased in the presence of ASIC2a in SH-SY5Y cells

We also examined whether such membrane trafficking mechanisms of ASIC2 isoforms appear in SH-SY5Y cells, which are popularly used human neuroblastoma cells. GFP-tagged ASIC2a or ASIC2b was co-transfected with RFP-PH (PLC δ), which is a commonly used plasma membrane marker. Consistent with our observation in HEK293T cells, ASIC2a

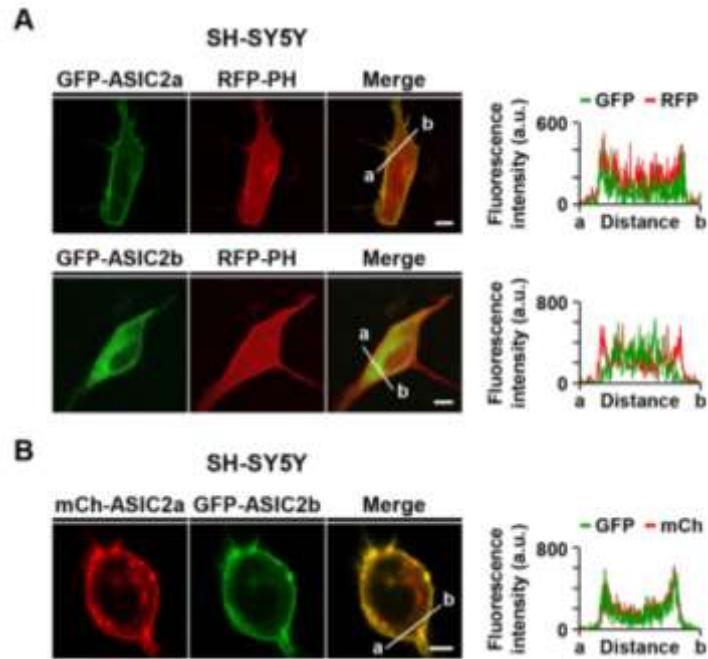


Fig. 16. Surface expression of ASIC2b is increased in the presence of ASIC2a in SH-SY5Y cells. (A) Representative confocal images of SH-SY5Y cells expressing GFP-tagged ASIC2a or ASIC2b with the plasma membrane marker, RFP-PH. In SH-SY5Y cells, ASIC2a and ASIC2b are localized in the cell surface and the ER, respectively, as observed in HEK293T cells. Line scanning of fluorescent images was processed by using ZEN2011 software (Carl Zeiss). **(B)** Representative confocal images of SH-SY5Y cells co-expressing ASIC2a and ASIC2b. In the presence of ASIC2a, surface expression of ASIC2b was increased, as indicated by a yellow color in the merged image and line scanning. The scale bar represents 5 μ m.

was predominantly localized in the cell surface like RFP-PH, as evidenced by overlapped line scanning results of GFP and RFP, while ASIC2b was accumulated in the ER in SH-SY5Y cells (Fig. 16A). However, when ASIC2b was co-expressed with ASIC2a, ASIC2b trafficked to the plasma membrane (Fig. 16B), as observed in HEK293T cells (Fig. 14).

The N-terminal region of ASIC2a is necessary for the ASIC2a-dependent membrane targeting of ASIC2b

Lastly, we tested whether Ch3 and 2b-TP containing the critical regions for membrane

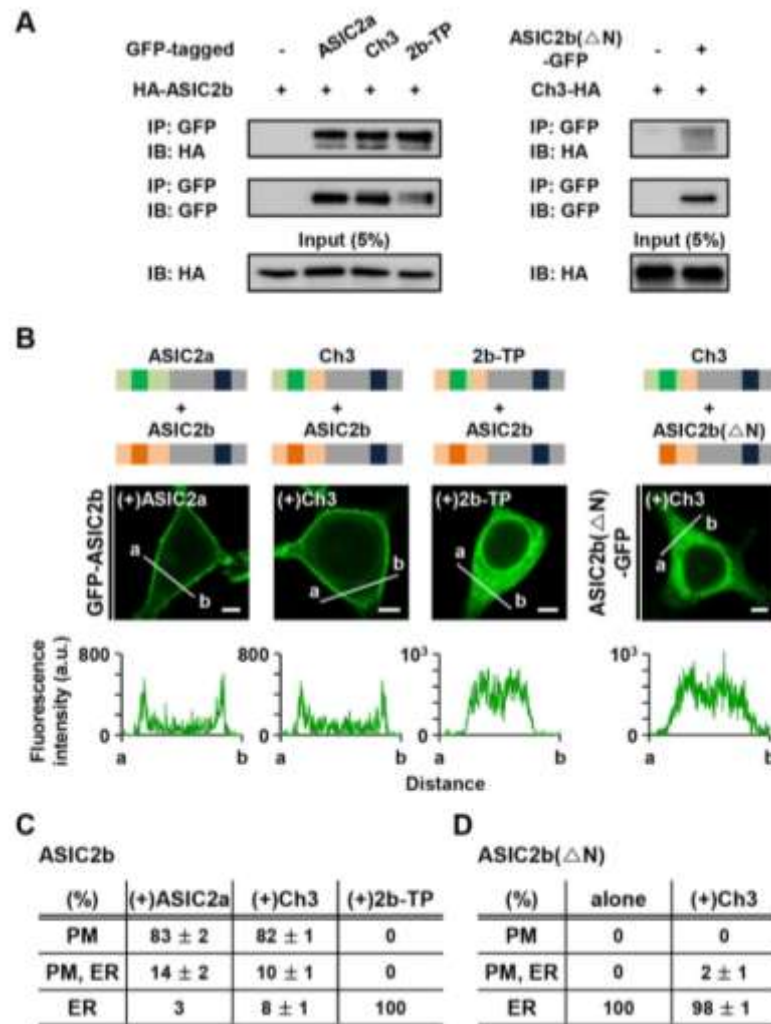


Fig. 17. The N-terminal region of ASIC2a is necessary for the ASIC2a-dependent membrane targeting of ASIC2b. (A) Co-immunoprecipitation assay in HEK293T cells. GFP-tagged ASIC2 proteins and HA-ASIC2b (left) or GFP-tagged ASIC2b(Δ N) and Ch3-HA were co-transfected into HEK293T cells, and cell lysates were immunoprecipitated using anti-GFP antibody. The immunoprecipitates were then examined by Western blotting using anti-HA antibody. (B) Schematic diagram depicting heteromeric assembly experiments and representative confocal images of HEK293T cells expressing GFP-tagged ASIC2b in the presence of each ASIC2 protein in pcDNA3.1(+). Line scanning of fluorescent images was processed by using ZEN2011 software (Carl Zeiss). The scale bar represents 5 μ m. (C) Percentage of cells showing ASIC2b in specific subcellular localizations in the presence of each ASIC2 protein in pcDNA3.1(+) (mean \pm SEM). For each experiment, 250 cells were counted from five independent experiments. (D) Percentage of cells showing N-terminal deleted ASIC2b in specific subcellular localizations in the absence or presence of Ch3 (mean \pm SEM). For each experiment, 250 cells were counted from five independent experiments.

targeting can also deliver ASIC2b to the cell surface, like ASIC2a. First of all, we investigated heteromeric interaction between ASIC2b and Ch3 or 2b-TP by Co-IP experiments. As shown in Fig. 17A, both Ch3 and 2b-TP strongly associate with ASIC2b, like ASIC2a. However, when the N-terminal region of ASIC2b was deleted (ASIC2b(Δ N)), the interaction with Ch3 was markedly reduced (Fig. 17A). Based on these results, we investigated the subcellular distribution of GFP-tagged ASIC2b in the presence of Ch3 or 2b-TP. We observed that, like ASIC2a, Ch3 can also deliver ASIC2b to the cell surface, indicating that 100 amino acids (86 to 185) of ASIC2a extracellular domain are not considerably involved in surface targeting of Ch3/ASIC2b heteromeric channels (Fig. 17, B and C). However, interestingly, ASIC2b remained in the ER when it was co-expressed with 2b-TP (Fig. 17, B and C). It suggests that the N-terminal region from ASIC2a is required for membrane targeting of 2b-TP/ASIC2b heteromeric channels, although it does not seem to be considerably necessary for that of 2b-TP homomeric channels (Fig. 11). These results suggest that surface trafficking of homomers and heteromers could be differentially regulated.

When the N-terminal region of ASIC2b was deleted, this ASIC2b(Δ N) was also accumulated in the ER, and co-expression with Ch3 had no effect on its localization (Fig. 17, B and D). It might be due to the reduced heteromeric interaction between two subunits, as observed in Co-IP experiments. Therefore, we can suggest that the N-terminus of ASIC2b is important for the heteromeric interaction with Ch3.

Different subcellular distribution of ASIC2a and ASIC3 in HEK293T cells

We also compared subcellular distribution of ASIC2a and ASIC3 in HEK293T cells. For this, we fused GFP to C-termini of ASIC proteins (ASIC2a-GFP and ASIC3-GFP, respectively) and transfected into cells with a plasma membrane or ER marker. As reported

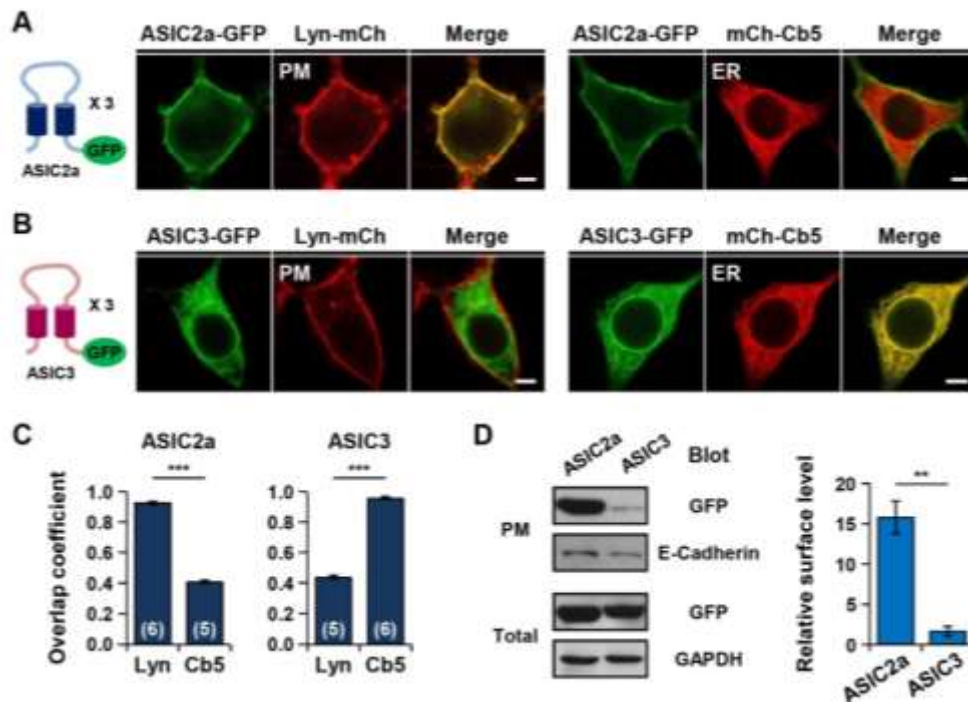


Fig. 18. Different subcellular distribution of ASIC2a and ASIC3 in HEK293T cells. (A, B) Confocal images of HEK293T cells expressing GFP-tagged (A) ASIC2a or (B) ASIC3 with a plasma membrane (Lyn-mCh) or ER (mCh-Cb5) marker. Scale bars are 5 μ m. (C) Overlap coefficient value of fluorescent signals (mean \pm SEM, *** $P < 0.001$, with Student's t -test). The number on each bar represents n for each condition. (D) Western blotting on the plasma membrane (PM) fraction and the total lysates of cells expressing GFP-tagged ASIC2a or ASIC3 using anti-GFP antibody. As controls, the PM and the total lysates were blotted using anti-E-Cadherin and anti-GAPDH antibodies, respectively. The surface level of ASIC2a or ASIC3 was normalized to that of E-Cadherin (mean \pm SEM, $n=3$ for ASIC2a; $n=3$ for ASIC3, ** $P < 0.01$, with Student's t -test).

by the previous literature, we observed the substantial distribution of ASIC2a at the cell surface (Chai et al., 2007; Chai et al., 2010). However, ASIC3 was mostly accumulated in the ER and around the nuclear envelop (Hruska-Hageman et al., 2004; Deval et al., 2006). ASIC2a was highly overlapped with the plasma membrane marker, Lyn-mCherry (Fig. 18, A and C). However, ASIC3 displayed a high overlap coefficient value with the ER marker, mCherry-Cb5 (Fig. 18, B and C), consistent with the previous reports describing a reticular

pattern of ASIC3 (Hruska-Hageman et al., 2004; Deval et al., 2006).

We also examined their subcellular localization by Western blotting on cells expressing GFP-tagged ASIC2a or ASIC3. Immunoblotting with an anti-GFP antibody also revealed a high expression of ASIC2a in the plasma membrane (Fig. 18D). However, we observed a weak ASIC3 band at predicted size in the plasma membrane fraction (Fig. 18D), suggesting that a portion of ASIC3 is also present at the cell surface, consistent with the previous study (Deval et al., 2006). The relative surface level of ASIC2a was about nine-fold higher than that of ASIC3 than that of ASIC3 (Fig. 18D).

N- or C-terminal deletion or both N- and C-terminal deletion from ASIC3 does not rescue ASIC3 from ER accumulation

Previous studies have shown that several membrane receptors or ion channels are retained in the ER when heterologously expressed (Ma and Jan, 2002; Michelsen et al., 2005). Such ER retention of synthesized proteins is generally caused by ER retention/retrieval signals that mostly reside in N- or C-terminal regions of proteins. We investigated whether ASIC3 contains ER retention/retrieval signals in its cytoplasmic tails by constructing N- or C-terminal deleted channels. However, deletion of neither N-terminal 2-43 amino acids (aa) (ASIC3(Δ N)) nor C-terminal 473-530 aa (ASIC3(Δ C)) rescued ASIC3 from ER accumulation, suggesting that ASIC3 may not contain ER retention/retrieval signals in either the N- or C-terminal region we deleted (Fig. 19). The deletion of both N- and C-termini from ASIC3 (ASIC3(Δ N,C)) was also ineffective for the localization of ASIC3 (Fig. 19).

ASIC2a enhances surface expression of ASIC3 by heteromeric assembly

Recently, it has been reported that ASIC2a enhances surface expression of ASIC1a

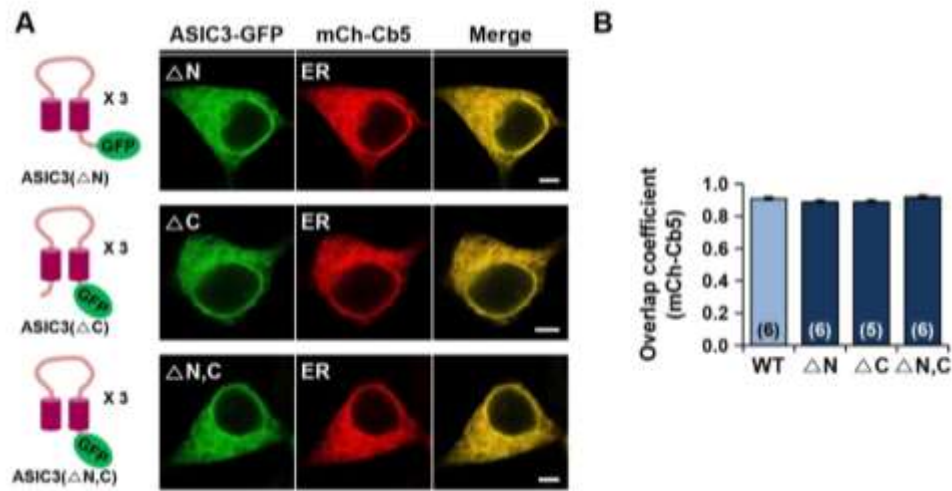


Fig. 19. N- or C-terminal deletion or both N- and C-terminal deletion from ASIC3 does not rescue ASIC3 from ER accumulation. (A) Confocal images of HEK293T cells expressing GFP-tagged ASIC3(Δ N), ASIC3(Δ C), or ASIC3(Δ N,C) with an ER marker (mCh-Cb5). For N- or C-terminal deletion, 2-43 amino acids or 473-530 amino acids were deleted, respectively. Scale bars are 5 μ m. (B) Overlap coefficient value of fluorescent signals (mean \pm SEM). Overlap coefficient value between wild-type (WT) ASIC3 and Cb5 in Fig. 1C was plotted as a control (*light blue*). The number on each bar represents n for each condition.

(Harding et al., 2014; Jiang et al., 2016). To test whether ASIC2a can also deliver ASIC3 to the cell surface, we co-expressed ASIC2a and ASIC3 in HEK293T cells. As shown in Fig. 20A, ASIC3 successfully targeted the cell surface when it was co-expressed with ASIC2a. It was supported by a high overlap coefficient value between two subunits (Fig. 20B). We also examined the relative surface level of ASIC3 in the absence or presence of ASIC2a by Western blotting. As shown in Fig. 20C, the surface level of ASIC3 significantly increased in the presence of ASIC2a.

We then tested heteromeric association between ASIC2a and ASIC3 by using a bimolecular fluorescence complementation (BiFC) assay, which allows the visualization of protein-protein interactions in living cells (Shyu et al., 2006). The C-termini of ASIC2a and

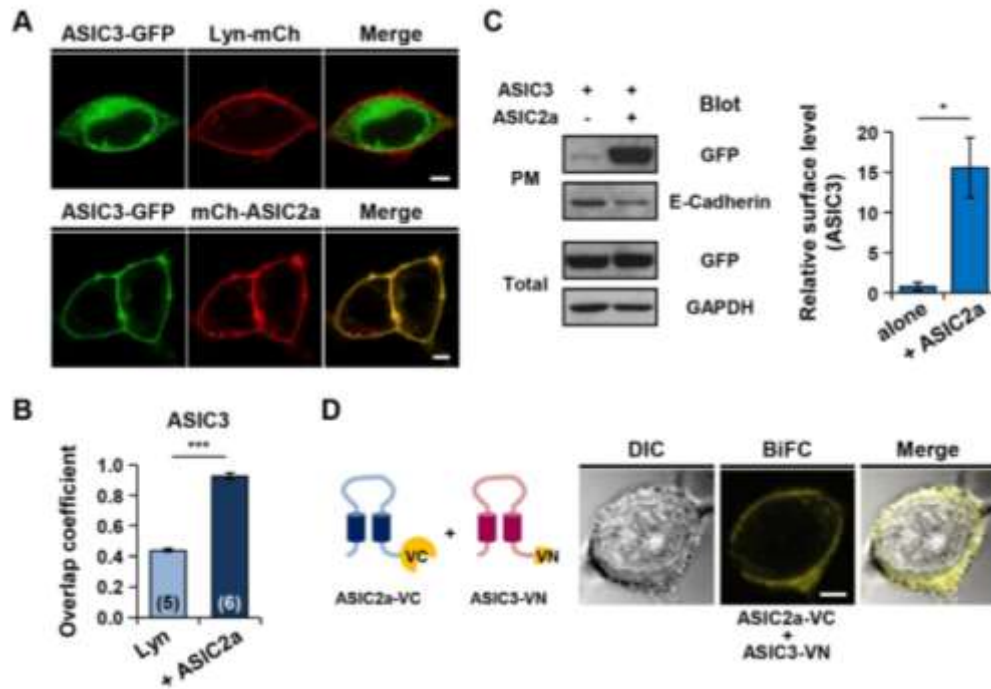


Fig. 20. ASIC2a enhances the surface expression of ASIC3 by heteromeric assembly. (A) Confocal images of HEK293T cells expressing GFP-tagged ASIC3 in the absence or presence of ASIC2a. (B) Overlap coefficient value of fluorescent signals (mean \pm SEM, *** $P < 0.001$, with Student's t -test). Overlap coefficient value between ASIC3 and Lyn in Fig. 1C was plotted as a control (*light blue*). The number on each bar represents n for each condition. (C) Western blotting on the plasma membrane (PM) fraction and the total lysates of cells expressing GFP-tagged ASIC3 in the absence or presence of ASIC2a in pcDNA3.1(+). As controls, the PM and the total lysates were blotted using anti-E-Cadherin and anti-GAPDH antibodies, respectively. The surface level of ASIC3 in the absence or presence of ASIC2a was normalized to that of E-Cadherin (mean \pm SEM, $n=3$ for ASIC3 alone; $n=3$ for ASIC3 with ASIC2a, * $P < 0.05$, with Student's t -test). (D) Confocal images of HEK293T cells co-expressing ASIC2a-VC and ASIC3-VN. Scale bars are 5 μm .

ASIC3 were fused by one of the complementary fragments of the Venus protein, C-terminal half (VC) and N-terminal half (VN), respectively. In cells co-expressing ASIC2a-VC and ASIC3-VN, we detected a BiFC signal in the plasma membrane, which was indicative of the heteromeric association between two subunits (Fig. 20D). However, we

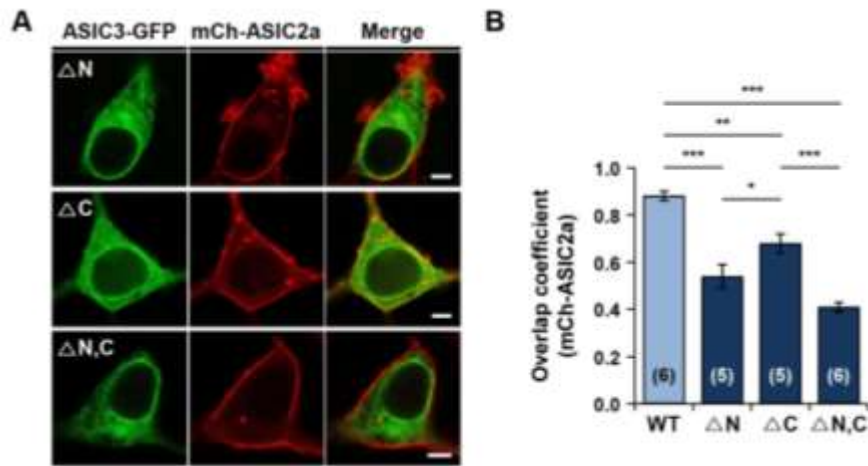


Fig. 21. N- and C-terminal regions of ASIC3 are involved in heteromeric assembly with ASIC2a. (A) Confocal images of HEK293T cells expressing GFP-tagged ASIC3(Δ N), ASIC3(Δ C), or ASIC3(Δ N,C) with ASIC2a. Scale bars are 5 μ m. (B) Overlap coefficient value of fluorescent signals (mean \pm SEM, * $P < 0.05$; ** $P < 0.01$; *** $P < 0.001$, with one-way ANOVA followed by Bonferroni post-hoc test). Overlap coefficient value between wild-type (WT) ASIC3 and ASIC2a in Fig. 2B was plotted as a control (*light blue*). The number on each bar represents n for each condition.

observed no fluorescence when either ASIC2a-VC or ASIC3-VN was expressed alone. These data suggest that ASIC2a delivers ASIC3 to the cell surface through heteromeric assembly. However, when the N- or C-terminus was deleted or both the N- and C-termini were deleted, the ASIC2a-dependent surface trafficking of ASIC3 was significantly decreased (Fig. 21), suggesting that both the N- and C-termini of ASIC3 are involved in the heteromeric assembly of ASIC2a and ASIC3 subunits.

ASIC2a-dependent surface trafficking of ASIC3 increases sustained component of currents

We also performed electrophysiological experiments to investigate whether the ASIC2a-dependent surface trafficking of ASIC3 results in any alterations in ASIC currents. Rapid extracellular pH drop elicited inward currents both in cells expressing ASIC2a or ASIC3

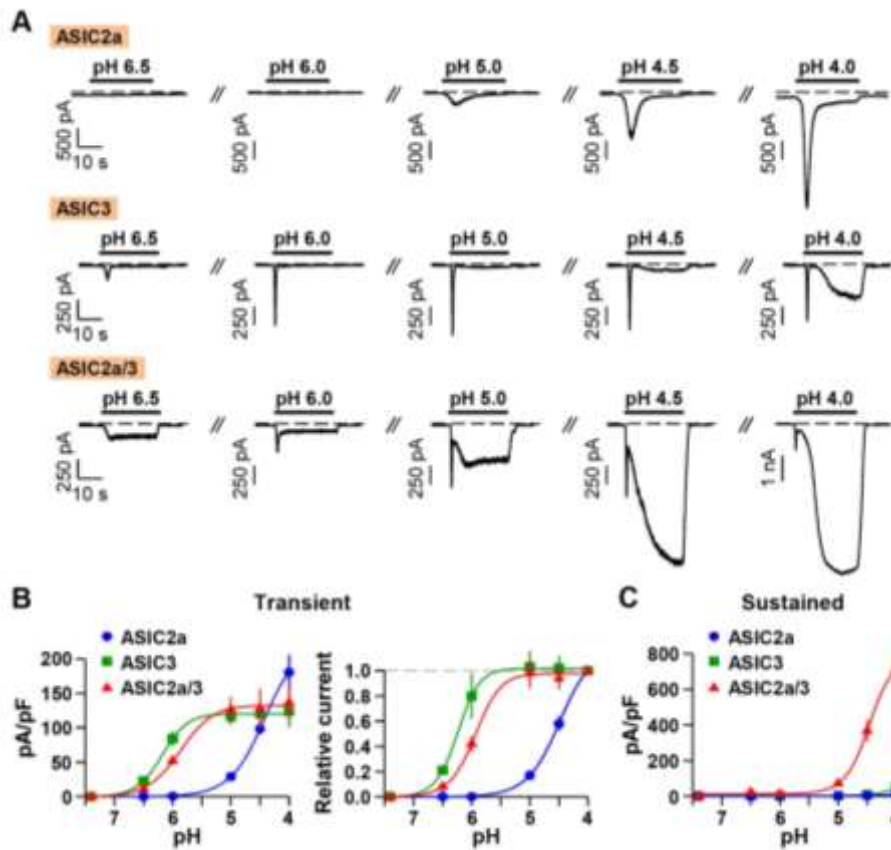


Fig. 22. ASIC2a-dependent surface trafficking of ASIC3 increases sustained currents. (A) Representative acid-evoked current traces of ASIC2a, ASIC3, or ASIC2a/3 channels. pH pulses were applied every 2 min for complete recovery from desensitization. Dashed line indicates the zero current level. (B) Left, pH-dependent current density of transient component of ASIC2a, ASIC3, or ASIC2a/3 currents (mean \pm SEM, $n=5$ for ASIC2a; $n=5$ for ASIC3; $n=7$ for ASIC2a/3). Right, relative current of ASIC2a, ASIC3, or ASIC2a/3 transient currents. Peak current at each pH was divided by pH 4.0-induced peak current in the left graph. (C) pH-dependent current density of sustained component of ASIC2a, ASIC3, or ASIC2a/3 currents (mean \pm SEM, $n=5$ for ASIC2a; $n=5$ for ASIC3; $n=7$ for ASIC2a/3). The pH-dependency curve was fitted with a Hill equation.

(Fig. 22A). As previously reported, ASIC2a generated slowly activating and desensitizing currents, while ASIC3 elicited fast activating and desensitizing transient currents followed by sustained currents (Fig. 22A). ASIC2a generated distinct currents in response to an extracellular pH drop to 5.0 or more acidic, while ASIC3 displayed higher sensitivity to

protons; the half-maximal pH value (pH_{50}) of the ASIC3 transient currents was 6.1 ± 0.2 ($n=5$), while the pH-dependency curve of ASIC2a did not reach a plateau even at pH 4.0, as previously reported (Fig. 22B) (Harding et al., 2014). The sustained currents of ASIC3 were steadily increased by a decreasing extracellular pH value, and it was significantly increased when a pH pulse of 4.0 was applied (Fig. 22, A and C).

In the ASIC2a/3 heteromeric channels, the current density of the transient component was not considerably altered compared with that of the ASIC3 homomeric channels. However, the pH-dependent response curve was shifted to the intermediate between those of ASIC2a and ASIC3; the pH_{50} value of the ASIC2a/3 transient currents was 5.8 ± 0.1 ($n=7$) (Fig. 22B). On the other hand, the sustained component of ASIC2a/3 currents was remarkably increased compared with those of ASIC2a or ASIC3 homomeric currents (Fig. 22, A and C). The current density of ASIC2a/3 sustained currents was about 14-fold higher than that of ASIC3 sustained currents at pH 4.0 (Fig. 22C). Several studies have reported that heterologously expressed ASIC2a/3 channels generate robust currents (Babinski et al., 2000; Hesselager et al., 2004; Hattori et al., 2009). Our data suggest that an ASIC2a-dependent increase of ASIC3 surface expression may underlie these significantly enhanced sustained currents in ASIC2a/3 heteromeric channels.

Surface expression of ASIC3 is increased in the presence of ASIC2a in SH-SY5Y cells

Since ASIC2a and ASIC3 are co-expressed in several human tissues (Babinski et al., 2000), we tested whether the ASIC2a-dependent trafficking of ASIC3 also occurred in neuroblastoma SH-SY5Y cells. As observed in HEK293T cells, ASIC2a and ASIC3 displayed differential subcellular localization. ASIC2a was primarily distributed at the cell surface, like RFP-PH (PLC δ), a plasma membrane PI(4,5)P₂ probe (Fig. 23A). However, ASIC3 was accumulated in the ER and efficiently trafficked to the cell surface in the

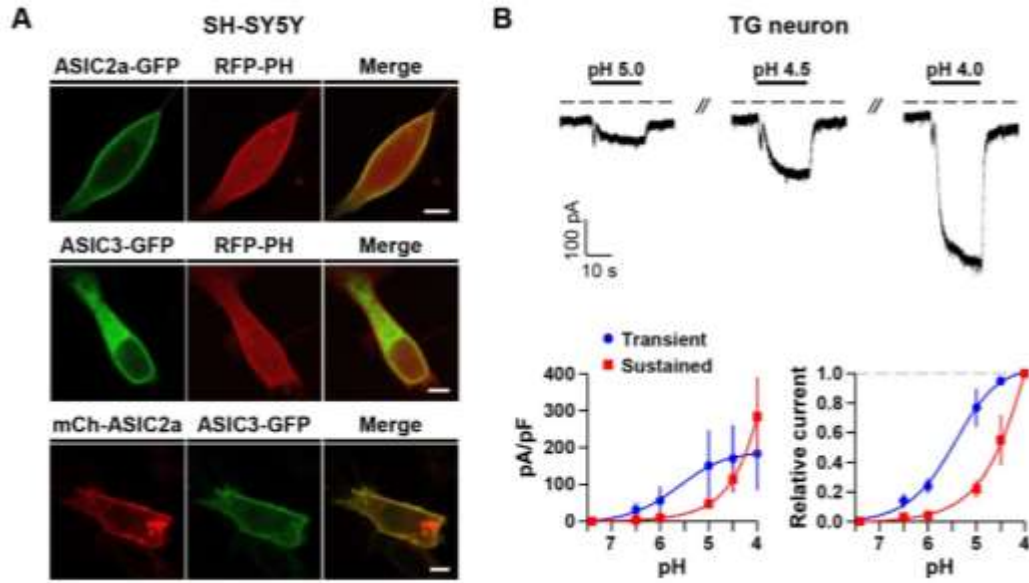


Fig. 23. ASIC2a-dependent surface expression of ASIC3 in SH-SY5Y cells and proton-induced currents in native neurons. (A) Confocal images of SH-SY5Y cells expressing GFP-tagged ASIC2a or ASIC3 with RFP-PH. Surface expression of ASIC3 is increased when it is co-expressed with ASIC2a. Scale bars are 5 μ m. (B) Proton-activated currents in trigeminal ganglion (TG) neurons. Left, pH-dependent current density (mean \pm SEM, n=4). Right, relative current. Peak current at each pH was divided by pH 4.0-induced peak current in the left graph. The pH-dependency curve was fitted with a Hill equation.

presence of ASIC2a (Fig. 23A). These results consistently demonstrate the significant role of ASIC2a in promoting the surface expression of ASIC3.

We also measured proton-induced currents in trigeminal ganglion (TG) neurons. According to the previous study, ASIC1, ASIC2a, and ASIC3 are highly expressed in TG neurons (Fu et al., 2016). In the middle-size (30–40 μ m in diameter) neurons, we observed similar current patterns to those observed in HEK293T cells co-expressing ASIC2a and ASIC3. The sustained currents remarkably increased at pH 4.0, and the pH₅₀ value of the transient currents was 5.4 ± 0.4 (n=4) (Fig. 23B).

Lastly, we tested whether ASIC2b, a splicing variant of ASIC2a, can also deliver ASIC3 to the cell surface. ASIC2b has different amino acid sequences in the N-terminus,

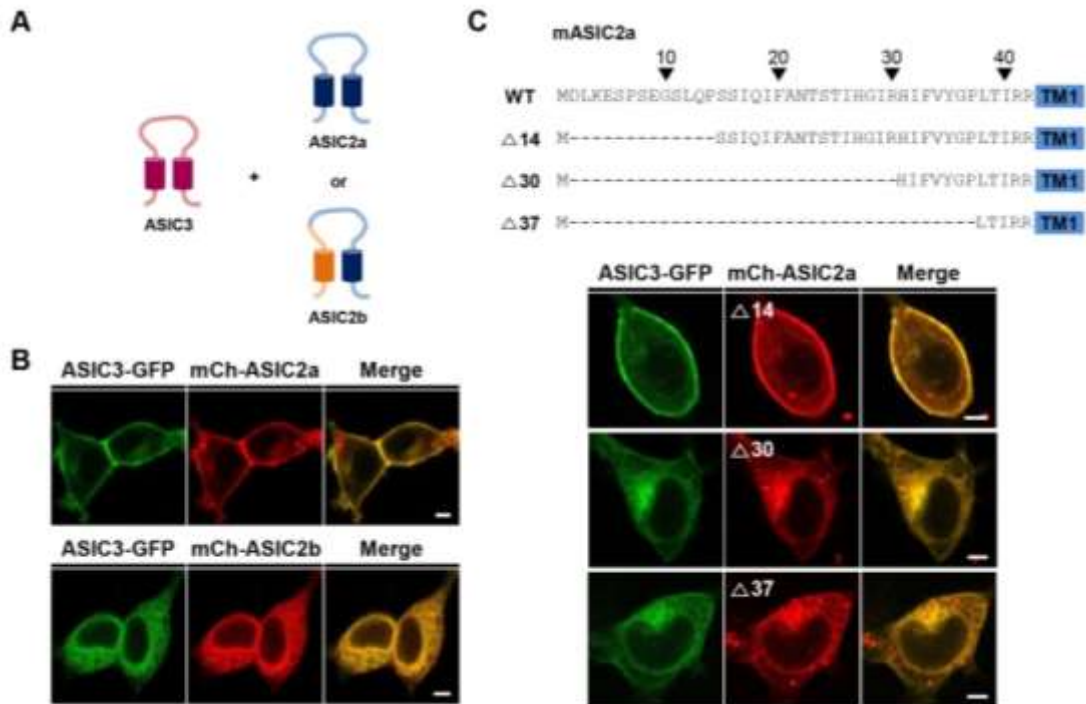


Fig. 24. N-terminal 15-30 amino acids of ASIC2a are critical for membrane targeting of ASIC2a and ASIC2a-dependent surface trafficking of ASIC3. (A) ASIC3 was co-expressed with ASIC2a or ASIC2b. ASIC2b has different amino acid sequences in the N-terminus, the first transmembrane domain, and one third of extracellular loop. (B) Confocal images of HEK293T cells expressing GFP-tagged ASIC3 in the presence of ASIC2a or ASIC2b. (C) Schematic diagram of N-terminal deletion of ASIC2a. Confocal images of HEK293T cells expressing GFP-tagged ASIC3 in the presence of ASIC2a(Δ 14), ASIC2a(Δ 30), or ASIC2a(Δ 37). Scale bars are 5 μ m.

the first transmembrane domain, and one third of the extracellular loop. Unlike ASIC2a, ASIC2b did not deliver ASIC3 to the cell surface (Fig. 24B). ASIC2b was not even localized in the plasma membrane alone, as previously reported (Wu et al., 2016). To test whether the N-terminus of ASIC2a has a critical region for the membrane targeting of ASIC2a, we deleted 2-37 aa from ASIC2a. ASIC2a(Δ 37) mostly resided in the cytoplasmic area with ASIC3, and this mutated ASIC2a did not deliver ASIC3 to the cell surface (Fig. 24C). For further analysis, we made more deleted ASIC2a. The deletion of 2-

14 aa from ASIC2a had no effect on the membrane localization of ASIC2a and delivery of ASIC3 to the cell surface. However, the further deletion of ASIC2a disrupted the membrane localization of ASIC2a, and this ASIC2a(Δ 30) could not deliver ASIC3 to the cell surface, suggesting that the critical region responsible for the membrane targeting of ASIC2a and for enhancing the surface expression of ASIC3 is located in 15-30 aa of ASIC2a.

IV. DISCUSSION

4. 1. Regulation of acid-sensing ion channels (ASICs) by membrane phospholipids

In this study, we observed that the activities of ASICs are independent of membrane phosphoinositides such as PI(4)P, PI(4,5)P₂, and possibly PI(3,4,5)P₃ by using the translocatable phosphatase system. This is the first report to show the sensitivities of ASICs toward phosphoinositides with direct manipulation of membrane phosphoinositides in intact cells. On the other hand, studies about TRPV1 sensitivity toward phosphoinositides have been undertaken by various research groups. In our system, we observed that proton-activated TRPV1 currents can be regulated by simultaneous manipulation of PI(4)P and PI(4,5)P₂ level, not PI(3,4,5)P₃ level, in intact cells.

Although both ASICs and TRPV1 channels can sense proton-mediated signaling, their expression and biophysical properties are different. ASICs are widely distributed throughout the CNS and the PNS, and they act as transducers of multiple sensory and synaptic signaling. TRPV1 is highly expressed in peripheral nerve endings of primary sensory neurons. Multimodal response of TRPV1 to various noxious stimuli elicits pain and leads to the development of hyperalgesia (Basbaum et al., 2009). According to previous studies, ASICs and TRPV1 are co-localized in a great part of subpopulation of DRG neurons, although there are differences between species (Ugawa et al., 2005; Leffler et al., 2006). In rat DRG neurons, ASIC1a and ASIC3 transcripts were detected in approximately 40–45% and 30% of the TRPV1-positive neurons, respectively (Ugawa et al., 2005). In these subsets of native sensory neurons, it is highly possible that the currents elicited by tissue acidosis are contributed from both ASICs and TRPV1 channels.

It is noteworthy that two channels are activated by different ranges of pH value. TRPV1 is activated by more severe acidification (pH_{0.5} activation of 5.4) than that required

to activate most ASIC subunits (Tominaga et al., 1998; Kweon and Suh, 2013). ASIC1a and ASIC3 are sensitive to moderate pH drop (pH_{0.5} activation of 6.2–6.8 for ASIC1a and 6.2–6.7 for ASIC3), whereas ASIC2a requires more severe acidification for activation (pH_{0.5} activation of 3.8–5.0) (Kweon and Suh, 2013). Interestingly, extracellular protons have a dual effect on TRPV1 currents. At low pH (< 6.0), protons themselves activate the channel at room temperature. However, protons potentiate the channel already opened by other stimuli (capsaicin or heat) by lowering the threshold for channel activation at higher pH levels (6–7.4) (Tominaga et al., 1998; Jordt et al., 2000; Aneiros et al., 2011). Therefore, ASICs are considered main mediators of pain induced by moderate tissue acidosis, while TRPV1 is thought to contribute to more severe acidosis-mediated pain perception, together with ASICs in peripheral sensory neurons (Deval et al., 2010). Hence, the complementary roles of these two proton-sensitive ion channels, ASICs and TRPV1, have great significance for perception of pH changes; thus, to understand the regulatory mechanisms of those channels is quite important.

Phosphoinositides have emerged as general regulators of ion channels, and PI(4,5)P₂ is known to stabilize the open state of many ion channels (Kweon and Suh, 2013; Suh and Hille, 2002; Yue et al., 2002; Pochynyuk et al., 2006; Suh et al., 2006; Hardie, 2007; Pochynyuk et al., 2007; Suh and Hille, 2008; Suh et al., 2010). However, regulation of TRPV1 by phosphoinositides is controversial (Chuang et al., 2001; Liu et al., 2005; Stein et al., 2006; Lukacs et al., 2007; Klein et al., 2008; Cao et al., 2013; Lukacs et al., 2013a, Lukacs et al., 2013b, Senning et al., 2014). In this study, we simply tested the effects of phosphoinositides on proton-activated TRPV1 currents by using a rapamycin-inducible PJ system, and compared the results with that of ASICs. We observed that proton-activated TRPV1 currents are significantly inhibited by the recruitment of PJ, while the translocation of INPP5E had no statistically significant effect on the currents (Fig. 2).

These results are consistent with the study by Hammond *et al.* (Hammond et al., 2012). They observed that capsaicin-activated TRPV1 currents in HEK293 cells are inhibited when both PI(4)P and PI(4,5)P₂ are depleted by the translocation of PJ (Hammond et al., 2012). In contrast to TRPV1 channels, the function of ASICs does not rely on PM phosphoinositides. By using the PJ system, we confirmed that homomeric ASIC1a, ASIC2a, and ASIC3 channels and heteromeric ASIC1a/2a, ASIC1a/3, and ASIC2a/3 channels are insensitive to PI(4)P and PI(4,5)P₂. These results are, in fact, unexpected since one previous study reported that activation of M₁R by its agonist, oxotremorine-M (Oxo-M), inhibited ASIC currents in Chinese hamster ovary (CHO) cells heterologously expressing ASIC1a and M₁R, and also in isolated rat hippocampus CA1 and striatum interneurons (Dorofeeva et al., 2009). That study suggested that muscarinic inhibition of ASIC1a currents could be due to depletion of PI(4,5)P₂ available to the channel (Dorofeeva et al., 2009); however, we observed no dependence of ASICs on PI(4)P or PI(4,5)P₂ (Figs. 3 and 4). Therefore, it is possible that inhibition of ASIC currents by M₁R activation might occur through mechanisms other than direct action of PI(4,5)P₂ hydrolysis. We also tried to test whether the activation of M₁R by Oxo-M modulates the function of homomeric ASIC1a channels in either tsA201 or CHO cells. However, we observed no inhibition of ASIC1a currents by M₁R activation in either type of cells (unpublished observations). In another previous study by Li et al. (2012), they found that supplementing the pipette solution with a short-chain PIP₂ was not effective to decrease the desensitization of ASIC1a currents. Furthermore, they observed that the currents were not regulated by activation of muscarinic receptor (Li et al., 2012). The discrepancy between the studies is not clear; however, in our system, using the translocatable PJ system, we verified that the activities of ASICs are independent from PM phosphoinositides.

We also investigated the dependence of ASICs and TRPV1 channels on

PI(3,4,5)P₃. ENaC and some families of TRP channels such as TRPM4 are known to have sensitivities toward PI(3,4,5)P₃ as well as PI(4,5)P₂ (Yue et al., 2002; Zhang et al., 2005; Pochynyuk et al., 2006; Pochynyuk et al., 2007). To selectively dephosphorylate PI(3,4,5)P₃, we generated a novel engineered phosphatase tool from PTEN, which is a well characterized 3-phosphatase that prefers PI(3,4,5)P₃ as a substrate (Iwasaki et al., 2008). By using a chimeric protein CF-PTEN, we observed that neither ASICs nor TRPV1 currents were altered by depletion of membrane PI(3,4,5)P₃ in intact cells.

Finally, we compared differential regulatory features of ASICs and TRPV1 by AA, a pro-inflammatory mediator released from phospholipids. In our experiments, AA induced significant potentiation of all ASIC1a, ASIC2a, ASIC3, and TRPV1 channels. TRPV1 currents were particularly more sensitive to AA than ASIC currents were. It is noteworthy that potentiated ASIC currents by AA were, remarkably, almost fully recovered to the initial level of the currents, while TRPV1 currents were partially recovered after washout of AA (Figs. 6 and 7). We propose that this is likely due to the difference in regulatory mechanisms of those channels by AA. The potentiating effect of AA on TRPV1 currents has been reported to result from the AA metabolites of lipoxygenase pathways, such as 12- and 15-hydroperoxyeicosatetraenoic acid (HPETE) (Hwang et al., 2000; Shin et al., 2002). However, a recent study suggested that both AA and its metabolites can produce marked sensitization of TRPV1 currents in the reconstituted liposome, allowing them to observe the direct effects of factors in the absence of other cellular enzymes (Cao et al., 2013). Therefore, AA seems to regulate the TRPV1 channels by both a direct and an indirect action through the metabolism pathways. On the other hand, ASICs are thought to be directly regulated by AA (Smith et al., 2007a). One previous study reported that inhibition of lipoxygenase or cyclooxygenase pathway did not impair the potentiating effect of AA on ASIC currents (Smith et al., 2007a). Therefore, ASICs and TRPV1 channels are

differentially regulated by a pro-inflammatory mediator AA.

In this study, we observed that two proton-sensitive ion channels, ASICs and TRPV1, display differential regulatory features by membrane phosphoinositides and AA. Their different topology, distribution, and biophysical properties might establish different sensitivities toward phospholipids. Understanding the relationship between these two groups of channels, and their relative contributions in proton-mediated signaling, is quite important for comprehending the complementary roles of ASICs and TRPV1 in the nervous system.

4. 2. Surface trafficking mechanisms of acid-sensing ion channels (ASICs)

This study concerns different surface trafficking mechanism and proton-sensitivity of ASIC2 isoforms, ASIC2a and ASIC2b. We took advantage of the recombinant expression system to discern hidden trafficking mechanisms of ASIC2 proteins. We observed that two subunits display dramatically different subcellular localization when expressed alone in heterologous expression systems including HEK293T and neuroblastoma SH-SY5Y cells: ASIC2a targets the cell surface by itself, while ASIC2b resides in the ER. This finding is quite unexpected, because several studies previously reported that ASIC2b normally traffics to the cell surface (Smith et al., 2007b; Schuhmacher et al., 2015). However, quite recently, one research group reported that ASIC2a and ASIC2b have different subcellular distribution in NIH 3T3 cells (Wu et al., 2016). In our study, we further investigated underlying mechanisms for this differential localization. By constructing a series of chimeras, we identified the TM1 and the proximal post-TM1 domain of ASIC2a as critical regions required for membrane targeting of ASIC2.

When these regions in ASIC2b were replaced by equivalent sequences of ASIC2a (Fig. 11, cf. 2b-TP), this chimera successfully trafficked to the cell surface. Moreover, this

chimeric channel evoked proton-activated currents, although the biophysical properties were different from those of ASIC2a currents (Figs. 11 and 12). The alterations in the current shape, time constant for desensitization, activation rate, and desensitizing property to successive pH stimuli were largely dependent on the intracellular N-terminus. When the N-terminus in 2b-TP was replaced by that of ASIC2a (Fig. 10, cf. Ch3), this chimera produced ASIC2a-like currents in response to protons, although the current density was smaller than that of ASIC2a (Figs. 10 and 12). Considering 2a-N and 2a-T, which showed similar current density to that of ASIC2a, we can infer that the decrease in the current density of Ch3 and 2b-TP might be due to the lack of ASIC2a amino acid sequences from 86 to 185, and that proton-binding sites involved in the current density are present in this region.

In the chimera assay, we found that proton-sensitivity of Ch3, 2b-TP, 2a-N, and 2a-T are critically dependent on their proximal post-TM1 domain (17 amino acids) sequences from ASIC2a as well as surface expression. We could not detect any proton-activated currents from the chimeras containing the proximal post-TM1 domain sequences from ASIC2b, even though they were apparently expressed in the plasma membrane (Figs. 10 and 11; Ch2, 2a-P, and 2b-T). Indeed, 17 amino acids from ASIC2a after the TM1 domain include H72, D77, and E78 of five putative proton-binding sites previously identified by others (Baron et al., 2001; Smith et al., 2007b). By using site-directed mutagenesis, we determined that H72 and E78 are critical residues for proton-sensitivity of Ch3 (Fig. 13). However, D77 seems to be involved in determining subcellular localization as well as proton-sensitivity of channels, inconsistent with the previous report (Smith et al., 2007b). Based on these results, we concluded that three amino acids (H72, D77, and E78) are all necessary for proton-sensitivity of channels. However, importantly, the chimera containing the proximal post-TM1 domain from ASIC2a was still insensitive to protons,

since it was not expressed in the cell surface (Fig. 11, cf. 2b-P). This result indicates that the proximal post-TM1 domain from ASIC2a does not always ensure proton-sensitivity of channels.

Through these studies, we identified the minimum region of ASIC2a extracellular domain required for proton-sensing of ASIC2 proteins as the first 17 amino acids that include H72, D77, and E78 after the TM1 domain. These results are quite different with the previous study that identified the first 87 amino acids after the TM1 domain as the minimal region required for ASIC2 activation by protons (Schuhmacher et al., 2015). In that study, they could not detect any proton-activated currents from five chimeras (AB3, AB4, AB10, AB11, and AB11-4). This was the case even though all of the chimeras contained H72, D77, and E78, which had been previously identified as putative proton-binding sites by the same group (Smith et al., 2007b). They reported that proton-insensitivity of these chimeras is due to inability of protons to activate the chimeric channels rather than disrupted surface expression (Schuhmacher et al., 2015). Their study is different from ours in several points, such as species of clones, cell type used in the experiments, and the length of the TM1 domains. Our chimeras were constructed based on the sequences from the study of Jasti and colleagues (V43 to F68 for the TM1 of ASIC2a; A87 to L112 for the TM1 of ASIC2b) (Jasti et al., 2007), while they used shorter amino acid sequences for the TM1 domains. However, it is not clear whether these factors can account for the discrepancy in the minimal region of ASIC2a extracellular domain required for proton-sensitivity.

For the efficient trafficking of ASIC2 to the plasma membrane, orchestrated work of the TM1 domain and neighboring regions such as the N-terminus and the proximal post-TM1 domain is necessary. As illustrated in Fig. 11, exchange of the TM1 domain in ASIC2a to that of ASIC2b markedly decreased surface expression of the channel (cf. 2a-T).

In addition, insertion of ASIC2a TM1 domain into ASIC2b promoted forward trafficking of ASIC2b (Fig. 11, cf. 2b-T), indicating that the TM1 domain of ASIC2a is critical for targeting the cell surface. However, when the N-terminus and the proximal post-TM1 domain were further replaced, the ability of the chimeric channel for trafficking was completely abolished (Fig. 11, cf. 2a-NTP) or enhanced (Fig. 10, cf. Ch3). These results indicate that neighboring regions of the TM1 domain are also involved in trafficking of the channel.

Finally, we showed that ASIC2b can traffic to the cell surface when it is co-expressed with ASIC2a. We verified the association between two subunits using Co-IP, Duolink PLA, and BiFC assay. According to the BiFC experiments, ER accumulation of ASIC2b is due to the lack of forward trafficking signals rather than inability to assemble by itself (Fig. 14). Surface trafficking of ASIC2b by the association with ASIC2a might be facilitated by membrane targeting domains that reside in ASIC2a. However, we also found that the N-terminal region of ASIC2a is necessary for the ASIC2a-dependent membrane targeting of ASIC2b (Fig. 17).

Recently, emerging role of ASIC2a in facilitating surface expression of ASIC1a has been reported (Harding et al., 2014; Jiang et al., 2016). Our finding further proves an important role of ASIC2a in surface trafficking of ASIC2b. We directly showed another critical meaning of heteromerization of ASICs other than the alterations in the biophysical properties of channels. However, we could not find a specific forward trafficking signal motif that might reside in the TM1 and the proximal post-TM1 domain of ASIC2a. Further investigation to find an anterograde signal that resides in ASIC2a and the role of ASIC2a in trafficking of other ASIC subunits will provide insight into surface targeting mechanisms of ASICs as well as strategies for developing therapeutic agents.

In the last part of this study, we additionally show that ASIC3 traffics to the cell

surface in an ASIC2a-dependent manner. Since sustained currents are primarily mediated by ASIC3, the largely increased sustained currents in ASIC2a/3 heteromeric channels seem to be caused by the ASIC2a-dependent surface trafficking of ASIC3. According to the previous studies, the co-expression of ASIC2a and ASIC3 elicits proton-activated currents with changed biophysical properties (Babinski et al., 2000; Hesselager et al., 2004; Hattori et al., 2009). These alterations were recognized as evidence for the functional interaction between two subunits (Babinski et al., 2000; Hesselager et al., 2004; Hattori et al., 2009). By using BiFC and the patch clamp technique, we found that the heteromeric association between ASIC2a and ASIC3 subunits forms proton-sensitive channels with remarkably enhanced sustained currents. We directly show another significant finding of the heteromerization of two subunits by revealing new trafficking mechanisms of ASICs.

V. REFERENCES

1. Allen, N. J. and Attwell, D. (2002) Modulation of ASIC channels in rat cerebellar Purkinje neurons by ischaemia-related signals. *J. Physiol.* **543**, 521-529.
2. Aneiros, E., Cao, L., Papakosta, M., Stevens, E. B., Phillips, S., et al. (2011) The biophysical and molecular basis of TRPV1 proton gating. *EMBO J.* **30**, 994-1002.
3. Askwith, C. C., Wemmie, J. A., Price, M. P., Rokhlina, T., and Welsh, M. J. (2004) Acid-sensing ion channel 2 (ASIC2) modulates ASIC1 H⁺-activated currents in hippocampal neurons. *J. Biol. Chem.* **279**, 18296-18305.
4. Babinski, K., Catarsi, S., Biagini, G., and Séguéla, P. (2000) Mammalian ASIC2a and ASIC3 subunits co-assemble into heteromeric proton-gated channels sensitive to Gd³⁺. *J. Biol. Chem.* **275**, 28519-28525.
5. Balla, A., Kim, Y. J., Varnai, P., Szentpetery, Z., Knight, Z., et al. (2008) Maintenance of hormone-sensitive phosphoinositide pools in the plasma membrane requires phosphatidylinositol 4-kinase III α . *Mol. Biol. Cell* **19**, 711-721.
6. Baron, A., Schaefer, L., Lingueglia, E., Champigny, G., and Lazdunski, M. (2001) Zn²⁺ and H⁺ are coactivators of acid-sensing ion channels. *J. Biol. Chem.* **276**, 35361-35367.
7. Basbaum, A. I., Bautista, D. M., Scherrer, G., and Julius, D. (2009) Cellular and molecular mechanisms of pain. *Cell* **139**, 267-284.
8. Bermak, J. C., Li, M., Bullock, C., and Zhou, Q. Y. (2001) Regulation of transport of the dopamine D1 receptor by a new membrane-associated ER protein. *Nat. Cell Biol.* **3**, 492-498.

9. Bichet, D., Cornet, V., Geib, S., Carlier, E., Volsen, S., et al. (2000) The I-II loop of the Ca²⁺ channel α_1 subunit contains an endoplasmic reticulum retention signal antagonized by the β subunit. *Neuron* **25**, 177-190.
10. Burke, J. E. and Dennis, E. A. (2009) Phospholipase A₂ structure/function, mechanism, and signaling. *J. Lipid Res.* **50**, S237-242.
11. Cao, E., Cordero-Morales, J. F., Liu, B., Qin, F., and Julius, D. (2013) TRPV1 channels are intrinsically heat sensitive and negatively regulated by phosphoinositide lipids. *Neuron* **77**, 667-679.
12. Chai, S., Li, M., Lan, J., Xiong, Z. G., Saugstad, J. A., et al. (2007) A kinase-anchoring protein 150 and calcineurin are involved in regulation of acid-sensing ion channels ASIC1a and ASIC2a. *J. Biol. Chem.* **282**, 22668-22677.
13. Chai, S., Li, M., Branigan, D., Xiong, Z. G., and Simon, R. P. (2010) Activation of acid-sensing ion channel 1a (ASIC1a) by surface trafficking. *J. Biol. Chem.* **285**, 13002-13011.
14. Chang, X. B., Cui, L., Hou, Y. X., Jensen, T. J., Aleksandrov, A. A., et al. (1999) Removal of multiple arginine-framed trafficking signals overcomes misprocessing of delta F508 CFTR present in most patients with cystic fibrosis. *Mol. Cell* **4**, 137-142.
15. Chen, X. and Gründer, S. (2007) Permeating protons contribute to tachyphylaxis of the acid-sensing ion channel (ASIC) 1a. *J. Physiol.* **579**, 657-670.
16. Chen, C. C. and Wong, C. W. (2013) Neurosensory mechanotransduction through acid-sensing ion channels. *J. Cell Mol. Med.* **17**, 337-349.
17. Chuang, H. H., Prescott, E. D., Kong, H., Shields, S., Jordt, S. E., et al. (2001) Bradykinin and nerve growth factor release the capsaicin receptor from PtdIns(4,5)P₂-mediated inhibition. *Nature* **411**, 957-962.

18. Chyb, S., Raghu, P., and Hardie, R. C. (1999) Polyunsaturated fatty acids activate the *Drosophila* light-sensitive channels TRP and TRPL. *Nature* **397**, 255-259.
19. Cunningham, M. R., McIntosh, K. A., Pediani, J. D., Robben, J., Cooke, A. E., et al. (2012) Novel role for proteinase-activated receptor 2 (PAR₂) in membrane trafficking of proteinase-activated receptor 4 (PAR₄). *J. Biol. Chem.* **287**, 16656-16669.
20. Das, S., Dixon, J. E., and Cho, W. (2003) Membrane-binding and activation mechanism of PTEN. *Proc. Natl. Acad. Sci. U.S.A.* **100**, 7491-7496.
21. DeRose, R., Miyamoto, T., and Inoue, T. (2013) Manipulating signaling at will: chemically-inducible dimerization (CID) techniques resolve problems in cell biology. *Pflugers. Arch.* **465**, 409-417.
22. Deval, E., Friend, V., Thirant, C., Salinas, M., Jodar, M., et al. (2006) Regulation of sensory neuron-specific acid-sensing ion channel 3 by the adaptor protein Na⁺/H⁺ exchanger regulatory factor-1. *J. Biol. Chem.* **281**, 1796-1807.
23. Deval, E., Noël, J., Lay, N., Alloui, A., Diochot, S., et al. (2008) ASIC3, a sensor of acidic and primary inflammatory pain. *EMBO J.* **27**, 3047-3055.
24. Deval, E., Gasull, X., Noël, J., Salinas, M., Baron, A., et al. (2010) Acid-sensing ion channels (ASICs): pharmacology and implication in pain. *Pharmacol. Ther.* **128**, 549-558.
25. Donier, E., Rugiero, F., Jacob, C., and Wood, J. N. (2008) Regulation of ASIC activity by ASIC4- new insights into ASIC channel function revealed by a yeast two-hybrid assay. *Eur. J. Neurosci.* **28**, 74-86.
26. Dorofeeva, N. A., Karpushev, A. V., Nikolaev, M. V., Bolshakov, K. V., Stockand, J. D., et al. (2009) Muscarinic M₁ modulation of acid-sensing ion channels. *Neuroreport* **20**, 1386-1391.

27. Du, J., Reznikov, L. R., Price, M. P., Zha, X. M., Lu, Y., et al. (2014) Protons are a neurotransmitter that regulates synaptic plasticity in the lateral amygdala. *Proc. Natl. Acad. Sci. U.S.A.* **111**, 8961-8966.
28. DuBridge, R. B., Tang, P., Hsia, H. C., Leong, P. M., Miller, J. H., et al. (1987) Analysis of mutation in human cells by using an Epstein-Barr virus shuttle system. *Mol. Cell Biol.* **7**, 379-387.
29. Falkenburger, B. H., Jensen, J. B., Dickson, E. J., Suh, B. C., and Hille, B. (2010) Phosphoinositides: lipid regulators of membrane proteins. *J. Physiol.* **588**, 3179-3185.
30. Fu, H., Fang, P., Zhou, H. Y., Zhou, J., Yu, X. W., et al. (2016) Acid-sensing ion channels in trigeminal ganglion neurons innervating the orofacial region contribute to orofacial inflammatory pain. *Clin. Exp. Pharmacol. Physiol.* **43**, 193-202.
31. Ghosh, M., Tucker, D. E., Burchett, S. A., and Leslie, C. C. (2006) Properties of the Group IV phospholipase A₂ family. *Prog. Lipid Res.* **45**, 487-510.
32. Gonzales, E. B., Kawate, T., and Gouaux, E. (2009) Pore architecture and ion sites in acid-sensing ion channels and P2X receptors. *Nature* **460**, 599-604.
33. Grifoni, S. C., McKey, S. E., and Drummond, H. A. (2008) Hsc70 regulates cell surface ASIC2 expression and vascular smooth muscle cell migration. *Am. J. Physiol. Heart Circ. Physiol.* **294**, H2022-2030.
34. Hardie, R. C. (2007) TRP channels and lipids: from Drosophila to mammalian physiology. *J. Physiol.* **578**, 9-24.
35. Hammond, G. R., Fischer, M. J., Anderson, K. E., Holdich, J., Koteci, A., et al. (2012) PI4P and PI(4,5)P₂ are essential but independent lipid determinants of membrane identity. *Science* **337**, 727-730.

36. Harding, A. M., Kusama, N., Hattori, T., Gautam, M., and Benson, C. J. (2014) ASIC2 subunits facilitate expression at the cell surface and confer regulation by PSD-95. *PLoS one* **9**, e93797.
37. Hattori, T., Chen, J., Harding, A. M., Price, M. P., Lu, Y., et al. (2009) ASIC2a and ASIC3 heteromultimerize to form pH-sensitive channels in mouse cardiac dorsal root ganglia neurons. *Circ. Res.* **105**, 279-286.
38. Hesselager, M., Timmermann, D. B., and Ahring, P. K. (2004) pH Dependency and desensitization kinetics of heterologously expressed combinations of acid-sensing ion channel subunits. *J. Biol. Chem.* **279**, 11006-11015.
39. Hilgemann, D. W. and Ball, R. (1996) Regulation of cardiac Na^+ , Ca^{2+} exchange and K_{ATP} potassium channels by PIP_2 . *Science* **273**, 956-959.
40. Horowitz, L. F., Hirdes, W., Suh, B. C., Hilgemann, D. W., Mackie, K., et al. (2005) Phospholipase C in living cells: activation, inhibition, Ca^{2+} requirement, and regulation of M current. *J. Gen. Physiol.* **126**, 243-262.
41. Hruska-Hageman, A. M., Benson, C. J., Leonard, A. S., Price, M. P., and Welsh, M. J. (2004) PSD-95 and Lin-7b interact with acid-sensing ion channel-3 and have opposite effects on H^+ -gated current. *J. Biol. Chem.* **279**, 46962-46968.
42. Hruska-Hageman, A. M., Wemmie, J. A., Price, M. P., and Welsh, M. J. (2002) Interaction of the synaptic protein PICK1 (protein interacting with C kinase 1) with the non-voltage gated sodium channels BNC1 (brain Na^+ channel 1) and ASIC (acid-sensing ion channel). *Biochem. J.* **361**, 443-450.
43. Hwang, E. M., Kim, E., Yarishkin, O., Woo, D. H., Han, K. S., et al. (2014) A disulphide-linked heterodimer of TWIK-1 and TREK-1 mediates passive conductance in astrocytes. *Nat. Commun.* **5**, 3227.

44. Ikeuchi, M., Kolker, S. J., Burnes, L. A., Walder, R. Y., and Sluka, K. A. (2008) Role of ASIC3 in the primary and secondary hyperalgesia produced by joint inflammation in mice. *Pain* **137**, 662-669.
45. Iwasaki, H., Murata, Y., Kim, Y., Hossain, M. I., Worby, C. A., et al. (2008) A voltage-sensing phosphatase, Ci-VSP, which shares sequence identity with PTEN, dephosphorylates phosphatidylinositol 4,5-bisphosphate. *Proc. Natl. Acad. Sci. U.S.A.* **105**, 7970-7975.
46. Jasti, J., Furukawa, H., Gonzales, E. B., and Gouaux, E. (2007) Structure of acid-sensing ion channel 1 at 1.9 Å resolution and low pH. *Nature* **449**, 316-323.
47. Jiang, N., Wu, J., Leng, T., Yang, T., Zhou, Y., et al. (2016) Region specific contribution of ASIC2 to acidosis-and ischemia-induced neuronal injury. *J. Cereb. Blood Flow Metab.* In press.
48. Jordt, S. E., Tominaga, M., and Julius, D. (2000) Acid potentiation of the capsaicin receptor determined by a key extracellular site. *Proc. Natl. Acad. Sci. U.S.A.* **97**, 8134-8139.
49. Klein, R. M., Ufret-Vincenty, C. A., Hua, L., and Gordon, S. E. (2008) Determinants of molecular specificity in phosphoinositide regulation. Phosphatidylinositol (4,5)-bisphosphate (PI(4,5)P₂) is the endogenous lipid regulating TRPV1. *J. Biol. Chem.* **283**, 26208-26216.
50. Kweon, H. J., Yu, S. Y., Kim, D. I., and Suh, B. C. (2015) Differential regulation of proton-sensitive ion channels by phospholipids: a comparative study between ASICs and TRPV1. *PLoS one* **10**, e0122014.
51. Kweon, H. J. and Suh, B. C. (2013) Acid-sensing ion channels (ASICs): therapeutic targets for neurological diseases and their regulation. *BMB Rep.* **46**, 295-304.

52. Lacroix, J., Halaszovich, C. R., Schreiber, D. N., Leitner, M. G., Bezanilla, F., et al. (2011) Controlling the activity of a phosphatase and tensin homolog (PTEN) by membrane potential. *J. Biol. Chem.* **286**, 17945-17953.
53. Lee, J., Shin, M. K., Ryu, D. K., Kim, S., and Ryu, W. S. (2010). Insertion and deletion mutagenesis by overlap extension PCR. *Methods Mol. Biol.* **634**, 137-146.
54. Leffler, A., Mönter, B., and Koltzenburg, M. (2006) The role of the capsaicin receptor TRPV1 and acid-sensing ion channels (ASICs) in proton sensitivity of subpopulations of primary nociceptive neurons in rats and mice. *Neuroscience* **139**, 699-709.
55. Li, T., Yang, Y., and Canessa, C. M. (2012) Impact of recovery from desensitization on acid-sensing ion channel-1a (ASIC1a) current and response to high frequency stimulation. *J. Biol. Chem.* **287**, 40680-40689.
56. Lingueglia, E., de Weille, J. R., Bassilana, F., Heurteaux, C., Sakai, H., et al. (1997) A modulatory subunit of acid sensing ion channels in brain and dorsal root ganglion cells. *J. Biol. Chem.* **272**, 29778-29783.
57. Liu, B., Zhang, C., and Qin, F. (2005) Functional recovery from desensitization of vanilloid receptor TRPV1 requires resynthesis of phosphatidylinositol 4,5-bisphosphate. *J. Neurosci.* **25**, 4835-4843.
58. Lukacs, V., Thyagarajan, B., Varnai, P., Balla, A., Balla, T., et al. (2007) Dual regulation of TRPV1 by phosphoinositides. *J. Neurosci.* **27**, 7070-7080.
59. Lukacs, V., Rives, J. M., Sun, X., Zakharian, E., and Rohacs, T. (2013a) Promiscuous activation of transient receptor potential vanilloid 1 (TRPV1) channels by negatively charged intracellular lipids: the key role of endogenous phosphoinositides in maintaining channel activity. *J. Biol. Chem.* **288**, 35003-35013.

60. Lukacs, V., Yudin, Y., Hammond, G. R., Sharma, E., Fukami, K., et al. (2013b) Distinctive changes in plasma membrane phosphoinositides underlie differential regulation of TRPV1 in nociceptive neurons. *J. Neurosci.* **33**, 11451-11463.
61. Ma, D., Zerangue, N., Lin, Y. F., Collins, A., Yu, M., et al. (2001) Role of ER export signals in controlling surface potassium channel numbers. *Science* **291**, 316-319.
62. Ma, D. and Jan, L. Y. (2002) ER transport signals and trafficking of potassium channels and receptors. *Curr. Opin. Neurobiol.* **12**, 287-292.
63. Ma, D., Zerangue, N., Raab-Graham, K., Fried, S. R., Jan, Y. N., et al. (2002) Diverse trafficking patterns due to multiple traffic motifs in G protein-activated inwardly rectifying potassium channels from brain and heart. *Neuron* **33**, 715-729.
64. Margeta-Mitrovic, M., Jan, Y. N., and Jan, L. Y. (2002) A trafficking checkpoint controls GABA_B receptor heterodimerization. *Neuron* **27**, 97-106.
65. Meves, H. (2008) Arachidonic acid and ion channels: an update. *Br. J. Pharmacol.* **155**, 4-16.
66. Michelsen, K., Yuan, H., and Schwappach, B. (2005) Hide and run. Arginine-based endoplasmic-reticulum-sorting motifs in the assembly of heteromultimeric membrane proteins. *EMBO Rep.* **6**, 717-722.
67. Miesenböck, G., De Angelis, D. A., and Rothman, J. E. (1998) Visualizing secretion and synaptic transmission with pH-sensitive green fluorescent proteins. *Nature* **394**, 192-195.
68. Murase, K., Ryu, P. D., and Randic, M. (1989) Excitatory and inhibitory amino acids and peptide-induced responses in acutely isolated rat spinal dorsal horn neurons. *Neurosci. Lett.* **103**, 56-63.
69. Nishimura, N. and Balch, W. E. (1997) A di-acidic signal required for selective export from the endoplasmic reticulum. *Science* **277**, 556-558.

70. Otsu, W., Kurooka, T., Otsuka, Y., Sato, K., and Inaba, M. (2013) A new class of endoplasmic reticulum export signal $\Phi X \Phi X \Phi$ for transmembrane proteins and its selective interaction with Sec24C. *J. Biol. Chem.* **288**, 18521-18532.
71. Pochynyuk, O., Tong, Q., Staruschenko, A., Ma, H. P., and Stockand, J. D. (2006) Regulation of the epithelial Na^+ channel (ENaC) by phosphatidylinositides. *Am. J. Physiol. Renal Physiol.* **290**, F949-957.
72. Pochynyuk, O., Tong, Q., Medina, J., Vandewalle, A., Staruschenko, A., et al. (2007) Molecular determinants of $\text{PI}(4,5)\text{P}_2$ and $\text{PI}(3,4,5)\text{P}_3$ regulation of the epithelial Na^+ channel. *J. Gen. Physiol.* **130**, 399-413.
73. Price, M. P., Snyder, P. M., and Welsh, M. J. (1996) Cloning and expression of a novel human brain Na^+ channel. *J. Biol. Chem.* **271**, 7879-7882.
74. Rahdar, M., Inoue, T., Meyer, T., Zhang, J., Vazquez, F., et al. (2009) A phosphorylation-dependent intramolecular interaction regulates the membrane association and activity of the tumor suppressor PTEN. *Proc. Natl. Acad. Sci. U.S.A.* **106**, 480-485.
75. Ryu, S., Liu, B., and Qin, F. (2003) Low pH potentiates both capsaicin binding and channel gating of VR1 receptors. *J. Gen. Physiol.* **122**, 45-61.
76. Schuhmacher, L. N., Srivats, S., and Smith, E. S. (2015) Structural domains underlying the activation of acid-sensing ion channel 2a. *Mol. Pharmacol.* **87**, 561-571.
77. Schwartz, V., Friedrich, K., Polleichtner, G., and Gründer, S. (2015) Acid-sensing ion channel (ASIC) 4 predominantly localizes to an early endosome-related organelle upon heterologous expression. *Sci. Rep.* **5**, 18242.
78. Senning, E. N., Collins, M. D., Stratiievska, A., Ufret-Vincenty, C. A., and Gordon, S. E. (2014) Regulation of TRPV1 ion channel by phosphoinositide (4,5)-bisphosphate: the role of membrane asymmetry. *J. Biol. Chem.* **289**, 10999-11006.

79. Sevier, C. S., Weisz, O. A., Davis, M., and Machamer, C. E. (2000) Efficient export of the vesicular stomatitis virus G protein from the endoplasmic reticulum requires a signal in the cytoplasmic tail that includes both tyrosine-based and di-acidic motifs. *Mol. Biol. Cell* **11**, 13-22.
80. Sherwood, T. W., Lee, K. G., Gormley, M. G., and Askwith, C. C. (2011) Heteromeric acid-sensing ion channels (ASICs) composed of ASIC2b and ASIC1a display novel channel properties and contribute to acidosis-induced neuronal death. *J. Neurosci.* **31**, 9723-9734.
81. Shyu, Y. J., Liu, H., Deng, X., and Hu, C. D. (2006) Identification of new fluorescent protein fragments for bimolecular fluorescence complementation analysis under physiological conditions. *Biotechniques* **40**, 61-66.
82. Smith, M. L., von Hanwehr, R., and Siesjö, B. K. (1986) Changes in extra- and intracellular pH in the brain during and following ischemia in hyperglycemic and in moderately hypoglycemic rats. *J. Cereb. Blood Flow Metab.* **6**, 574-583.
83. Smith, E. S., Cadiou, H., and McNaughton, P. A. (2007a) Arachidonic acid potentiates acid-sensing ion channels in rat sensory neurons by a direct action. *Neuroscience* **145**, 686-698.
84. Smith, E. S., Zhang, X., Cadiou, H., and McNaughton, P. A. (2007b) Proton binding sites involved in the activation of acid-sensing ion channel ASIC2a. *Neurosci. Lett.* **426**, 12-17.
85. Söderberg, O., Gullberg, M., Jarvius, M., Ridderstråle, K., Leuchowius, K. J., et al. (2006) Direct observation of individual endogenous protein complexes in situ by proximity ligation. *Nat. Methods* **3**, 995-1000.

86. Standley, S., Roche, K. W., McCallum, J., Sans, N., and Wenthold, R. J. (2000) PDZ domain suppression of an ER retention signal in NMDA receptor NR1 splice variants. *Neuron* **28**, 887-898.
87. Stein, A. T., Ufret-Vincenty, C. A., Hua, L., Santana, L. F., and Gordon, S. E. (2006) Phosphoinositide 3-kinase binds to TRPV1 and mediates NGF-stimulated TRPV1 trafficking to the plasma membrane. *J. Gen. Physiol.* **128**, 509-522.
88. Suh, B. C. and Hille, B. (2002) Recovery from muscarinic modulation of M current channels requires phosphatidylinositol 4,5-bisphosphate synthesis. *Neuron* **35**, 507-520.
89. Suh, B. C., Inoue, T., Meyer, T., and Hille, B. (2006) Rapid chemically induced changes of PtdIns(4,5)P₂ gate KCNQ ion channels. *Science* 314, 1454-1457.
90. Suh, B. C. and Hille, B. (2008) PIP₂ is a necessary cofactor for ion channel function: how and why? *Annu. Rev. Biophys.* **37**, 175-195.
91. Suh, B. C., Leal, K., and Hille, B. (2010) Modulation of high-voltage activated Ca²⁺ channels by membrane phosphatidylinositol 4,5-bisphosphate. *Neuron* **67**, 224-238.
92. Tominaga, M., Caterina, M. J., Malmberg, A. B., Rosen, T. A., Gilbert, H., et al. (1998) The cloned capsaicin receptor integrates multiple pain-producing stimuli. *Neuron* **21**, 531-543.
93. Ugawa, S., Yamamoto, T., Ueda, T., Ishida, Y., Inagaki, A., et al. (2003) Amiloride-insensitive currents of the acid-sensing ion channel-2a (ASIC2a)/ASIC2b heteromeric sour-taste receptor channel. *J. Neurosci.* **23**, 3616-3622.
94. Ugawa, S., Ueda, T., Yamamura, H., and Shimada, S. (2005) In situ hybridization evidence for the coexistence of ASIC and TRPV1 within rat single sensory neurons. *Brain Res. Mol. Brain Res.* **136**, 125-133.

95. Vazquez, F., Matsuoka, S., Sellers, W. R., Yanagida, T., Ueda, M., et al. (2006) Tumor suppressor PTEN acts through dynamic interaction with the plasma membrane. *Proc. Natl. Acad. Sci. U.S.A.* **103**, 3633-3638.
96. Waldmann, R., Champigny, G., Bassilana, F., Heurteaux, C., and Lazdunski, M. (1997) A proton-gated cation channel involved in acid-sensing. *Nature* **386**, 173-177.
97. Wemmie, J. A., Chen, J., Askwith, C. C., Hruska-Hageman, A. M., Price, M. P., et al. (2002) The acid-activated ion channel ASIC contributes to synaptic plasticity, learning, and memory. *Neuron* **34**, 463-477.
98. Wemmie, J. A., Askwith, C. C., Lamani, E., Cassell, M. D., Freeman, J. H., Jr., et al. (2003) Acid-sensing ion channel 1 is localized in brain regions with high synaptic density and contributes to fear conditioning. *J. Neurosci.* **23**, 5496-5502.
99. Wemmie, J. A., Taugher, R. J., and Kreple, C. J. (2013) Acid-sensing ion channels in pain and disease. *Nat. Rev. Neurosci.* **14**, 461-471.
100. Wu, J., Xu, Y., Jiang, Y. Q., Xu, J., Hu, Y., et al. (2016) ASIC subunit ratio and differential surface trafficking in the brain. *Mol. Brain* **9**, 4.
101. Yue, G., Malik, B., Yue, G., and Eaton, D. C. (2002) Phosphatidylinositol 4,5-bisphosphate (PIP₂) stimulates epithelial sodium channel activity in A6 cells. *J. Biol. Chem.* **277**, 11965-11969.
102. Zerangue, N., Schwappach, B., Jan, Y. N., and Jan, L. Y. (1999) A new ER trafficking signal regulates the subunit stoichiometry of plasma membrane K_{ATP} channels. *Neuron* **22**, 537-548.
103. Zha, X. M., Costa, V., Harding, A. M., Reznikov, L., Benson, C. J., et al. (2009) ASIC2 subunits target acid-sensing ion channels to the synapse via an association with PSD-95. *J. Neurosci.* **29**, 8438-8446.

104. Zhang, Z., Okawa, H., Wang, Y., and Liman, E. R. (2005) Phosphatidylinositol 4,5-bisphosphate rescues TRPM4 channels from desensitization. *J. Biol. Chem.* **280**, 39185-39192.

요 약 문

산-감지 이온채널 (acid-sensing ion channel, ASIC) 의 세포막 운송 및 지질에 의한 활성화 조절 메커니즘

ASIC 은 수소이온에 의해 활성화되는 양이온 채널로서 신경계에서 대표적 pH 센서로 작용한다. 수소이온은 통증을 유발하는 염증, 국소 빈혈, 감염, 암과 같은 병리생리학적인 상태에서 분비되며, 정상적인 시냅스 활동에서도 신경전달 물질로 역할을 하는 것으로 알려져 있다. ASIC 을 통한 생리학적 pH 변화의 감지는 침해 수용 (nociception), 가려움증, 통각, 미각, 학습과 기억, 공포 등에 관련되어 있다. 이러한 ASIC 의 중요성에도 불구하고, 이 이온채널에 관한 조절 기작에 대해서는 아직 구체적인 연구가 많이 되어 있지 않다. 본 연구에서는 ASIC 의 조절 기작에 대해 크게 두 부분으로 나누어 연구하였다. 첫 번째 연구에서는 ASIC 이 많은 수용체와 이온채널들의 활성화에 중요한 보조요인으로 작용하는 세포막 인지질에 의해 조절 받는가에 관해 연구하였다. 두 번째 연구에서는 ASIC 소단위체들 간에 서로 다른 세포막 운송 기작에 대해 연구하였다.

먼저, ASIC 이 세포막 인지질에 의해 조절 받는지 연구하기 위해 또 다른 수소이온을 감지할 수 있는 이온채널인 TRPV1 (transient receptor potential vanilloid 1) 을 이용하여 이들의 세포막 인지질에 대한 민감도를 비교하였다. 그 결과, ASIC 은 활성화에 세포막 인지질인 PI(4)P 과 PI(4,5)P₂ 를 필요로 하지 않는 반면, TRPV1 의 활성화는 PI(4)P 과 PI(4,5)P₂ 를 동시에

고갈시켰을 때 감소되는 것을 관찰하였다. PI(3,4,5)P₃ 의 D3 위치의 인산기만 특징적으로 탈인산화시킬 수 있는 새로운 키메라 단백질인 CF-PTEN 을 이용하여 ASIC 뿐 아니라 TRPV1 의 활성화도 PI(3,4,5)P₃ 에 의해 조절 받는다는 것을 관찰하였다. 마지막으로 이 이온채널들에 대한 아라키돈산의 효과를 살펴보았다. 아라키돈산이 ASIC 과 TRPV1 의 전류를 모두 증가시켰지만, 전류가 회복되는 양상은 다름을 알 수 있었다. 따라서, ASIC 과 TRPV1 은 수소이온의 센서로서 같은 역할을 하고 있지만 세포막 인지질인 PI(4)P, PI(4,5)P₂, 그리고 아라키돈산에 의해 다르게 조절 받는다는 것을 알 수 있다.

두 번째 연구에서는 ASIC 의 세포막 운송 기작을 밝힘으로 이 이온채널의 세포 내 활성화 조절 기전을 연구하였다. 세포 내에서 새롭게 합성된 수용체 혹은 이온채널들은 세포 내의 알맞은 위치로 운송되어야 활성화될 수 있기 때문에 세포 내에서 이온채널의 운송은 매우 중요하다. 다양한 질병들이 이온채널의 세포막 운송에 있어서의 결함으로 인해 발생된다. 본 연구에서는 특별히 ASIC2 소단위체에 초점을 맞추었다. ASIC 의 소단위체들 중 ASIC2a 와 ASIC2b 는 ACCN1 이라는 유전자에서 파생된 splicing variants 이다. ASIC2a 와는 달리 ASIC2b 는 수소이온을 감지하지 못하는데, 이에 관한 기전에 대해서는 깊은 연구가 필요하다. 본 연구에서는 ASIC2 소단위체들이 세포 내에서 서로 다른 위치에 분포하고 있음을 밝혔다. ASIC2a 는 그 자체만으로도 세포막으로 잘 운송되는 반면, ASIC2b 는 소포체에 머물러 있다. 서로 다른 세포 내 운송 기작을 밝히기 위해 유전자 변형기법을 이용하여 ASIC2 키메라들을 만들었고, 이를 통해 ASIC2a 의 TM1 (the first transmembrane) 도메인과 TM1 근접의 17개 아미노산이 세포막으로의 운송에 중요한 부분이

라는 것을 발견했다. ASIC2b 에서 이 부분을 ASIC2a 의 해당 아미노산 서열로 치환했을 경우, 세포막으로 이동하고 수소이온도 감지할 수 있음을 관찰하였다. 이에 더해, TM1 근접의 17개 아미노산이 ASIC2 의 수소이온 감지에 중요한 역할을 한다는 것을 발견하였다. 마지막으로 ASIC2b 가 ASIC2a 와 복합체 (heteromer) 를 형성함으로써 소포체로부터 이탈되어 세포막으로 운송될 수 있다는 것을 발견하였고, 복합체를 형성하는데 소단위체들 간의 N-말단 상호작용이 중요하다는 것을 밝혔다.

추가적으로, ASIC2a 가 다른 소단위체인 ASIC3 의 세포막 운송 또한 증가시킨다는 것을 발견하였다. ASIC2a 는 대부분 소포체에 분포하는 ASIC3 를 세포막으로 이동시켰으며, ASIC2a 에 의한 ASIC3 의 세포막으로의 운송은 전류의 sustained component 을 상당히 증가시켰다. 본 연구 결과는 ASIC 의 지금까지 알려져 있지 않았던 세포막 운송 기작을 밝힘으로 매우 큰 의미를 내포하고 있다.

핵심어: 산-감지 이온채널 (ASIC), 소포체, 세포막 지질, 단백질 결합, 세포막 운송

